

12-13-2003

## **New Visualization Techniques for Multi-Dimensional Variables in Complex Physical Domains**

Rhonda J. Vickery

Follow this and additional works at: <https://scholarsjunction.msstate.edu/td>

---

### **Recommended Citation**

Vickery, Rhonda J., "New Visualization Techniques for Multi-Dimensional Variables in Complex Physical Domains" (2003). *Theses and Dissertations*. 3286.  
<https://scholarsjunction.msstate.edu/td/3286>

This Dissertation - Open Access is brought to you for free and open access by the Theses and Dissertations at Scholars Junction. It has been accepted for inclusion in Theses and Dissertations by an authorized administrator of Scholars Junction. For more information, please contact [scholcomm@msstate.libanswers.com](mailto:scholcomm@msstate.libanswers.com).

NEW VISUALIZATION TECHNIQUES FOR MULTI-DIMENSIONAL  
VARIABLES IN COMPLEX PHYSICAL DOMAINS

By

Rhonda J. Vickery

A Dissertation  
Submitted to the Faculty of  
Mississippi State University  
in Partial Fulfillment of the Requirements  
for the Degree of Doctor of Philosophy  
in Computational Engineering  
in the College of Engineering

Mississippi State, Mississippi

December 2003

Copyright by

Rhonda J. Vickery

2003

NEW VISUALIZATION TECHNIQUES FOR MULTI-DIMENSIONAL  
VARIABLES IN COMPLEX PHYSICAL DOMAINS

By

Rhonda J. Vickery

Approved:

---

Robert J. Moorhead II  
Professor of Electrical and  
Computer Engineering  
(Major Professor and Dissertation  
Director)

---

David H. Huddleston  
Associate Professor of  
Civil Engineering  
(Committee Member)

---

Joerg Meyer  
Adjunct Assistant Professor of  
Computer Science and Engineering  
(Committee Member)

---

Clarence O. E. Burg  
Assistant Research Professor of  
Computational Engineering  
(Committee Member)

---

Timothy R. Keen  
Naval Research Laboratory  
(Committee Member)

---

Boyd Gatlin  
Associate Professor of  
Aerospace Engineering  
(Graduate Coordinator)

---

A. Wayne Bennett  
Dean of the College of Engineering



Name: Rhonda J. Vickery

Date of Degree: December 13, 2003

Institution: Mississippi State University

Major Field: Computational Engineering

Major Professor: Dr. Robert J. Moorhead II

Title of Study: NEW VISUALIZATION TECHNIQUES FOR MULTI-DIMENSIONAL VARIABLES IN COMPLEX PHYSICAL DOMAINS

Pages in Study: 163

Candidate for Degree of Doctor of Philosophy

This work presents the new Synthesized Cell Texture (SCT) algorithm for visualizing related multiple scalar value fields within the same 3D space. The SCT method is particularly well suited to scalar quantities that could be represented in the physical domain as size fractionated particles, such as in the study of sedimentation, atmospheric aerosols, or precipitation.

There are two components to this contribution. First a Scaling and Distribution (SAD) algorithm provides a means of specifying a multi-scalar field in terms of a maximum cell resolution (or density of represented values). This information is used to scale the multi-scalar field values for each 3D cell to the maximum values found throughout the data set, and then randomly distributes those values as particles varying in number, size, color, and opacity within a 2D cell slice. This approach facilitates viewing of closely spaced layers

commonly found in sigma-coordinate grids. The SAD algorithm can be applied regardless of how the particles are rendered.

The second contribution provides the Synthesized Cell Texture (SCT) algorithm to render the multi-scalar values. In this approach, a texture is synthesized from the location information computed by the SAD algorithm, which is then applied to each cell as a 2D slice within the volume. The SCT method trades off computation time (to synthesize the texture) and texture memory against the number of geometric primitives that must be sent through the graphics pipeline of the host system.

Analysis results from a user study prove the effectiveness of the algorithm as a browsing method for multiple related scalar fields.

The interactive rendering performance of the SCT method is compared with two common basic particle representations: flat-shaded color-mapped OpenGL points and quadrilaterals. Frame rate statistics show the SCT method to be up to 44 times faster, depending on the volume to be displayed and the host system.

The SCT method has been successfully applied to oceanographic sedimentation data, and can be applied to other problem domains as well. Future enhancements include the extension to time-varying data and parallelization of the texture synthesis component to reduce startup time.

## DEDICATION

This dissertation is dedicated to my children, Axel and Kate, and my husband John, who all shared this journey with me.

This dissertation is also dedicated to my brother Rob. Every time I think of him I am reminded of two important things:

- Ambitious dreams do not have to come true, so long as you enjoy reaching for them.
- You can teach and be a positive influence on other people without being a teacher.

Sail home, Rob. Sail home.

## ACKNOWLEDGMENTS

I thank Dr. Robert Moorhead for directing this research and providing the long term support necessary for me to complete this work. I also thank my committee members for their constructive comments during the preparation of this document, and their insight during the research phase. My family deserves much of the credit for my successful completion of this degree. Their support and sacrifice made it all possible.

Portions of this research were funded by ONR grant N00014-001-0560.

SGI, OpenGL, and OpenGL Performer are trademarks or registered trademarks of Silicon Graphics, Inc., in the United States and other countries worldwide. CAVE is a registered trademark of the University of Illinois Board of Trustees. All other trademarks are the property of their respective owners.

## TABLE OF CONTENTS

	Page
DEDICATION . . . . .	ii
ACKNOWLEDGMENTS . . . . .	iii
LIST OF TABLES . . . . .	vi
LIST OF FIGURES . . . . .	viii
CHAPTER	
I. INTRODUCTION . . . . .	1
1.1 Multiple Scalar Field Visualization for Environmental Data . . . . .	3
1.2 Hypotheses . . . . .	9
II. BACKGROUND . . . . .	13
2.1 Perceptual Visualization . . . . .	14
2.2 Particle Rendering . . . . .	17
2.3 Volume Visualization . . . . .	17
2.4 Sedimentation . . . . .	19
III. APPROACH . . . . .	21
3.1 Sedimentation Data Grid Characteristics . . . . .	22
3.2 SCT Algorithm Implementation . . . . .	25
3.2.1 System Design . . . . .	29
3.2.2 Texture Calculations . . . . .	31
3.2.3 SCT Implementation Details . . . . .	34
IV. USER STUDY . . . . .	41
4.1 Methodology . . . . .	41
4.1.1 Design . . . . .	42
4.1.2 Hypotheses . . . . .	46

CHAPTER	Page
4.1.3 Operationalization of Variables . . . . .	48
4.1.4 Final User Study Experimental Configuration . . . . .	49
4.1.5 Statistical Methods . . . . .	53
4.2 Results . . . . .	55
4.2.1 Task 1 Analysis . . . . .	59
4.2.2 Task 2 Analysis . . . . .	63
V. PERFORMANCE STUDY . . . . .	69
5.1 Design . . . . .	70
5.2 Results . . . . .	72
VI. CONCLUSIONS . . . . .	81
6.1 Future Work . . . . .	83
REFERENCES . . . . .	85
APPENDIX	
A. DATASET AND TEST CASE INFORMATION . . . . .	92
B. DISTRIBUTION NORMALIZATION PROCESS . . . . .	119
C. ACCURACY INFORMATION . . . . .	126
D. SUMMARY STATISTICS . . . . .	128
E. SPSS OUTPUT . . . . .	134

## LIST OF TABLES

TABLE	Page
3.1 Dataset Descriptions. . . . .	25
3.2 Oceanside Dataset Grain Size Distribution. . . . .	36
3.3 USDA Consolidated Grain Size Classification. . . . .	37
3.4 Oceanside Dataset Example Calculations. . . . .	38
3.5 Bin Categories With USDA Pixel and Color Assignments. . . . .	38
4.1 Method Characteristics Comparison. . . . .	46
4.2 Task 1 Cases. . . . .	50
4.3 Task 2 Cases. . . . .	50
4.4 Task 1 Multivariate and Univariate Significance Test Results. . . . .	60
4.5 Task 2 Multivariate and Univariate Significance Test Results. . . . .	64
5.1 Machine Configurations for Benchmark Tests. . . . .	71
5.2 Number of Actual Consolidated Glyphs Used in Volume for Machine B SRBCR. . . . .	77
A.1 User Study Test Cases: Main Experiment. . . . .	115
A.2 User Study Test Cases: Training. . . . .	115
A.3 User Study Test Cases: Examples. . . . .	116
A.4 Performance Study Test Cases. . . . .	117
B.1 Task 1 Original <i>Time</i> Statistics for 50 Users. . . . .	122

TABLE	Page
B.2 Task 2 Original <i>Time</i> Statistics for 50 Users. . . . .	123
B.3 Task 1 Adjusted <i>Time</i> Statistics for 49 Users. . . . .	124
B.4 Task 2 Adjusted <i>Time</i> Statistics for 49 Users. . . . .	125



## LIST OF FIGURES

FIGURE	Page
1.1 Littoral Region. . . . .	2
1.2 Example Points Visualization of Sediment Concentration. . . . .	5
1.3 Point Detail View Showing SSC for the Hill Location. . . . .	6
1.4 Point Detail View Showing SSC for the Hole Location. . . . .	6
1.5 Twelve Layer Visualization With Point Detail Profiles. . . . .	8
1.6 Close-up of the Hole Location. . . . .	8
2.1 Wedges Method Over Nine Grid Locations on One Layer. . . . .	16
3.1 Plot of a Sigma-coordinate System at a Single Time Step. . . . .	23
3.2 Typical Grain Size Distribution for Oceanside Dataset (in Units of $\Phi$ and $m$ ). . . . .	24
3.3 New Grid Slice With Eight Triangles Superimposed on the Original Grid. . . . .	26
3.4 Example Showing Difference Between Blended and Constant Value Coloring. . . . .	28
3.5 System Design. . . . .	30
3.6 Particle Primitive for Each USDA Sedimentation Category. . . . .	39
3.7 Single Cell Texture Generated by the SCT Algorithm. . . . .	40
4.1 Oriented Sliver Textures in the VE. . . . .	44
4.2 Top-down View of Typical Wedges Scene in Practice. . . . .	45
4.3 Top-down View of Typical SCT Scene in Practice. . . . .	45

FIGURE	Page
4.4 Early Wedges Showing Ineffective Use of Transparency. . . . .	47
4.5 Wedges Task 1 Effect of Changing <i>XY</i> Area. . . . .	52
4.6 SCT Task 2 Effect of Changing <i>XY</i> Area. . . . .	52
4.7 Task 2 No Pattern Example for Both Methods. . . . .	52
4.8 Task 1 <i>Time</i> vs. <i>Method</i> for 50 Subjects. . . . .	61
4.9 Task 1 <i>Time</i> vs. <i>Area</i> for 50 Subjects. . . . .	61
4.10 Task 1 <i>Time</i> vs. <i>Area</i> for 50 Subjects. . . . .	62
4.11 Task 1 <i>Time</i> vs. <i>Area</i> by <i>Method</i> for 50 Subjects. . . . .	63
4.12 Task 2 <i>Time</i> vs. <i>Method</i> for 50 Subjects. . . . .	65
4.13 Task 2 <i>Correct</i> vs. <i>Method</i> for 50 Subjects. . . . .	65
4.14 Task 2 <i>Time</i> vs. <i>Area</i> for 50 Subjects. . . . .	66
4.15 Task 2 <i>Time</i> vs. <i>Area</i> for 50 Subjects. . . . .	66
4.16 Task 2 <i>Time</i> vs. <i>Area</i> by <i>Method</i> for 50 Subjects. . . . .	67
5.1 Frame Rate vs. Number of Layers for Machine A SRALA. . . . .	72
5.2 Frame Rate Speedup Ratio vs. Number of Layers for Machine A SRALA. . . . .	73
5.3 Frame Rate vs. Number of Layers for Machine B SRBDP. . . . .	74
5.4 Frame Rate Speedup vs. Number of Layers for Machine B SRBDP. . . . .	75
5.5 Frame Rate vs. Slice Resolution for Machine B SRBCR. . . . .	76
5.6 Startup Time vs. Number of Layers for Machine A SRALA. . . . .	78
5.7 Total Memory vs. Number of Layers for Machine A SRALA. . . . .	79

FIGURE	Page
5.8 Startup Time Speedup Ratio vs. Number of Layers for Machine A SRALA. . . . .	79
A.1 Louisiana Coast Hurricane Andrew Dataset Location. . . . .	92
A.2 Duck, North Carolina Dataset Location. . . . .	93
A.3 Great Bay, New Jersey Dataset Location. . . . .	94
A.4 Mississippi Sound MSB Dataset Location. . . . .	94
A.5 Mississippi Sound Hurricane Camille Dataset Location. . . . .	95
A.6 Oceanside, California Dataset Location. . . . .	95
A.7 Microsoft Copyright Permission for Maps. . . . .	118
B.1 Histogram frequency distribution of <i>Time</i> by <i>Case</i> for Task 1. . . . .	121
C.1 Accuracy Distributions for Task 1. . . . .	127
D.1 Task 1 <i>Time</i> vs. <i>Color</i> for 50 subjects. . . . .	128
D.2 Task 1 <i>Correct</i> vs. <i>Method</i> for 50 subjects. . . . .	129
D.3 Task 1 <i>Correct</i> vs. <i>Color</i> for 50 subjects. . . . .	129
D.4 Task 1 <i>Time</i> vs. <i>Color</i> by <i>Method</i> for 50 subjects. . . . .	130
D.5 Task 1 <i>Correct</i> vs. <i>Area</i> by <i>Method</i> for 50 subjects. . . . .	130
D.6 Task 1 <i>Correct</i> vs. <i>Color</i> by <i>Method</i> for 50 subjects. . . . .	131
D.7 Task 2 <i>Time</i> vs. <i>Pattern</i> for 50 subjects. . . . .	131
D.8 Task 2 <i>Correct</i> vs. <i>Pattern</i> for 50 subjects. . . . .	132
D.9 Task 2 <i>Time</i> vs. <i>Pattern</i> by <i>Method</i> for 50 subjects. . . . .	132
D.10 Task 2 <i>Correct</i> vs. <i>Area</i> by <i>Method</i> for 50 subjects. . . . .	133

FIGURE	Page
D.11 Task 2 <i>Correct vs. Pattern by Method</i> for 50 subjects. . . . .	133

# CHAPTER I

## INTRODUCTION

The magnitude of the problems scientists are trying to solve today necessitates the creation of new methods for understanding complex interrelated processes. This often requires the comparison of large amounts of acquired measurement data with model generated data to improve the prediction capability of the models and gain better understanding of the problems. Additionally, models are now being tied together into systems to make large scale predictions that are influenced by many small scale processes that affect the accuracy of the output. In summary, scientists develop complicated models dealing with large amounts of data that must be accurate to be useful.

For global environmental data, the accuracy is being improved by breaking down general variables into their smaller components. One class of problems where this is the case are those variables that represent concentrations of particulates differentiated by size. Examples include:

- *Precipitates*: water droplets, snow, ice crystals, and water-particulate combinations.
- *Aerosols*: pollutants, sea salt, and dust.
- *Sediment*: clay, silt, sand, and gravel.

The interrelationships of these particulates can be seen in Figure 1.1. The atmospheric effects from various sized precipitates are present in the prevailing weather, separated into

layers. Winds cause mixing in the aerosol dome, which may have several grain sizes of sand or dust from dry areas onshore, as well as size differentiated pollutants. Within the shallow water region, the influence of waves, tides, and changing bottom types cause mixing of various sizes of sediment. All of the processes involved have a volumetric influence, not just a surface area influence, which makes understanding the overall effect more complicated. Models are incorporating variables that describe these detailed subprocesses in order to improve the accuracy of future predictions.

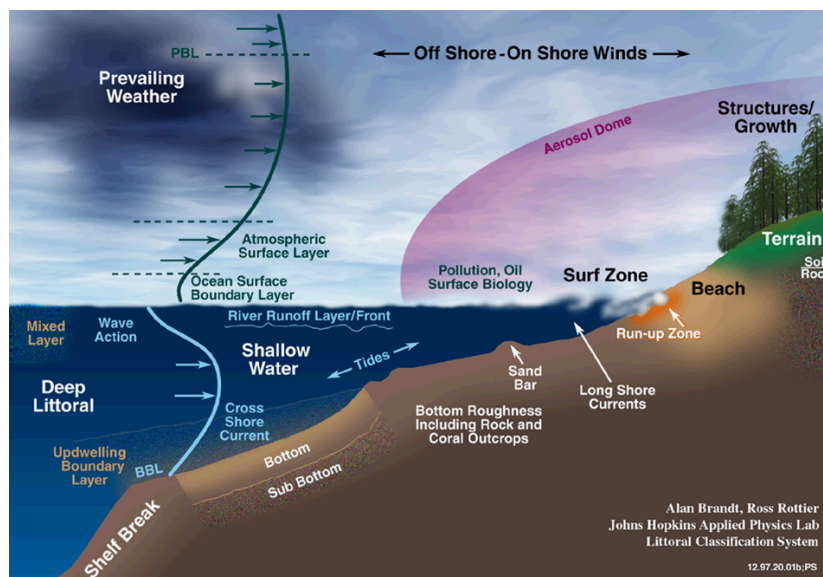


Figure 1.1 Littoral Region.

An area of focus for this dissertation is in the visualization of output from coupled sediment dynamics and optics models in shallow water [30]. These models compute quantities of sediment being entrained and transported in complex coastal environments with mixed

sediment types. Some studies use bottom boundary layer models to examine near-bottom processes, while others are concerned with upper water column sediment distributions. The goal is to develop the ability to predict the impact of the suspended sediment optical fields on visibility in support of naval operations such as mine warfare. Intelligently designed visualization techniques can help the scientist with the analysis of these physical processes. This research presents the *Synthesized Cell Texture* (SCT) algorithm, which is a new browsing method to view concentrations of size fractionated particulates in large datasets. The SCT method can be applied as one layer to see effects over large areas, or as multiple layers at once over a small area so volumetric effects can be understood. The scientist can use the SCT method as an analysis tool to help visually determine whether there are problems in the model output and to help assess the accuracy of the processes represented.

### **1.1 Multiple Scalar Field Visualization for Environmental Data**

Concentrations of related environmental variables are often reported as mass per unit volume magnitudes, or multi-valued scalar fields. Although this puts all quantities on an equal basis for comparison, it does not give a direct indication of how many particles of different sizes are actually suspended. What this means is that for each physical point in space, or grid point in the model, there are concentration values for a number of different grain sizes. Since the magnitudes are differentiated by size, the values form a group of related scalar fields, sometimes referred to as “profiles.” The combined effect is important

for the production of accurate model results, but the added dimension creates difficulties for existing visualization methods. In addition to longitude, latitude, depth (or altitude), and time, there is now a fifth dimension, grain size, making it difficult to display values individually using conventional methods [32, 68]. This extra dimension is problematic for off-the-shelf visualization software, and has until recently only been visualized as a single combined entity throughout a volume, or as individual scalar values.

An example is shown in Figure 1.2<sup>1</sup>, where columns of color-mapped spheres on a texture-mapped ocean bottom show the combined magnitudes for suspended sediment concentrations (SSC) in a shallow water region near Oceanside, California. Each sphere in the column represents the magnitude of the summation of 20 scalar fields for one of the 31 layers in the visualization. Although the columns are rendered at every other grid location on the texture-mapped surface, the display is still cluttered, and the visualization is not very useful. Color-mapped 2D (horizontal) depth layers are another method commonly used to show combined or single valued SSC.

The full profiles themselves have only been visualized at individual points or columns of points aligned in the third dimension. For example, point profiles for overall SSC have been used for visualization of sedimentation processes [32, 68]. For the point profile visualization from the Oceanside dataset shown in Figure 1.3, the sediment concentration

---

<sup>1</sup>The red box marks the presence of the wand in the virtual environment simulator. This desktop version of the application was used to capture screenshots at various stages of development. The wand icon may also have a pointer extension to facilitate selection of points in the application. The virtual environment is described in Section 1.2.



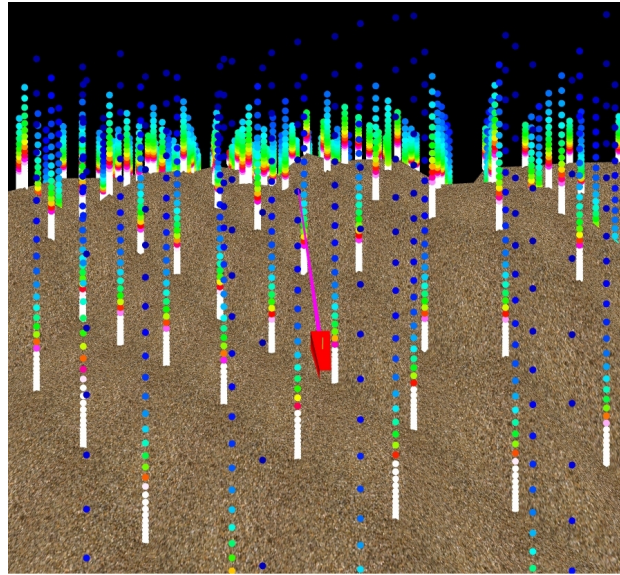


Figure 1.2 Example Points Visualization of Sediment Concentration.

values are color-mapped on a  $\log_{10}$  scale for a column of water<sup>2</sup> at a grid location on a raised area within a shallow water region (or hill location). The semicircular columns of points indicate the individual SSC for each grain size from smallest (left) to largest (right), where zero values are dark blue. In this case the largest grain size represented is 3000 times larger than the smallest, but concentration values very close to zero for the smaller grain sizes are still significant. Figure 1.4 shows a similar profile for a deeper grid location within the same shallow water region (hole location). To the novice analyst, it is not clear how much sediment, in terms of relative numbers of suspended particles, is represented from these views, and this method does not display an integrated view for all grid locations throughout a volume.

<sup>2</sup>The column represents depth in the vertical direction as defined in Section 3.1.

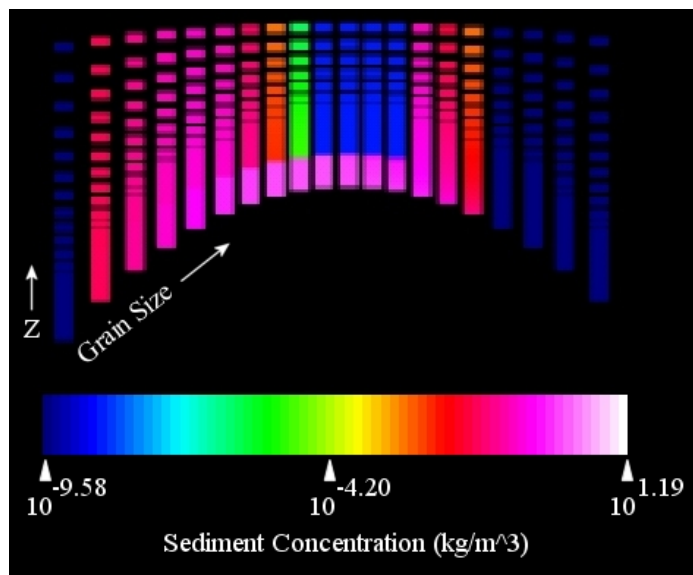


Figure 1.3 Point Detail View Showing SSC for the Hill Location.

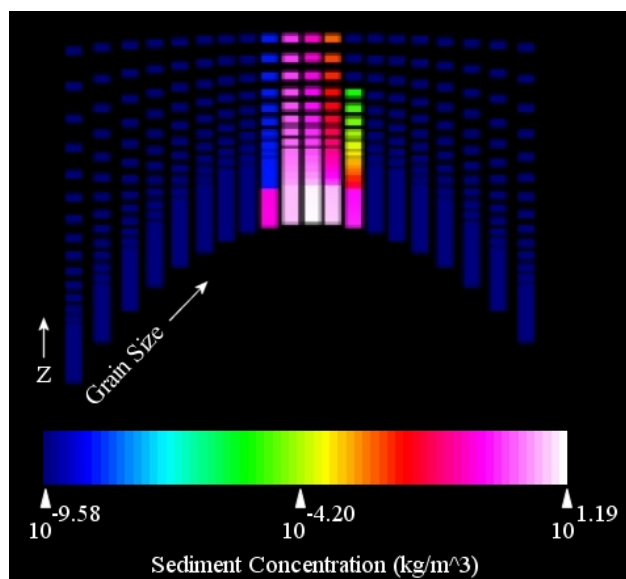


Figure 1.4 Point Detail View Showing SSC for the Hole Location.

Given the densities and particle volume information of the suspended particulates, the concentration values can be converted to numbers of particles per unit volume. These quantities can then be rendered using multidimensional, multivariate (MDMV) methods [77], including those for direct volume or particle rendering, as shown in Figure 1.5. In this example rendered using the new SCT method, a twelve layer volume visualization is depicted with the point profiles for the hill and hole locations. For the SCT method, the magnitudes of the scalar fields are depicted with quantities of particles. Without knowing any of the details of the implementation, it can be quickly seen that certain particles are stripped away within the depression, an effect known as armoring, shown in more detail in Figure 1.6. This type of “at a glance” information can be useful for browsing large datasets. The presence of other environmental information, such as a vector field of currents, may provide insight into the visibility conditions near the ocean bottom over time. For instance, mine counter measures operations require the identification or location of objects, and a detailed visual representation of the ocean bottom may improve the understanding of underwater conditions affecting decision making policies.

Other areas where accuracy is important are related to aerosol dispersion of such fine particulates as sulfates, soot, dust, and sea salt [2, 18]. Climate models used to study problems, such as global warming, generate atmospheric and oceanic circulations that can be greatly affected by the accuracy of estimates of sunlight absorption in the atmosphere. Models in the 1990’s greatly miscalculated the effects of sunlight absorption because they did not account for substantial amounts of atmospheric aerosols [18]. Recent

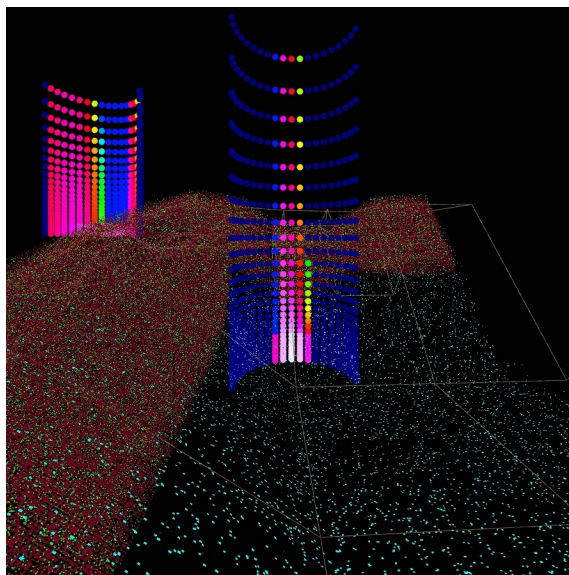


Figure 1.5 Twelve Layer Visualization With Point Detail Profiles.

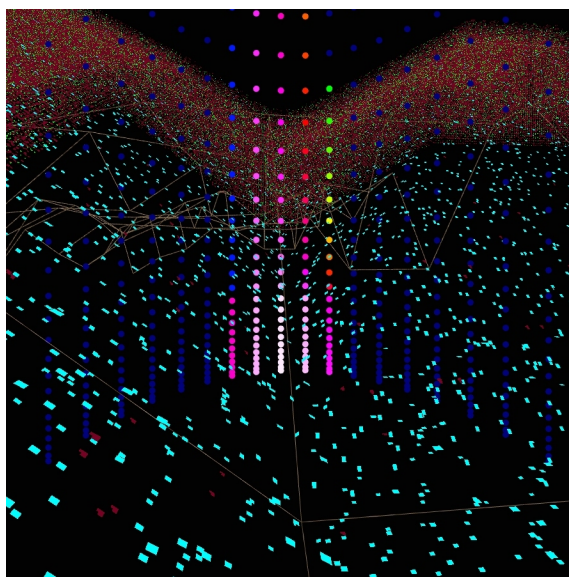


Figure 1.6 Close-up of the Hole Location.

models account for these effects through the inclusion of size fractionated source distributions [11, 12, 13, 16, 61], and are validating the accuracy of these models with comparisons to observed conditions [1, 43, 55, 73]. Visual techniques that can show the magnitudes of these related scalar fields at once may help scientists better understand the complex inter-related processes affecting the accuracy of these models.

## 1.2 Hypotheses

The problem domains just described are good candidates for exploration in our four-wall virtual environment (VE)<sup>3</sup> [4], especially for combination views involving concentrations, vector quantities, and other scalar fields [32]. In this room-size VE, a scientist can get “inside” the visualization by physically walking around a displayed grid location to see the data from multiple viewpoints in three dimensions. This capability gives the scientist additional depth to view higher dimensional data that is not available on conventional desktop displays. However, rendering concentrations as particles at interactive frame rates using traditional methods, such as texture-mapped primitives or basic points [36, 42], is computationally expensive and can easily overload the VE graphics pipeline. Therefore, this work describes an alternate means of visualizing multi-scalar data with the introduction of the new SCT algorithm. This hybrid technique indicates the added dimension of a scalar profile variable within a three-dimensional (3D) cell in terms of relative quantities of different size particles.

---

<sup>3</sup>The VE is similar to a CAVE®, and the recursive acronym stands for CAVE Automatic Virtual Environment.

Given the particle representation of the SCT method, there are instances where this technique can be applied to some advantage over other state-of-the-art methods. The type of information conveyed is not easily quantified against a visual scale, yet the SCT method does give the viewer a general idea about what is present that can be ascertained quickly, or “at a glance”. Thus the SCT method has certain characteristics that make it a useful browsing technique. Using perceptual concepts from Healey [20, 22] and Ware [71], a visual browsing technique can be developed that enables the user to quickly perform:

1. *Feature Detection*: whether information is present, and
2. *Feature Identification*: whether some feature stands out that should be investigated.

The goal of this research is to show that the SCT method satisfies these requirements by comparing it with another new glyph-based Wedges visualization method that also incorporates state-of-the-art perceptual characteristics in a user study. Statistical analysis will prove that the SCT method can be used for feature detection and identification for several size areas (regions) from multiple sedimentation datasets. The amount of time taken for a person to complete a task that centers around these requirements is measured and compared, as well as the correctness of the result. This is expressed in the form of two formal (paired) hypotheses:

$HT_0$ : There is no significant difference in the amount of time it takes to complete a browsing task between the two methods over different size areas. This is the null hypothesis for time.

$HT_A$ : It takes significantly less time to complete a browsing task using the SCT method vs. using the Wedges method over different size areas (the alternate hypothesis for time).

$HC_0$ : There is no significant difference in the correctness of the result during the completion of a browsing task between the two methods over different size areas. This is the null hypothesis for correctness.

$HC_A$ : There is a significant difference in the correctness of the result during the completion of a browsing task between the two methods over different size areas (the alternate hypothesis for correctness).

Statistical analysis of the results will prove that the null hypothesis  $HT_0$  is rejected, showing that it takes significantly less time to perform two specific browsing tasks using the SCT method for feature identification and detection for several different size areas. Additionally it will be shown that hypothesis  $HC_0$  will not be rejected, and the SCT method will be proven to be no less accurate than the Wedges method. Chapter 4 documents the user study results that prove these hypotheses.

Note that this study is conducted with sedimentation data in the Mississippi State University ERC CAVE-like VE facility, known as the *COVE*. The results are only shown to be valid in this context, although it is fully expected that similar results could be achieved with other types of related data (such as precipitation, airborne pollutants, dust, etc.) in other visualization environments.

The SCT algorithm can display the additional information throughout a prescribed volume at a desired slice resolution, given existing hardware constraints. The performance

and interactivity of the SCT method is of interest when compared with other particle rendering methods. As a measure of how well this method can be applied in the COVE, the rendering performance of the SCT method is compared with two basic particle rendering methods as part of this research: flat-shaded color-mapped points and quadrilaterals. Both methods can be considered simpler (and faster) forms of the general texture-mapped primitives approach. Results show that the SCT method can render scenes interactively up to 44 times faster than the other two particle rendering methods. These results are presented in Chapter 5.

The structure of this document is organized into sections on the research, implementation, and analysis required to introduce the SCT visualization technique for representing related multi-dimensional variables in complex physical domains. Chapter 2 describes the background and related work for visualization of scalar data. Chapter 3 presents the approach used in the development of the algorithm along with the implementation and application to sedimentation data sets [68]. The user study design, execution, and results are included in Chapter 4. Performance comparisons are made in Chapter 5 [69], and Chapter 6 provides conclusive remarks and points out areas for future work.

Portions of this research have been published in citations [32, 67, 68, 69] and should be consulted for additional information.



## CHAPTER II

### BACKGROUND

Effectively representing MDMV scalar fields is an active area of research in information visualization. Two important goals are: (i) to discover the values for data within a region, and (ii) locate data with specific values [75]. Good visual methods often help the researcher find areas of interest and correlations between variables. With the ability of computers to convey more information at once comes a challenge to determine what visual attributes are best perceived by humans [71]. Hence evaluating the effectiveness of a technique is dependent on perception-based user studies [7], as well as rendering speed and memory efficiency.

An excellent overview and classification scheme for MDMV visualizations is presented by Wong and Bergeron [77]. Statistical and information analysis motivates the use of various 2D and 3D graphical methods [33, 62, 63, 64], with the objective of conveying information about  $m$ -dimensional dependent variables (the multivariate aspect) for  $n$ -dimensional independent variables (the multidimensional aspect). For our sedimentation application, SSC represents the dependent variable for the 5D independent variables of longitude, latitude, depth, time, and grain size. Animation is often used to convey changes in dependent variables over time, but displaying SSC values for the remaining

four dimensions in 3D space is more problematic. One category of MDMV methods encodes data information to color and geometric attributes of an object (often termed a glyph or icon) [38, 39].

This chapter describes related literature from the fields of perceptual visualization (Section 2.1), particle rendering (Section 2.2), and volume visualization (Section 2.3). Concepts from these areas were applied iteratively to develop the effective texture-based SCT method, as well as another state-of-the-art glyph-based method, termed *Wedges*.

## 2.1 Perceptual Visualization

The study of perceptual characteristics played a key role in the development of both the SCT and *Wedges* methods. Lessons learned from understanding how artists employ techniques to draw the viewer's interest to certain areas of a painting helped considerably in the effective use of textures in the SCT method. How well certain information “pops out” from the surrounding visualization is the focus of literature on pre-attentive processing, which influenced the glyph design of both methods. This section describes how the work in these areas of perceptual visualization relate to the SCT and *Wedges* methods. For details about the implementation of the SCT method, see Chapter 3. The evolution of the *Wedges* method is described in Chapter 4.

Laidlaw [37] summarizes the recent work in using textures for visualization by comparing concepts from computer visualization and the art of three famous painters: van Gogh, Monet, and Cezanne. These artists were proficient at using multiple layers to con-

vey subtle differences in visualization. He presents the concept of “underpainting” to describe how Van Gogh used “rough value sketching” of the entire painting as a way to help organize or group the canvas into distinct parts. Then detailed brush strokes would be added to define specific areas to draw the attention of the viewer. From this article the following quote describing how these artists use underpainting and detail strokes to draw the viewer into the scene is extremely relevant:

Similarly, brush-stroke size and proximity depict density, weight, and velocity. In our visualizations, we want to capture this marriage between direct representation of independent data and the overall intuitive feeling of the data as a whole.

Other authors describe similar concepts, often combining traditional techniques with textures to represent multiple data values at a point [21, 22, 26, 34, 60, 71, 72, 76]. The SCT method is an excellent example of a technique that gives that “overall intuitive feeling of the data as a whole.” This is one attribute that makes it a viable method for information browsing (see Figure 1.5).

In the area of pre-attentive processing, the following attributes are employed in the SCT and Wedges methods to make certain information “pop out” [20, 71]:

- hue,
- intensity,
- size,
- orientation,
- numerosity, and
- spatial position.

The SCT method makes particularly good use of hue, numerosity, and particle size to distinguish between amounts of different categories of sediment. The Wedges method primarily uses grayscale intensity, size, hue, and orientation to display differences in the multiple scalar fields. Both methods depend heavily on spatial positioning to convey location information. Whereas the SCT method is useful for identifying small regions of interest, the Wedges method provides more detailed information at a particular grid location. This method uses an oriented grouping of wedges where intensity represents the number of particles of each scalar field, color shows the category of sediment, and the size of the wedges indicates the relative grain size of the bin particle size, as shown in Figure 2.1. In Chapter 4 both state-of-the-art methods are evaluated in a user study to measure their effectiveness for visual browsing tasks.

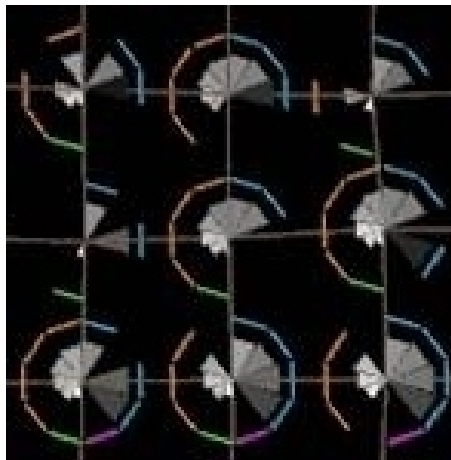


Figure 2.1 Wedges Method Over Nine Grid Locations on One Layer.

## 2.2 Particle Rendering

In terms of rendering particle information, a quadrilateral can be considered a glyph with the attributes of color (four components), shape, size, and texture. Any number of these attributes could be mapped to the magnitude of a different scalar field, but perception-based studies determine which attributes can be effectively utilized [71]. Flow visualization often uses texture-mapped quadrilaterals (or basic color-mapped points) to represent particles [36, 42, 44, 45, 57]. The SCT algorithm incorporates the concept of a glyph at two levels. In this study, an SCT particle primitive is considered to be a  $4 \times 4$  array of pixels from a 2D texture with the same attributes as a quadrilateral. However, an SCT glyph could also represent the information for a 3D cell volume (containing many particles) at a spatial location.

Particles for flow visualization may also be rendered by some number of pixels in an overall texture that are then advected over time. These include such methods as spot noise [5], line integral convolution (LIC) [54], and texture advection [23, 27, 28]. These pixel-based particles are generally massless and are injected into the flow at a specific time. Size, color, and shape variability are often used to indicate direction and orientation of flow, or magnitude of a scalar field.

## 2.3 Volume Visualization

Scalar fields are commonly represented by volume visualization methods, which generally involves the rendering of volumetric data sets representing 1D scalar quantities at

specific points [29, 47]. Historically these were medical data sets containing values at regularly sampled points (as on an implicit regular 3D grid), but now the field has expanded to include other types of data. The challenge is to classify what the scalar values represent (such as tissue or bone) as indicated by different colors and opacities. Rendering the values is often done using one of two general approaches. The first renders 3D polygonal surfaces constructed from scalar values in the volume, and the second renders the scalar values directly [47]. The latter approach is known in the literature as direct volume rendering (DVR) [40]. Several methods approximate the underlying integral defining the blending of values (such as splatting or texture-based methods), or show 2D slices of the volume (such as projection-based methods).

The SCT method is similar in concept to the DVR approach. Different colors and opacities depict the various classifications of scalar values. In order for a DVR method to be rendered, the colors and opacities must be obtained at discrete intervals along a linear path and then composited in a front to back order. How the colors and opacities are computed at specific points along the path differentiates the various DVR algorithms. The time spent computing the values determines how interactive the algorithm will be. Many basic DVR algorithms use trilinear interpolation to compute the values within 3D cells (or voxels) defined by the grid points.

Research has also been done on trying to show two or three independent variables at once in a volume visualization [3]. More work is needed on effectively representing larger

numbers of scalars simultaneously. The SCT algorithm represents multiple scalar fields as particles differentiated by size and color in a synthesized texture.

With the advent of 3D texture mapping hardware, direct volume rendering can be accomplished at interactive frame rates [17]. The basic idea is to use the scalar field as a 3D texture. A number of equidistant planes parallel to the image plane are clipped against the bounding volume boundaries, and the texture hardware trilinear interpolation mechanism computes the values on the planes. Then the hardware blending capability blends the planes from back to front, such that the viewer sees the combined contribution of all the planes. A 2D texture mapping algorithm can provide a 3D rendered image if the planes are perpendicularly aligned along one of the primary axes, and viewing is parallel to the chosen axis. The SCT approach utilizes 2D texture mapping.

Details about the texture synthesis portion of the SCT method are presented in Chapter 3.

## 2.4 Sedimentation

SSC is one of the most difficult sedimentation variables to visualize, since it varies with longitude, latitude, depth, time, and grain size. At each grid point, there are values of SSC for 20 different sediment grain sizes. The order-of-magnitude range in sediment size makes it difficult to visually show differences in grain size on a linear scale, and so detailed views are shown with log scale color mapping (see Figure 1.3). Although this method allows viewing all grain sizes for a column of water, multiple simultaneous detail

views across large areas are not readily viewed as a single combined visualization. Other methods for viewing either overall combined SSC or individual grain size values for SSC include: point visualizations throughout a volume of interest as shown in Figure 1.2, or 2D color-mapped surfaces for a particular depth. Generally, SSC cannot be visualized directly using popular off-the-shelf tools, since the SSC variable is 5D. Thus the analysis of the SSC distribution can be difficult [32].



## CHAPTER III

### APPROACH

This chapter describes the approach used to develop the SCT visualization algorithm. The environmental data and grid characteristics are detailed in Section 3.1, and the algorithm implementation is presented in Section 3.2, including texture calculations described in Section 3.2.2.

First this method provides a means of creating a visualization of a volumetric multi-scalar field that can be specified in terms of a maximum cell resolution (or density of represented values). This maximum resolution is used to scale the multi-scalar field for the data over the entire volumetric area, including all time series. Therefore a prescribed volume of data for any time step can be displayed and compared relative to the same scale with other areas within the same time step or across multiple time steps. The values within a 3D cell are positioned as nonoverlapping entities equally distributed within a 2D slice centered at the original grid point. In other words, this algorithm scales the data for each cell to the maximum values found throughout the data set, and then randomly distributes the values within a cell slice. This portion of the SCT method is termed the *Scaling and Distribution (SAD)* algorithm. This approach facilitates viewing of closely spaced layers commonly found in sigma-coordinate (terrain following) grids that have

logarithmic spacing in the vertical direction [51]. The SAD portion of the algorithm can be applied regardless of how the multi-scalar entities are rendered (i.e. as parts of a 2D texture-mapped slice, color-mapped point primitives, or color-mapped quadrilaterals).

The second contribution provides a hardware texture mapping algorithm to render the multi-scalar values. In this approach, a texture is synthesized from the location information from the first step, which is then applied to each cell 2D slice within the volume. This method trades off computation time (to synthesize the texture) and texture memory against the number of geometric primitives that must be sent through the graphics pipeline of the host system. This algorithm will be referred to as the *Synthesized Cell Texture* (SCT) algorithm. The SCT algorithm incorporates the SAD algorithm as part of the rendering of the volume visualization. Therefore SCT will also refer to the visualization algorithm in general.

### 3.1 Sedimentation Data Grid Characteristics

Although the SCT method can be applied to any scalar where different characteristics can be represented by pixel color, pixel opacity, and number of pixels per color, it is particularly well suited to multi-dimensional variables that have typically been represented as profiles of size fractionated scalar values. Grids used in numerical models often have a sigma-coordinate in the vertical direction. This is not a requirement for the algorithm, but since slicing is done along these vertical layers, the resulting visualization will appear more volumetric when the layers are close together.

The wave-current interaction bottom boundary layer model (BBLM) described by Keen and Glenn [31] is used to calculate suspended sediment profiles. This model is an extended version of the suspended-sediment-stratified BBLM of Glenn and Grant [14]. The model computes sediment concentrations for a number of size bins on a structured sigma-coordinate grid that has 30 levels and varies in time. A typical grid with the coordinate axes conventions used throughout the rest of this document is shown in Figure 3.1. The grid spacing is dependent on the height of the wave boundary layer and is variable in space and time. The resulting resolution near the ocean bed can be less than 0.001 *m*. For more information about coastal sediment transport and modeling see Nielson [49] and Fredsoe [9].

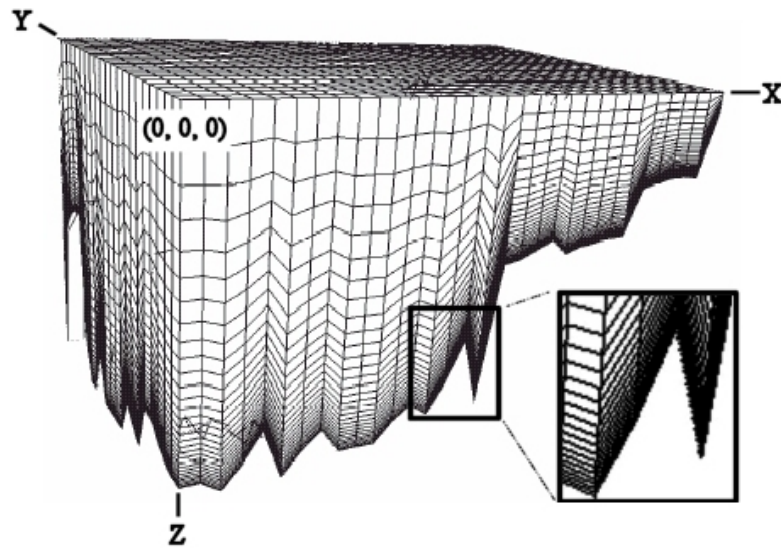


Figure 3.1 Plot of a Sigma-coordinate System at a Single Time Step.

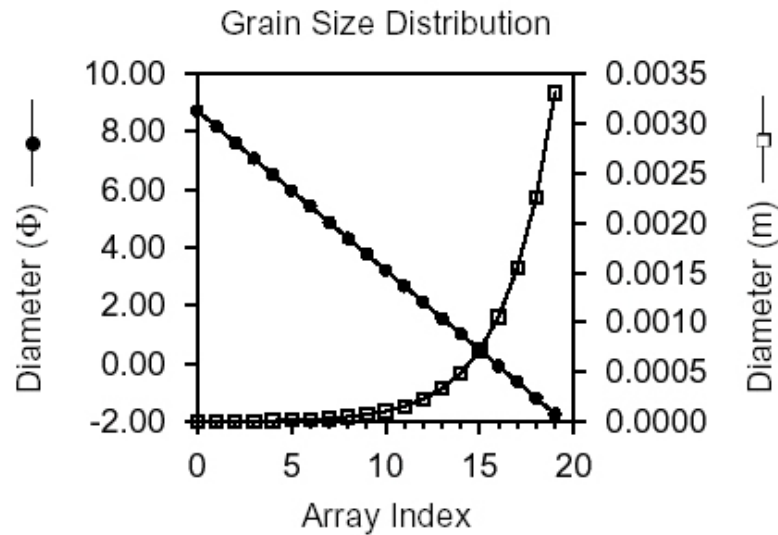


Figure 3.2 Typical Grain Size Distribution for Oceanside Dataset (in Units of  $\Phi$  and  $m$ ).

A typical sedimentation model contains up to 20 different size classes (bins) of sediment, ranging from  $9 \Phi$  ( $\sim 2 \times 10^{-6} m$ ), to  $-1.73 \Phi$  ( $\sim 3 \times 10^{-3} m$ ) in diameter [35], as shown in Figure 3.2. In this context,  $\Phi = -\log_2(d)$  where  $d$  is the diameter of a grain in  $mm$  ( $10^{-3} m$ ).  $\Phi$  is a commonly used binary logarithmic scale in sedimentation that converts the grain size distributions to a linear scale. This  $\Phi$  scale is used in the implementation of the SCT algorithm as described in Section 3.2. The 5D suspended sediment concentration (SSC) varies with longitude, latitude, depth, time, and grain size. In other words, at each grid point, there are values of SSC for up to 20 different sediment grain sizes, with relevant information densely packed near the boundary layer just above the sea floor.

Seven datasets were used in this research representing various geographic locations, weather conditions, dimensions, sediment sizes, and time increments as shown in Table 3.1. Maps illustrating the geographical locations for each dataset are available in Appendix A.

Table 3.1 Dataset Descriptions.

Name	Description	Dimensions			Sediment Classes	Time Steps	Time Range	Increment (hours)
		I	J	K				
andrew	LA Coast Hurricane Andrew	355	262	31	20	30	08/24/1992 12:00 08/27/1992 00:00	2
duck10	Duck, NC Northeaster	36	30	31	10	41	10/14/1997 12:00 10/24/1997 12:00	6
duck20	Duck, NC Northeaster	36	30	31	20	41	10/14/1997 12:00 10/24/1997 12:00	6
gbay	Great Bay, NJ Northeaster	177	198	31	20	29	07/27/2000 12:00 07/28/2000 16:00	1
msb	MS Sound Weak Cold Front	182	139	31	15	32	03/04/1997 03:00 03/08/1997 00:00	3
mssnd	MS Sound Hurricane Camille	111	51	31	10	3	08/18/1969 06:00 08/18/1969 08:00	1
oside	Oceanside, CA Normal	32	22	31	20	11	10/18/1995 00:28 10/27/1996 21:42	varies

### 3.2 SCT Algorithm Implementation

In this discussion, the term **cell** refers to a 3D volume immediately surrounding a grid location in the physical domain with dimensions  $\Delta x \Delta y \Delta z$ . A **slice** refers to the 2D texture-mapped primitive for a cell centered at the grid location as described by Vickery in [68] and shown in Figure 3.3. The 2D texture is generated from information about the physical scalar quantities within a 3D cell. The term **pixel** refers to the smallest unit of the 2D texture that has both color and opacity. Since the grid points are packed so densely in

the vertical direction close to the sea floor (the main area of interest), the physical scalar quantities for an entire 3D volume can be visualized as layers comprised of 2D slices. The term **glyph** will refer to the entity that represents the scalar values for a cell, whether it is a slice of the SCT algorithm, a Wedges glyph, or any similar construct. The term **particle primitive** will refer to the entity that represents a particle, whether it is a  $4 \times 4$  grouping of pixels in the texture, a color-mapped point primitive specified using the OpenGL® computer graphics language (an OpenGL point), or a color-mapped quadrilateral [78]. The term **slice resolution** is the program selectable option that sets the maximum number of particle primitives per grid location. This is computed as  $R_{slice}$  in Section 3.2.2, and can be adjusted based on hardware capability.

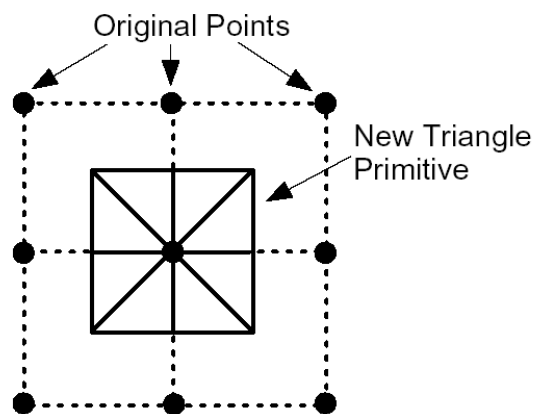


Figure 3.3 New Grid Slice With Eight Triangles Superimposed on the Original Grid.

The basis of the SCT method is a 2D texturing algorithm rendered in the CAVE-like VE. When data values are located at the grid points, choices must be made as to how

coloring or texture mapping is done for the areas between the grid points. In the simplest case, this can be considered in terms of color mapping, where the color represents the value of the data. If the data values between grid points vary by some linear or other relationship, then the color also varies and is blended as shown in the upper left corner of Figure 3.4. In this 2D example, the colored circles represent the current data value at the grid points. For the four points in the upper left of the figure, the data varies between the grid points, and so the color is blended between the two colors red and green. The problem with this approach is that the color value for a particular grid point might be difficult to see, especially if all the surrounding points are different colors. Since the scientists generally like to see the actual data values from the model output, and not approximated values between grid points, a constant value approach can be applied. In Figure 3.4, the colored circles in the lower right section illustrate this concept. In this case the value at the point is constant throughout the quadrilateral surrounding it, making it the same color as the point. The scientist knows that the color value shown is from the model output data, and not some interpolated value. The boundaries of the region surrounding the grid point are midway between the grid points. Extending this concept to 3D means that the surrounding volume of the grid point contains the same color.

For the SCT method, instead of color mapping the area around the grid point, a texture map is applied that contains a representation of the data value. In this case, it is the profile of scalar values for each grain size of SSC represented as particle primitives within the texture slice. Additionally, since the layers in the vertical  $z$  direction are so closely packed

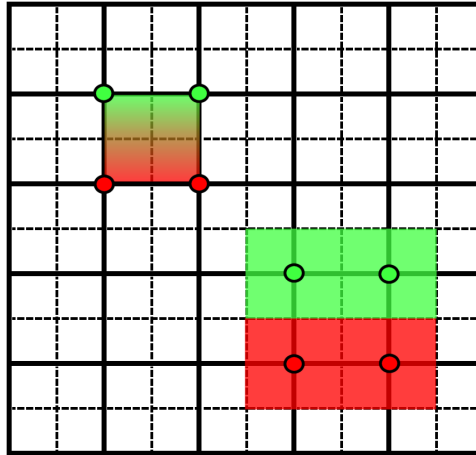


Figure 3.4 Example Showing Difference Between Blended and Constant Value Coloring.

at the ocean bottom, the information for that 3D volume surrounding the grid point is represented in the 2D slice primitive as shown in Figure 3.3. The grid is regular in  $x$  and  $y$ , and interpolating values in these directions is trivial, but care must be taken to correctly interpolate  $z$ , since not all points in the original quadrilateral cell are coplanar. Whereas the OpenGL rendering pipeline breaks down the original quadrilateral into two triangles, the new slice primitive consists of eight triangles arranged as an OpenGL triangle-fan. This primitive accommodates all of the irregularities in the  $z$  direction within a cell.

Several horizontal texture mapped layers can be viewed together and represent the information for the volume containing the grid points. Because the horizontal layers are used directly, no hardware interpolation is required to represent values between grid points. Therefore there are no extra calculations (such as a Jacobian transformation) required to transform data from the structured sigma-coordinate grid to a regular grid, as is often done in volume visualization [24, 46]. The data are represented directly, and colors are



not "smoothed" or blended within a texture slice, other than what is desired to represent opacity.

### **3.2.1 System Design**

This section describes the overall design of the immersive visualization system, and the choices made in the integration of existing software with custom routines to implement the SCT algorithm.

One of the main goals of the application design was to allow the development of new algorithms without spending large amounts of time reimplementing common visualization techniques. One way to do this is to use the popular Visualization Toolkit (VTK), which is an object-oriented C++ graphics library commonly used for desktop applications [57]. In order to visualize the 5D SSC data, the convenience and flexibility offered by VTK had to be balanced against the efficiency needed to obtain interactive frame rates in the four wall VE [4]. This was accomplished by using the OpenGL Performer™ application programming interface (API) developed by Silicon Graphics, Incorporated (SGI). [6, 56]. The Performer API enables developers to optimize their applications for SGI® computer systems without requiring extensive knowledge of the internals for specific machines. In this case the computer hardware that drives the CAVE-like VE has an Infinite Reality 2 graphics system specifically designed to deliver high-quality rendering of complex scenes at consistent frame rates [48]. Effective use of the Performer API in conjunction with the normal CAVE libraries [4] allows an application to take advantage of the specialized

hardware functionality in the Infinite Reality 2 engine to increase performance. Since Performer lacks the common visualization algorithms, an additional VTK class called `vtkActorToPF` developed by Paul Rajlich provided the means to integrate VTK with the Performer API [52]. This class allows normal VTK pipelines to generate graphics primitives (polydata), which are then translated into Performer scene graph nodes (geodes) for rendering in the VE.

The integrated system design is shown in Figure 3.5. One advantage of using this combination of libraries is that a desktop display can be used at several stages of development to verify results and isolate problems. For instance, desktop interfaces using either scripting languages or C++ can be developed to test new VTK classes before integration with the Performer API. Likewise, visualization can be done from the combined VTK and Performer application before integration with the CAVE libraries.

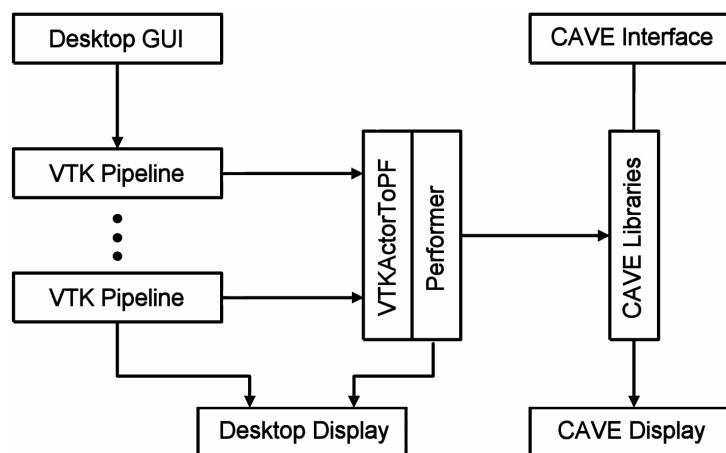


Figure 3.5 System Design.

### 3.2.2 Texture Calculations

The equations described in this section determine how the texture map is generated for the grid points of interest, and the details about the number of pixels calculated for each color (representing different grain sizes) to include in the texture map portion for each cell.

The sediment concentration values are in units of  $kg/m^3$ , and are calculated based on spherical sand grains with a density  $\rho$  of  $2650 kg/m^3$  (quartz). Therefore the equation for SSC for a specific grain size (or diameter)  $d$  is

$$S = P V \rho, \quad (3.1)$$

where

$S$  represents the SSC for individual grain size  $d$  within a cell ( $kg/m^3$ ),

$P$  is the number of particles per cubic meter for grain size  $d$ ,

$V$  is the volume of a spherical particle of grain size  $d$  given by  $\frac{\pi d^3}{6}$ , and

$\rho$  is the density of the particle in  $kg/m^3$ .

Substituting for  $V$ , Equation (3.1) can be rewritten to give the number of particles per cubic meter as

$$P \approx \frac{S}{1387.5 d^3}. \quad (3.2)$$

The fractional contribution of particles for each grain size is given by

$$F = \frac{P}{\sum_{i=1}^n P_i}, \quad (3.3)$$

where

$n$  is the number of grain sizes or bins,

$F$  is the fractional particle contribution for grain size  $d$ , and

$\sum_{i=1}^n P_i$  represents the total number of particles within a cell.

Substituting Equation (3.2) into (3.3) and reducing yields

$$F = \frac{\frac{S}{d^3}}{\sum_{i=1}^n \frac{S_i}{d_i^3}} = \frac{C}{\sum_{i=1}^n C_i} = \frac{C}{C_{cell}}, \quad (3.4)$$

where

$C$  is the individual grain size particle contribution given by  $\frac{S}{d^3}$ , and

$C_{cell}$  is the total particle contribution for the cell

(or the cell particle contribution).

Equation (3.4) can be used to compute the number of pixels in a texture that should have the color representing  $d$ . However, we want each 2D texture slice to represent one cell of a volume of particles. We also want the visualization to show the differences between higher particle concentrations near the ocean bottom, and lower concentrations at the surface, as well as differences in concentrations at the same grid location at different times. This means that the cell with the highest concentration of particles (referred to as

the maximum cell particle contribution described in Equation 3.5 below) should have all pixels in the associated texture colored, and all other cells will have some lesser amount of pixels colored. This is called the *limiting resolution* of the texture<sup>1</sup>. In the same way that the maximum value of a scalar quantity is used to scale the other values so that a color mapping can be applied, the limiting resolution sets the maximum cell particle contribution to be represented by the texture.

The end result is that for each cell in the volume of interest, there will be some number of pixels colored out of a 2D texture slice that represents that cell's particle contribution relative to the maximum cell particle contribution. This relationship can be written as

$$\frac{N_{slice}}{R_{slice}} = \frac{C_{cell}}{(C_{cell})_{max}}, \quad (3.5)$$

where

$N_{slice}$  is the number of colorable pixels in a texture slice (representing one cell),

$R_{slice}$  is the 2D texture slice resolution

$(C_{cell})_{max}$  is the maximum cell particle contribution throughout the volume over all time steps (the limiting resolution).

Equation (3.5) can be rewritten to find the number of colorable pixels for a specific cell

$$N_{slice} = R_{slice} \frac{C_{cell}}{(C_{cell})_{max}}. \quad (3.6)$$

---

<sup>1</sup>The huge numbers of particles represented here means that each pixel of the 2D texture slice represents many particles, and comparisons of quantities in the visualization are relative, not absolute.

Note that  $(C_{cell})_{max}$  is calculated over all time steps, but all other quantities are calculated at a specific time step. Using Equation (3.4), the number of pixels to include for each grain size color for a specific cell then becomes

$$N = F N_{slice} = \frac{C}{C_{cell}} N_{slice} . \quad (3.7)$$

where

$N$  is the number of pixels to color for grain size  $d$ .

### 3.2.3 SCT Implementation Details

The first version of the SCT algorithm converted the twenty scalar values at each grid point represented in units of  $kg/m^3$  to numbers of particles of each bin<sup>2</sup> [68]. A 2D texture mapping scheme was employed to display the particles where a texture for each cell layer was synthesized to show the relative numbers of particles as *same size pixels* using a different color for each bin (twenty colors in all). This approach suffered from two major shortcomings: particles of vastly different sizes were displayed as the same size, and there were too many colors to distinguish between particle bins. From a perceptual viewpoint, this experience indicated that particle primitives representing different grain sizes needed to also vary in size so that the visual representation of mass rendered as particles reflected the same relative mass differences within the data (see Figure 1.5). Perceptual

---

<sup>2</sup>In the sedimentation data, each bin represents values of a particular grain size (diameter) of sediment.

guidelines also indicated that the number of hues used in a visualization should be limited to a maximum of seven [19].

The algorithm was enhanced to allow a custom bin consolidation scheme to be applied to reduce the number of bins to sixteen (or less), such that a particle primitive with a  $4 \times 4$  footprint could be used to show grain size differences<sup>3</sup> [50, 70]. Bins may also be grouped into more general categories to reduce the number of colors that must be represented, or an automatic color assignment algorithm can be used. Four colors were chosen to represent the sediment types: clay, silt, sand, and gravel [70]. The twenty bins were consolidated by taking advantage of the  $\Phi$  scale shown in Figure 3.2. For example, the Oceanside dataset grain size distribution is shown in Table 3.2 with the category and subcategory descriptions. After consolidation, the bins with redundant subcategories were combined into one bin subcategory where each integer value of  $\Phi$  is represented, as shown in Table 3.3. To more clearly see how this is accomplished, refer to Table 3.4, which shows the calculations for a volume of 396 grid point locations for a resolution of  $64 \times 64$  (4,096) particle primitives per grid slice. The maximum number of particle primitives for the volume is 1,622,016 ( $396 \cdot 4,096$ ), but only 678,951 are available, since the number used is scaled against the maximum concentration value. The number of particles per particle primitive is the total number of particles divided by the available primitives or 384,867,000. The percentage used is the number of available primitives divided by the maximum for the volume or 41%. The number of particles and particle primitives does not change as a result of

---

<sup>3</sup>For the sedimentation data, this is the USDA soil texture classification that reduced the bins to fourteen, although a generic bin grouping or reduction algorithm could also be used.

consolidation, but the number of different sizes of particle primitives is reduced to sixteen so that the  $4 \times 4$  footprint can be used. This restriction can be lifted with the implementation of a variable size footprint, as described in Section 6.1. Note that some bin values are zero where there are no particles of that particular grain size present in the volume of interest. In some datasets, the extreme differences in the numbers of particles in some bins required that a  $\log_{10}$  scale option be available so that these magnitude differences could be represented.

Table 3.2 Oceanside Dataset Grain Size Distribution.

Grain Size (mm)	$\Phi$	Category
0.002363	8.725165	clay - mix w a little silt
0.003460	8.175012	clay - mix w a little silt
0.005066	7.624937	silt - very fine
0.007417	7.074949	silt - very fine
0.01086	6.524832	silt - fine
0.01590	5.974829	silt - medium
0.02328	5.424765	silt - medium
0.03408	4.874931	silt - coarse
0.04989	4.325105	silt - coarse
0.07305	3.774972	sand - very fine
0.1069	3.225666	sand - very fine
0.1566	2.674844	sand - fine
0.2293	2.124692	sand - fine
0.3356	1.575185	sand - medium
0.4914	1.025030	sand - medium
0.7195	0.4749334	sand - coarse
1.053	-0.07450542	sand - very coarse
1.542	-0.6248027	sand - very coarse
2.258	-1.175045	gravel - granule
3.306	-1.725087	gravel - granule



Table 3.3 USDA Consolidated Grain Size Classification.

Grain Size (mm)	$\Phi$	Category
$< 0.0039 \left(\frac{1}{256}\right)$	$> 8$	clay - mix w a little silt
$0.0078 \left(\frac{1}{128}\right)$	7	silt - very fine
$0.0156 \left(\frac{1}{64}\right)$	6	silt - fine
$0.031 \left(\frac{1}{32}\right)$	5	silt - medium
$0.0625 \left(\frac{1}{16}\right)$	4	silt - coarse
$0.125 \left(\frac{1}{8}\right)$	3	sand - very fine
$0.25 \left(\frac{1}{4}\right)$	2	sand - fine
$0.5 \left(\frac{1}{2}\right)$	1	sand - medium
1	0	sand - coarse
2	-1	sand - very coarse
4	-2	gravel - granule
32	-5	gravel - pebble
256	-8	gravel - cobble
$> 256$	$< -8$	gravel - boulder

The number of pixels in the  $4 \times 4$  particle primitive are colored to show the relative sizing of particles. The smallest grain size is represented by one pixel in the particle primitive, and one pixel more is added for each larger grain size bin. For the case of the USDA consolidated bin breakdown for the Oceanside dataset, Table 3.5 indicates the range in number of pixels used in the particle primitive to represent each bin and sedimentation category. Figure 3.6 illustrates the sequence of pixels colored in the particle primitive and how it appears for the maximum pixels colored in each category. For the sedimentation application where the  $\Phi$  scale is based on  $\log_2$ , each pixel increase in particle primitive size corresponds to roughly a grain size that is two times larger than the previous bin.

Several different parameters were assigned to the pixel opacity ( $\alpha$ ), including SSC concentration, but an effective scalar turned out to be grain size. Larger grain sizes were

Table 3.4 Oceanside Dataset Example Calculations.

Bin	Actual Particles	Actual Primitives	Consolidated Particles	Consolidated Primitives
0	0	0	$7.57721 \times 10^{13}$	196,885
1	$7.57721 \times 10^{13}$	196,885	$1.11551 \times 10^{14}$	289,876
2	$6.39223 \times 10^{13}$	166,108	$3.13282 \times 10^{13}$	81,392
3	$4.76288 \times 10^{13}$	123,768	$2.89912 \times 10^{13}$	75,332
4	$3.13282 \times 10^{13}$	81,392	$1.00614 \times 10^{13}$	26,171
5	$1.85719 \times 10^{13}$	48,257	$3.37459 \times 10^{12}$	8,771
6	$1.04192 \times 10^{13}$	27,075	$2.24318 \times 10^{11}$	524
7	$6.07447 \times 10^{12}$	15,791	$2.78858 \times 10^9$	0
8	$3.98691 \times 10^{12}$	10,380	$2.52616 \times 10^7$	0
9	$2.27527 \times 10^{12}$	5,905	0	0
10	$1.09932 \times 10^{12}$	2,866	0	0
11	$2.04652 \times 10^{11}$	524	0	0
12	$1.96661 \times 10^{10}$	0	0	0
13	$2.49810 \times 10^9$	0	0	0
14	$2.90478 \times 10^8$	0		
15	$2.52616 \times 10^7$	0		
16	0	0		
17	0	0		
18	0	0		
19	0	0		
Totals	$2.61306 \times 10^{14}$	678,951	$2.61306 \times 10^{14}$	678,951
Particles Per Particle Primitive in Volume: 384,867,000				
Total Available Particle Primitives in Volume: 678,951				
Percent Used of 1,622,020 Maximum Particle Primitives: 41.9%				

Table 3.5 Bin Categories With USDA Pixel and Color Assignments.

Bins / Num Pixels	Soil Type	Color
1	Clay	Green
2-5	Silt	Red
6-10	Sand	Cyan
11-14	Gravel	Magenta

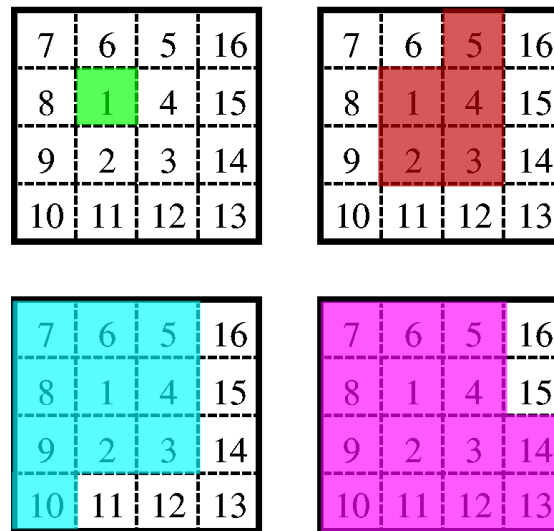


Figure 3.6 Particle Primitive for Each USDA Sedimentation Category.

indicated by higher opacity values within a set range between 0.3 and 1.0 (although this range was changeable)<sup>4</sup>. Using this criteria tended to emphasize the fewer larger diameter particle primitives among many smaller ones.

Figure 3.7 shows the results of these enhancements for a single texture slice with a slice resolution of  $32 \times 32$  for a cell at the hill location of the Oceanside dataset. Here bin differences are indicated by particle size and color. Large numbers of clay particles are shown by one pixel green particle primitives, as well as several sizes of silt particles (red), and very few larger sand particles (cyan). The twelve layer volume visualization described in Section 1.1, and shown in Figure 1.5, shows the benefits of the SCT algorithm in the CAVE-like VE. Consider the point detail profile of the hill location from Figure 1.3

<sup>4</sup> $\alpha$  is typically represented in floating point as a value between 0 and 1, where 0 is totally transparent and 1 is totally opaque

where the leftmost column depicting the clay bin category shows a very low value of dark blue on the  $\log_{10}$  scale. This hardly seems like a significant sediment concentration amount, but in terms of suspended particles, Figure 1.5 clearly shows numerous green clay particles in the hill region. This is an example where the SCT method quickly shows the difference between a grid location where many smaller particles result in very low sediment concentration (hill), and one where fewer larger particles make up a much larger sediment concentration (hole). This is contrary to what might be interpreted from the detail profiles (see Figure 1.3). This is due to the differences in the grain sizes (diameters of an assumed spherical particle) between bins, and the part it plays in the mass per volume computation for sediment concentration ( $kg/m^3$ ) [68, 70].

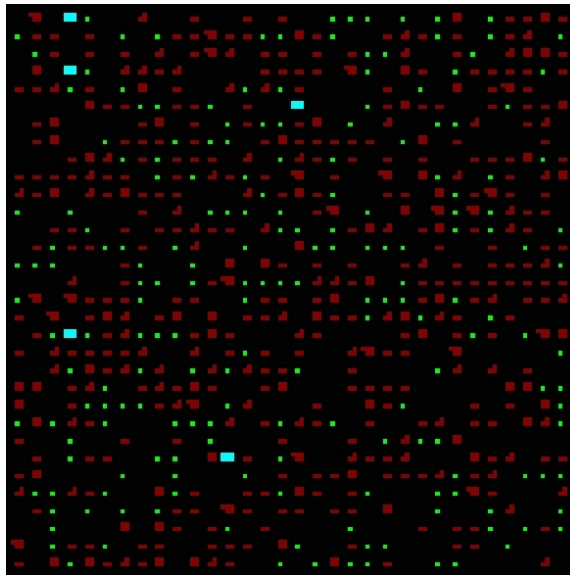


Figure 3.7 Single Cell Texture Generated by the SCT Algorithm.

## CHAPTER IV

### USER STUDY

The main purpose behind this study has been to quantitatively measure the effectiveness of the SCT technique as a browsing method. A good browsing method will allow the viewer to get an amount of basic information in a short time (“at a glance” type information). Using perceptual concepts from Healey [20, 22] and Ware [71], a visual browsing technique can be developed that enables the user to perform:

1. *Feature Detection*: whether information is present, and
2. *Feature Identification*: whether some feature stands out that should be investigated.

The user study experiment described in this chapter tests both criteria. Section 4.1 on methodology describes all aspects involved with designing and setting up the experiment. Section 4.2 describes the statistical results and analysis.

#### 4.1 Methodology

This section describes how the user study was designed, the data acquisition process, the physical aspects of the test environment, and the statistical methods used.

### 4.1.1 Design

The user study was conceived around several goals. It needed to be general enough to provide some external validity that the SCT algorithm could be applied as a browsing method. It also needed to be constrained enough such that a subject could complete the experiment in under an hour. In order to have enough subjects participate and guarantee unbiased results, the study did not include sedimentation experts or require visualization experts. To assess the effectiveness of the SCT method, it was compared with a state-of-the-art method with similar characteristics. This was accomplished by conducting pilot studies to determine the best comparative technique for the CAVE-like VE. Since the SCT method does not use color to show magnitude, but only to show categories, the comparative method was implemented using color the same way. The comparative method was required to be 2D within a layer, such that multiple layers could potentially be rendered to represent a volume.

Concepts from Taylor [60] on the characteristics of state-of-the-art information visualization techniques were used as a starting point for the comparative method implementation. The data acquisition process and physical conditions of the experiment were derived from a study on reaction times to name common objects by Watson [74], and a recent VE user study design outlined in Ziegeler [80]. From the pilot study, five parameters were determined to greatly affect how both techniques were perceived in the VE. These parameters were:

- Field-of-view,

- Vertical distance above surface,
- $XY$  area,
- Number of layers, and
- $Z$  scale.

The initial comparative method was heavily influenced by the “Oriented Sliver Textures” technique presented in Weigle [76], and possessing the advanced perceptual characteristics discussed in Taylor [60]. Weigle’s 2D method uses orientation of sparse fields of thin lines to differentiate between scalar fields and luminance intensity to show magnitude. According to Weigle, up to 15 separate orientations can be perceived, leading one to believe that perhaps 15 scalar fields can be visualized at once. In practice Weigle’s method was not effective in the VE, even with the incorporation of numerous options to randomize how the orientations and placements occurred. Adding hue to help differentiate the scalar fields created more difficulties due to differences in perceived intensity of hues [72, 79] (see Figure 4.1). The thinness of the slivers also made 3D interpretation difficult in the lower luminance VE environment and did not convey the size characteristic of the scalar fields well.

From these results, an ordered wedge glyph was implemented where the area of each wedge shape was related to the grain size characteristic of the scalar field, as shown in Figure 2.1. The ordering of the wedges improved interpretation of the information and grayscale intensity could then be used to convey scalar field magnitude. Colored bands were placed around the outside of the glyph to provide the same general sediment category

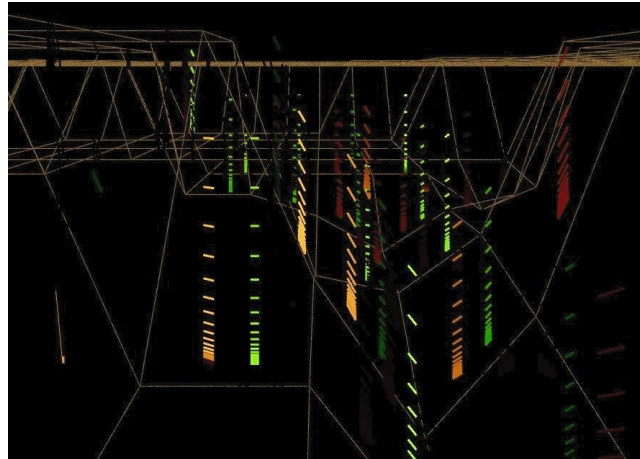


Figure 4.1 Oriented Sliver Textures in the VE.

information as the SCT method. The wedges and bands were separated by thin black areas to reduce proximity contrast effects [71]. Local visualization experts viewed the final glyph shape in the VE and considered it a viable state-of-the-art method incorporating perceptual characteristics as outlined in the research. The overall technique was aptly named *Wedges*, and an example of the implemented method is shown in Figure 4.2. The results of the SCT algorithm for the same scene are shown in Figure 4.3. A comparison of how the SCT and *Wedges* methods convey the sediment concentration information is summarized in Table 4.1.

Other problems were uncovered during consultations with local visualization experts while viewing various configurations in the VE. The *Wedges* method was not effective when multiple layers were rendered to show volumes, even with transparency applied (see Figure 4.4). Additionally, scenes with changing field-of-view, vertical distance, number of



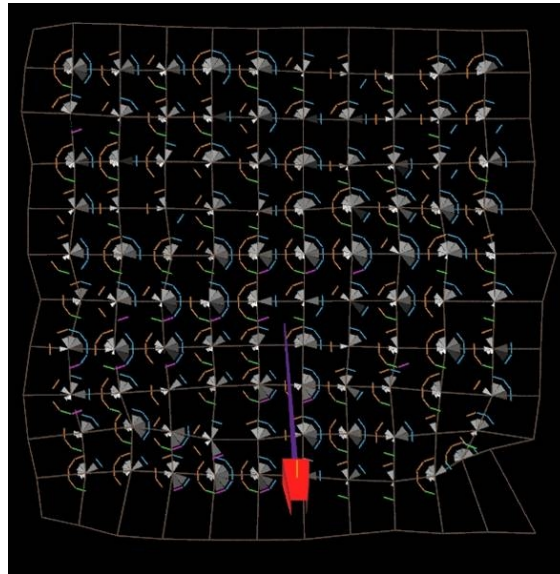


Figure 4.2 Top-down View of Typical Wedges Scene in Practice.

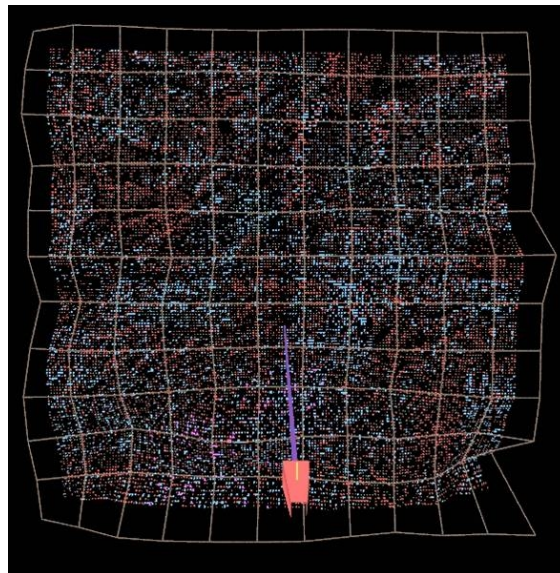


Figure 4.3 Top-down View of Typical SCT Scene in Practice.

Table 4.1 Method Characteristics Comparison.

Per Grid Location	SCT	Wedges
Glyph for Each Bin	Multiple PPs*	Individual Wedge
Relative Grain size of Each Bin	Number of Pixels in PP	Area Size of Wedge
Magnitude of Each Bin	Number of PPs	Grayscale Intensity of Wedge
Category of Sediment	Color of PPs	Color of Outer Bands

\*Particle Primitive

layers, and  $z$  scale were considered too difficult for novices to properly evaluate, so these parameters were held constant for the final experiment.

#### 4.1.2 Hypotheses

The general research question is to see if the SCT method has certain characteristics that could make it a useful browsing technique. A good browsing method will allow the viewer to get an amount of basic information in a short time while doing feature detection and feature identification. This is tested by comparing the SCT method against the Wedges method over increasing size  $xy$  areas (regions) of datasets. The amount of time it takes for a person to complete tasks to accomplish these goals can be measured and compared for the two methods.

This is expressed in the form of two formal (paired) hypotheses:

$HT_0$ : There is no significant difference in the amount of time it takes to complete a browsing task between the two methods over different size areas.

$HT_A$ : It takes significantly less time to complete a browsing task using the SCT method vs. using the Wedges method over different size areas.

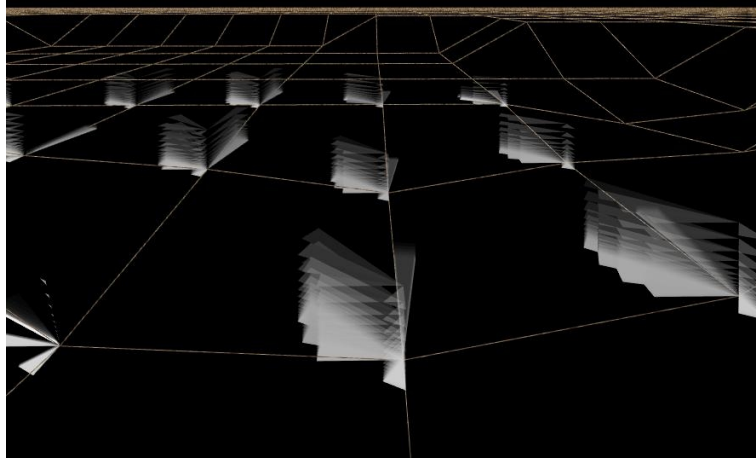


Figure 4.4 Early Wedges Showing Ineffective Use of Transparency.

$HC_0$ : There is no significant difference in the correctness of the result during the completion of a browsing task between the two methods over different size areas.

$HC_A$ : There is a significant difference in the correctness of the result during the completion of a browsing task between the two methods over different size areas.

These hypotheses can be written algebraically as:

$$HT_0 : T_s = T_w, \quad (4.1)$$

$$HT_A : T_s < T_w, \quad (4.2)$$

and

$$HC_0 : C_s = C_w, \quad (4.3)$$

$$HC_A : C_s \neq C_w, \quad (4.4)$$

where  $T_s$  and  $T_w$  represent the times using SCT and Wedges, respectively, and  $C_s$  and  $C_w$  represent the correctness.

The hypotheses were tested using a powerful statistical package from SPSS, Inc., called SPSS<sup>1</sup>. In the SPSS Analysis of Variance (ANOVA) procedure, the F-test is used to test for differences between groups, and then comparison T-type tests verify in which direction the differences exist and at which levels. Since there are three factors in this experiment, ANOVA performs the F-test for differences between each of the factors, and their combinations. For this analysis, the tests were run for *Method*, *Area*, and *Color*, as well as the interactions of *Method \* Area*, *Method \* Color*, *Area \* Color*, and *Method \* Area \* Color*. When there are multiple dependent variables involved (as in this case with *Time* and *Correct*), then a multivariate version of ANOVA, called MANOVA, is used. The advantage of using MANOVA is that the procedure tests for every condition at once, so that combination effects are more completely evaluated and the combined error is reduced.

#### 4.1.3 Operationalization of Variables

The test cases were developed for levels of the four independent variables:

- *Method*: SCT, Wedges.
- *Area*: Small, Medium, and Large.
- *Color* (Task1 Only): Red, Green, Blue.

---

<sup>1</sup>Historically the product was known as the “Statistical Package for the Social Sciences,” but is now simply referred to as SPSS.

- *Pattern* (Task 2 Only): Pattern, No Pattern.

For each combination of independent variables, the dependent variables of *Time* and *Correct* were recorded. There were 18 Task 1 cases as shown in Table 4.2, and 12 Task 2 cases (see Table 4.3). Details about the specific datasets and grid locations are contained in Appendix A.

#### **4.1.4 Final User Study Experimental Configuration**

The formal user study design was a  $2 \times 3 \times 3$  experiment with two methods, three levels of  $xy$  area, and three colors, as described in Section 4.1.3. A thorough design must often test at least three levels of each factor to avoid missing important results at values other than the extremes [7]. The other variables of field-of-view, vertical distance, number of layers, and  $z$  scale were held constant. This was accomplished by rotating scenes that would normally show up in a top-down view of the floor, up on the front wall such that each scene would take up the same amount of area on the screen. Only one layer was rendered at a flat  $z$  scale for each scene. The design was considered to be a repeated measure within-subject, completely randomized design. This means that all subjects did all parts of the experiment (so there were repeated measurements of the same subject), and the ordering of which method, task, and scene was randomly set at the start of the experiment. There were 50 subjects total and two tasks selected:

- *Task 1*: Find the single color cell.
- *Task 2*: Determine whether a checkerboard pattern exists.

Table 4.2 Task 1 Cases.

Case		Method	Area	Color
Number	Sequence			
0	000	SCT	Small	Red
1	001	SCT	Small	Green
2	002	SCT	Small	Blue
3	010	SCT	Medium	Red
4	011	SCT	Medium	Green
5	012	SCT	Medium	Blue
6	020	SCT	Large	Red
7	021	SCT	Large	Green
8	022	SCT	Large	Blue
9	100	Wedges	Small	Red
10	101	Wedges	Small	Green
11	102	Wedges	Small	Blue
12	110	Wedges	Medium	Red
13	111	Wedges	Medium	Green
14	112	Wedges	Medium	Blue
15	120	Wedges	Large	Red
16	121	Wedges	Large	Green
17	122	Wedges	Large	Blue

Table 4.3 Task 2 Cases.

Case		Method	Pattern	Area
Number	Sequence			
0	000	SCT	False	Small
1	001	SCT	False	Medium
2	002	SCT	False	Large
3	010	SCT	True	Small
4	011	SCT	True	Medium
5	012	SCT	True	Large
6	100	Wedges	False	Small
7	101	Wedges	False	Medium
8	102	Wedges	False	Large
9	110	Wedges	True	Small
10	111	Wedges	True	Medium
11	112	Wedges	True	Large

Each scene viewed in the VE represents one combination of the independent variables and is termed a *treatment* or *condition* of the experiment.

Once the tasks and parameters were chosen, time steps from the available datasets were viewed for scenes fitting the constraints. Although the scenes could have been artificially generated, the results from a study using scenes from sedimentation datasets better supports the external validity required to apply conclusions to real world usage. Scenes were taken from the seven datasets described in Section 3.1 and Appendix A.

The time steps were preprocessed to find minimums and maximums in the multiple scalar fields representing sediment concentration, then those time steps were viewed using both the SCT and Wedges methods. For Task 1, small to large  $xy$  areas were chosen where only one cell contained the desired color. The location of the cell within the scene was also varied such that subjects searched all four quadrants of the front wall display. For Task 2, small to large  $xy$  areas were chosen such that either a significant portion of the scene contained the checkerboard pattern or no pattern was discernable. The pattern was only present in datasets containing mostly silt and sand, so the colors were limited to red and blue. Since the subject would see the same scene rendered by both the SCT and Wedges methods, only regions with no recognizable geographical features were used with data represented at all grid points. Examples demonstrating the effect of changing  $xy$  area for the Wedges method and Task 1 are shown in Figure 4.5. A similar effect for the SCT method and Task 2 is shown in Figure 4.6. An example of a no pattern effect for both the SCT and Wedges methods is shown in Figure 4.7.



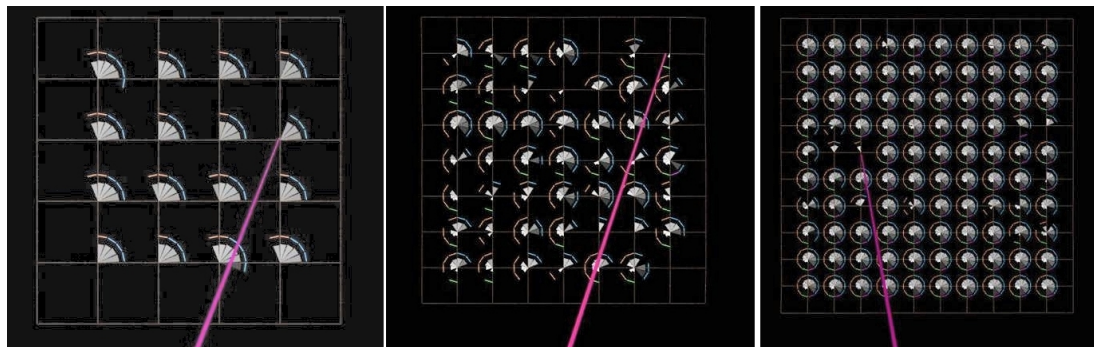


Figure 4.5 Wedges Task 1 Effect of Changing  $XY$  Area.

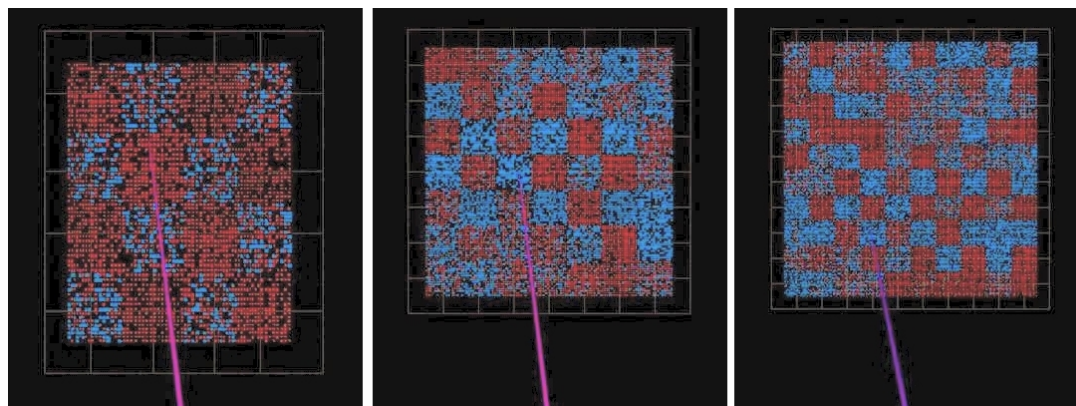


Figure 4.6 SCT Task 2 Effect of Changing  $XY$  Area.

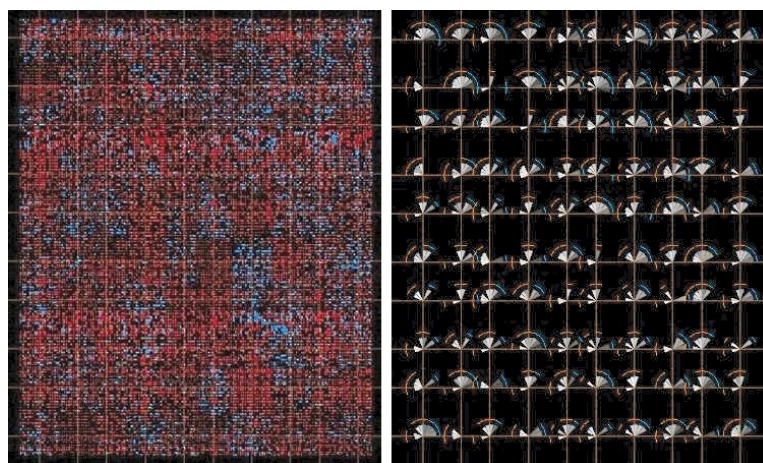


Figure 4.7 Task 2 No Pattern Example for Both Methods.



A person participating in the user study would spend a total of 40 to 60 minutes following a structured series of steps that would provide breaks to minimize fatigue, ask questions, and keep attention focused. These segments included:

1. Detailed background information about the visualizations they would be viewing,
2. Introductory training on the features of the VE,
3. Examples of each task with practice,
4. Training for each task,
5. The actual experiment for each task.

All subjects performed the first 3 segments in the same sequence. Segments 4 and 5 were randomized by method and task, and then randomized by scene such that each subject received a different ordering of treatments. The subject sat in a comfortable chair in the middle of the VE, and used the wand to indicate responses by pointing and clicking. The response time taken to select with the wand was recorded. The location and orientation of the wand was also recorded to determine the correctness of the response. Additionally, video and audio of each subject was digitally recorded, in case there was any ambiguity in the computer logs. This user study conformed to the Mississippi State University Institutional Review Board (IRB) guidelines for the protection of human subjects as documented in IRB docket number 02-308 [66].

#### **4.1.5 Statistical Methods**

For a randomized within-subjects experimental design, several observations (called repeated measures) are taken from the same subject. Parametric statistical methods such as

ANOVA for a single dependent variable can be employed under the following assumptions [8, 41]:

1. *Interval Data*: The dependent variable is measured on an equal interval scale.
2. *Independence*: The groups of measurements taken for each treatment are independent.
3. *Normally Distributed Data*: The measurements are sampled from a source population with a reasonably normal distribution.
4. *Homogeneity of Variance*: The groups of measurements have reasonably equal variances.

The *Independence* assumption is met since the major dependent variable measured is *Time*, which is on an equal interval (linear) scale. As an example, Subject A performs a task in 10 seconds, and Subject B performs the same task in 5 seconds. Subject A takes twice as long as Subject B, and so the scale for measuring time is linear. Since the same subject is measured for each treatment, the *Independence* assumption is satisfied by randomizing the presentation of each treatment. Additionally, the measurements between different participants are also independent. As long as the number of measurements in each treatment are the same, then ANOVA is quite robust with respect to assumptions 3 and 4. In this study each treatment group contains the response to one question by all subjects, making the size of each group constant. There are specific tests in SPSS to test for both *Homogeneity of Variance* and *Normally Distributed Data*. The results of testing these assumptions and the implications for the analysis are described in Section 4.2.

The accuracy of the subject's response was also recorded and analyzed as the second dependent variable. This was initially recorded as the  $x$  and  $y$  coordinates of the wand

intersection with the front wall. These values were compared with recorded correct responses and a value of 0 for an incorrect answer or 1 for a correct answer was assigned for the analysis. The resulting dichotomous *Correct* variable was analyzed together with the *Time* variable using an extension to ANOVA called Multiple Analysis of Variance, or MANOVA. MANOVA contains all of the same tests as ANOVA where each dependent variable is analyzed separately, in addition to statistics for testing combined effects.

The analysis for each task of the user study was performed in two stages. During the first stage the “Explore” group of statistics in SPSS was used to get basic information about the independent and dependent variables and test the *Normally Distributed Data* assumption. Repeated measures ANOVA was then applied to test the matrix of hypotheses.

## 4.2 Results

Prior to analysis, the variables *Time* and *Correct* were examined through SPSS exploratory programs for accuracy of data recorded and fit between the distributions for the 18 test cases against the assumptions of multivariate analysis. Although no values were missing, there were a few cases where multiple *Time* values were recorded. In almost all cases, the first value was used since supporting log file comments indicated that the selection button on the wand was held down just long enough to be recorded twice. *Correct* is a dichotomous variable with a poor split (roughly 90% *True* to 10% *False*), so analysis including correlations with other variables was limited. Variables of this type are often still

used in the analysis [8, 59], so *Correct* was retained. In order to meet the requirement for normal distributions, the following actions were taken [59]:

- The *Time* variable was logarithmically transformed.
- One subject with extremely long times was deleted in order to reduce its effect on all of the distributions, leaving 49 subjects for analysis.
- Long *Time* outliers were adjusted to maximum values based on Tukey's Hinges [59, 65], which effectively sets a time limit for each test case.
- For a few remaining cases, there were still too many time values at maximum times for the distributions to be classified as normal. For these cases, extremes were set to the original distribution average value. For Task 1: three extremes were set for Case 13. For Task 2: two extremes were set for Case 1, and seven for Case 5.

These actions resulted in treatments with equal numbers of responses and *Time* data distributions that met the *Normally Distributed Data* assumption.

For repeated measures designs, the *Homogeneity of Variance* assumption is often violated whenever *Time* is a within-subjects variable [59]. This was also the case for this study, but the SPSS significance tests produce output that is adjusted for violations of the *Homogeneity of Variance* assumption. Additionally, a conservative adjustment for univariate pairwise comparisons was made to control the Type I pooled error rate<sup>2</sup>, thereby reducing the probability of falsely rejecting the null hypothesis  $HT_0$ . Interpretation of the SPSS output was done using conservative significance test results. Although this approach tends to reduce the statistical power, which increases the probability of a Type II error<sup>3</sup>,

---

<sup>2</sup>A Type I error means falsely rejecting the null hypothesis, or finding a difference that does not exist. At a 0.05 level of significance, the probability of a Type I error is 5%. The pooled error rate is the combined error from all of the tests.

<sup>3</sup>A Type II error means rejecting an effect that actually exists, or finding no difference when one exists. Statistical power measures the probability of a Type II error.

the observed power for these results was the same as for less conservative tests, except as specifically noted in the analyses described in Sections 4.2.1 and 4.2.2.

The significance level used to construct confidence intervals and compute observed power can be changed in the SPSS Repeated Measures Option dialog. Separate analyses were run for values at both 0.01 and 0.05 levels of significance. The effects resulting from the pairwise mean difference comparisons were all significant at the 0.01 level. Except where noted in the detailed analysis for each task, the observed statistical power for all significant effects was still above 0.9. Values of power above 0.8 are considered adequate for research [10], although Field recommends a value above 0.9 [8].

The *Correct* variable was set to a value of 0 for incorrect or 1 for correct based on whether the subject chose the correct colored cell for Task 1, or the front or side walls to register *True* or *False* correctly for Task 2. For Task 2 the assignment was easily done, since whether the front or side walls were selected is straightforward, and the assignment was recorded directly in the log files. Each subject response was compared to the correct *True* or *False* answer to assign the *Correct* value. For Task1, the assignment was more difficult, since comparisons had to be made to determine if the subject selected the correct region on the front wall of the VE. To assign the value, the subject's wand vector intersection with the wall was compared to a distribution of correct values previously registered. This control distribution was gathered when the author selected the center point, corners, and sides of the correct region for each test case condition. Additionally, points were gathered from a left-handed and right-handed wand configuration, to account for different

directions and orientations. This resulted in a distribution of twenty correct responses for each condition. For each subject response, the intersection coordinates of the wand vector with the front wall were checked to see if they were within 1.5 times the range of the control distribution [59, 65]. If they were, then a 1 or correct value was assigned. Otherwise a 0 or incorrect value was assigned. The expanded 1.5 times range was included to account for slight differences in seating and wand positioning between subjects. To verify the reasonableness of this approach, the number of incorrect responses for each test case condition was compared with visual analysis of scatter plots of the subject responses for each condition. The number of subject responses outside the main region of majority responses was consistent with the number of incorrect responses counted for each condition. For details on the assignment of the *Correct* variable, see Appendix C. For details about the process of cleaning up data for statistical analysis and the process undertaken here, see Chapter 4 in Tabachnick [59], Garson [10], and Appendix B.

For each task a combined MANOVA analysis was performed that looks for significant differences among the treatments for both dependent variables  $\log_{10}(Time)$  and *Correct*. Multivariate results are reported for each main effect and all combinations. For results that are significant, separate univariate ANOVA results for each effect and combination are interpreted to see where the differences lie. Although all ANOVAs were conducted on the data with 49 subjects and outliers trimmed, the graphs show the original *Time* and *Correct* data with all 50 subjects<sup>4</sup>. As a validation check, the complete MANOVA analysis

---

<sup>4</sup>This approach is taken in practice and facilitates interpretation of the results.

was also run on the original data and similar significant results were obtained, but since the *Normally Distributed Data* assumption was not met, the reported  $F$  values are considered inaccurate and the overall power is less. Therefore the results of the significance tests are reported based on results from the  $\log_{10}(\text{Time})$  trimmed data as output by SPSS and contained in Appendix E. This combined approach provides a better overall understanding of the data.

#### 4.2.1 Task 1 Analysis

This section presents the results from testing the hypotheses  $HT_0$ ,  $HT_A$ ,  $HC_0$ , and  $HC_A$ , using SPSS MANOVA for repeated measures samples taken during the Task 1 portion of the experiment. MANOVA results are discussed for hypothesis testing using the *Time* dependent variable at the 0.01 and 0.05 significance levels. Results for the dependent variable *Correct* are also discussed.

Results of the MANOVA showed significant multivariate results for the effects of *Method*, *Area*, *Color*, and the combinations of all effects except  $Method * Color$ . For this study, the effects of *Method*, *Area*, and  $Method * Area$  are of particular interest and are shown in Table 4.4 as a combined multivariate effect, as well as the separate univariate effects on *Time* and *Correct*. Results are considered to be highly significant when the  $F$  value is greater than 2, and the probability  $p$  is less than 0.05 [8]. The “Combined” column of Table 4.4 shows that the effects of *Method*, *Area*, and  $Method * Area$  were highly significant for the combination of *Time* and *Correct* together.

Table 4.4 Task 1 Multivariate and Univariate Significance Test Results.

Effect	Combined	p <	Time	p <	Correct	p <
<i>Method</i>	$F(2, 47) = 161.20$	0.001	$F(1, 48) = 315.79$	0.001	Not Significant	NA
<i>Area</i>	$F(4, 192) = 37.64$	0.001	$F(1.75, 83.95) = 332.51$	0.001	$F(1.49, 71.56) = 9.68$	0.01
<i>Method * Area</i>	$F(4, 192) = 37.64$	0.001	$F(1.92, 92.04) = 33.57$	0.001	Not Significant	NA

Table 4.4 shows a significant effect of *Method* on *Time*, and this relationship is graphically presented in Figure 4.8. The average time for the SCT method was 5.3 seconds, while the average time for the Wedges method was 10.8 seconds, indicating that subjects completed the task using the SCT method on average 5.5 seconds faster. There was no significant effect of *Method* on *Correct*.

The significant multivariate effect of *Area* shown in Table 4.4 is broken down into the effects on *Time* and *Correct*. As shown in Figure 4.9, the time increased with area size from 4.5 seconds for small areas, to 11.5 seconds for large areas, and all pairwise differences between area sizes are significant. As would also be expected, the accuracy decreased with increasing area, but the analysis indicates that the effect is only significant between small and large areas (see Figure 4.10).

The significant effect of *Method \* Area* on *Time* can be seen in Figure 4.11. The length of time it took a subject to complete Task 1 using the Wedges method took increasingly longer with larger area size. The average difference between the two methods was only 1.3 seconds for small areas, but increased to 5.3 seconds for medium areas and 10.1



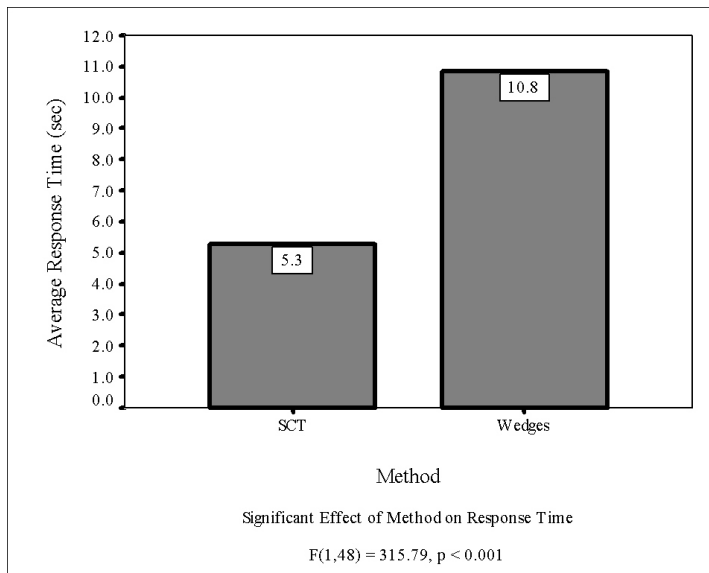


Figure 4.8 Task 1 *Time* vs. *Method* for 50 Subjects.

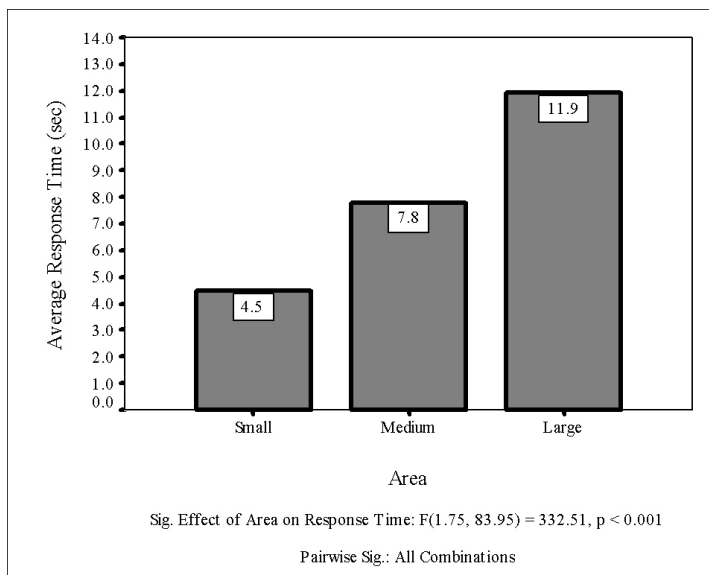


Figure 4.9 Task 1 *Time* vs. *Area* for 50 Subjects.

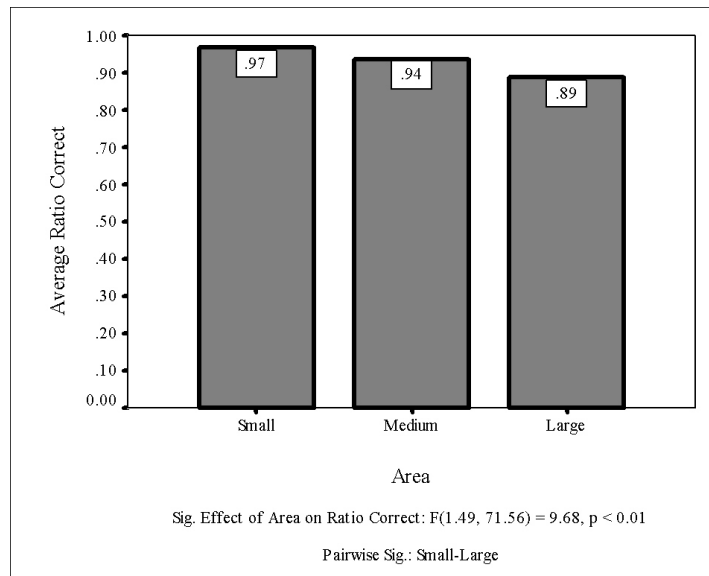


Figure 4.10 Task 1 *Time* vs. *Area* for 50 Subjects.

seconds for large areas. There was no significant effect of *Method* \* *Area* on *Correct*, presented in Table 4.4.

Therefore for Task 1, it is clear that the null hypothesis  $HT_0$  is rejected and  $HT_A$  is accepted. It took significantly less time for subjects to complete the task using the SCT method than using the Wedges method. Additionally, the null hypothesis  $HC_0$  is accepted and  $HC_A$  is rejected. There was no significant difference in the correctness of the result during the completion of a browsing task between the two methods over different size areas. Differences in accuracy were attributable to changes in *Area*, not *Method*.

Other significant results from the study of Task 1 are summarized in Appendix D, and the detailed MANOVA SPSS results are available in Appendix E.

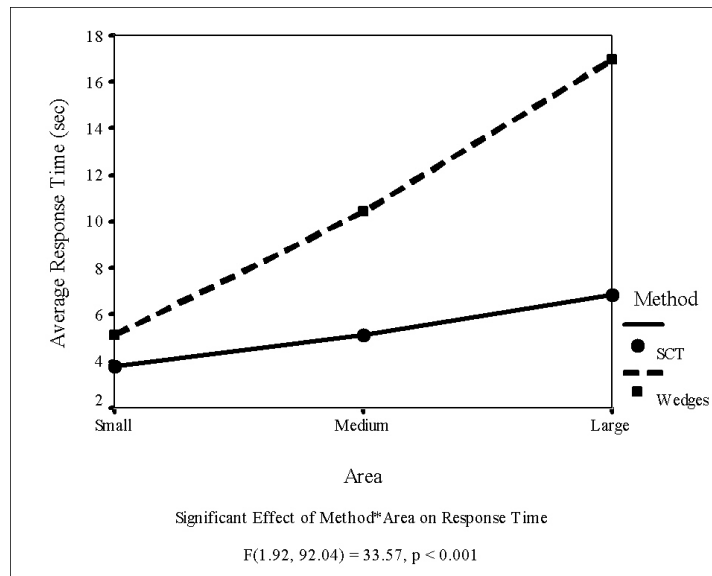


Figure 4.11 Task 1 *Time vs. Area by Method* for 50 Subjects.

#### 4.2.2 Task 2 Analysis

The main difference between the analysis for Task 1 and Task 2 is that instead of a *Color* factor, there was a *Pattern* factor. The only pattern tested was a checkerboard pattern, which only appeared in the data as a red and blue mix. The *Pattern* factor itself only has two levels: *None* (or False) and *Checkerboard* (or True).

Results of the MANOVA showed significant multivariate results for the effects of *Method*, *Area*, *Pattern*, and the combinations of all effects except *Method \* Pattern* and *Method\*Pattern\*Area*. For this study, the effects of *Method*, *Area*, and *Method\*Area* are of particular interest and are shown in Table 4.5. The “Combined” column of Table 4.5 shows that the effects of *Method*, *Area*, and *Method \* Area* were highly significant for the combination of *Time* and *Correct* together.

Table 4.5 Task 2 Multivariate and Univariate Significance Test Results.

Effect	Combined	p <	Time	p <	Correct	p <
<i>Method</i>	$F(2, 47) = 153.67$	0.001	$F(1, 48) = 303.76$	0.001	$F(1, 48) = 18.15$	0.001
<i>Area</i>	$F(4, 192) = 9.35$	0.001	$F(1.60, 76.86) = 10.19$	0.001	$F(1.51, 72.41) = 7.91$	0.01
<i>Method * Area</i>	$F(4, 192) = 13.28$	0.001	$F(1.97, 94.84) = 34.03$	0.001	Not Significant	NA

Table 4.5 shows a significant effect of *Method* on *Time*, and this relationship is graphically presented in Figure 4.12. The average time for the SCT method was 5.1 seconds, while the average time for the Wedges method was 16.0 seconds, indicating that subjects completed the task using the SCT method on average 10.9 seconds faster. Unlike Task 1, there was also a significant effect of *Method* on *Correct*. As shown in Figure 4.13, the average ratio of *Correct* was higher for subjects using the SCT method at 0.94, whereas the average ratio *Correct* was only 0.83 for subjects using the Wedges method.

The significant multivariate effect of *Area* shown in Table 4.5 is broken down into the effects on *Time* and *Correct*. As shown in Figure 4.14, the time increased with area size from 8.7 seconds for small areas, to 12.9 seconds for large areas. Small-Large and Medium-Large pairwise differences in area size are significant. As in Task 1, the accuracy decreased with increasing area, but only the *Area* pairwise difference of Small-Medium is significant (see Figure 4.15).

There was also a significant effect of *Method \* Area* on *Time*, which can be seen in Figure 4.16. The length of time it took a subject to complete Task 2 using the Wedges method took increasingly longer with larger area size, ranging from 12.3 seconds for small

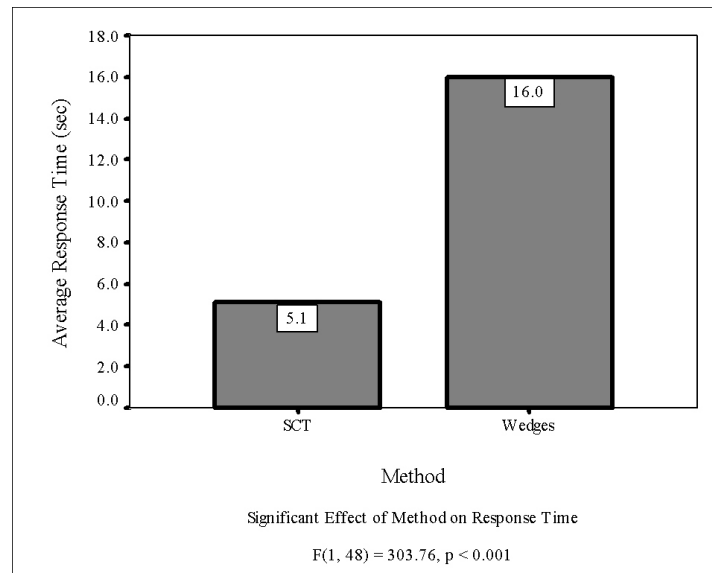


Figure 4.12 Task 2 *Time* vs. *Method* for 50 Subjects.

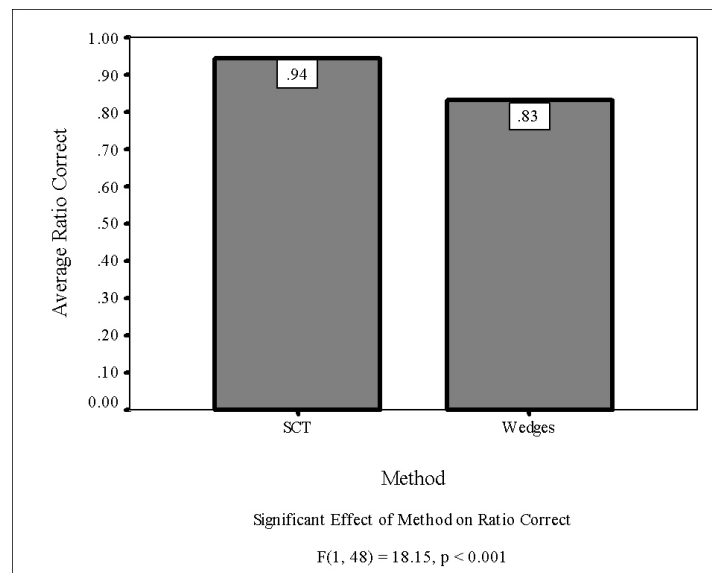


Figure 4.13 Task 2 *Correct* vs. *Method* for 50 Subjects.

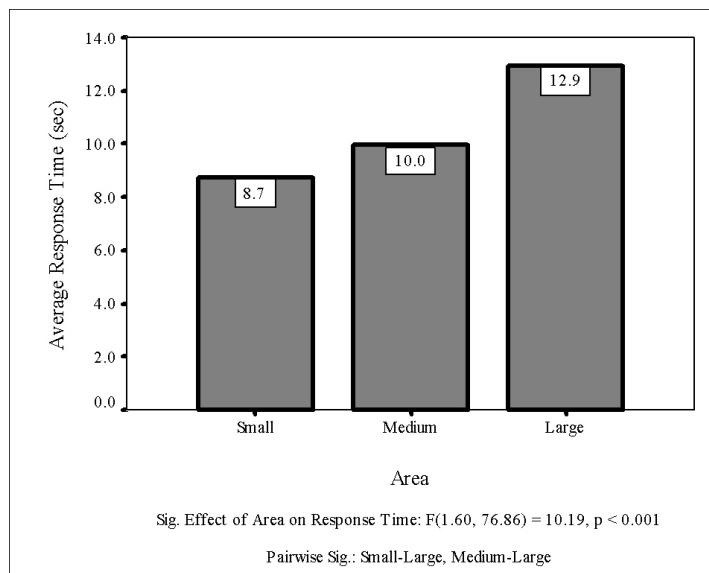


Figure 4.14 Task 2 *Time* vs. *Area* for 50 Subjects.

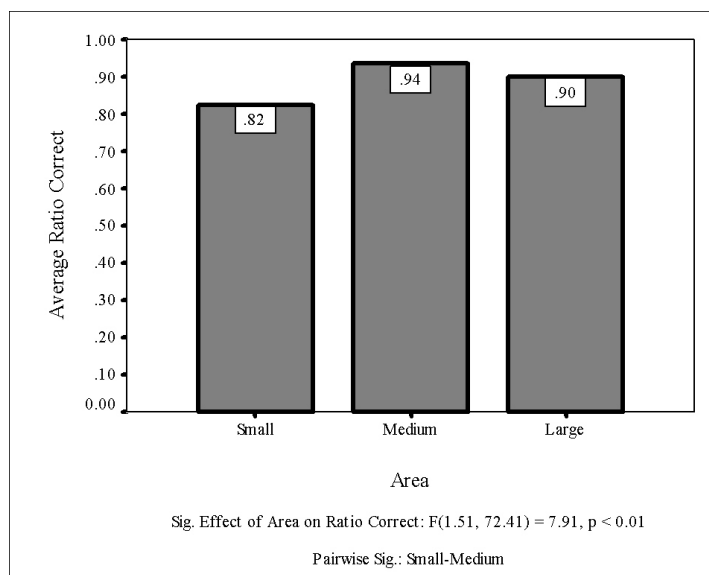


Figure 4.15 Task 2 *Time* vs. *Area* for 50 Subjects.

areas to 20.5 seconds for large areas. In contrast, subjects took on average about 5 seconds using the SCT method, regardless of area size. This result indicates that the SCT method is very good for quickly identifying the checkerboard pattern when browsing large datasets. There was no significant effect of *Method \* Area* on *Correct*, presented in Table 4.5.

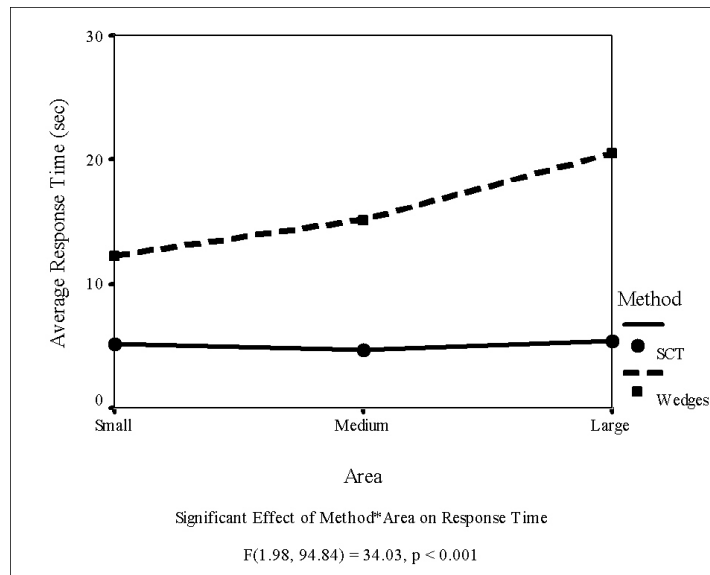


Figure 4.16 Task 2 *Time* vs. *Area* by *Method* for 50 Subjects.

Therefore for Task 2, it is clear that the null hypothesis  $HT_0$  is rejected, and  $HT_A$  is accepted. It took significantly less time for subjects to complete the task using the SCT method than using the Wedges method. Additionally, the null hypothesis  $HC_0$  is also rejected, and  $HC_A$  is accepted. Subjects using the SCT method were significantly more accurate than when using the Wedges method over different size areas. Differences in accuracy were attributable to changes in *Method* and *Area*.

Other significant results from the study of Task 2 are summarized in Appendix D, and the detailed MANOVA SPSS results are available in Appendix E.



## CHAPTER V

### PERFORMANCE STUDY

As described in Chapter 3, the SCT consists of the implementation independent portion that does the scaling and distribution, as well as the portion that uses texture mapping to implement the algorithm. The portion that renders the particles could have been implemented a number of ways. In practice, particles are often rendered as individual primitives, such as OpenGL points, quadrilaterals, or triangles. Quadrilaterals and triangles may themselves be texture-mapped to make them appear more like spheres, or to convey additional information other than just color. In their simplest and fastest form, these individual particle primitives are color-mapped with a single color (or flat-shaded), and sized according to some other criteria, such as grain size. The 2D texture mapping SCT method was developed because it was thought that for each grid location, rendering only eight triangles with the particle primitives synthesized into the texture vs. rendering hundreds or thousands of individual particle primitives would be faster. The results in this chapter confirm the logic of this decision. A performance study was completed that compares the SCT method with two other currently used methods for rendering particles: OpenGL® color-mapped points (Points) and flat-shaded, color-mapped quadrilaterals (Quads) [78].

Detailed results show where the performance of the SCT method is superior. The system was optimized for deployment in a four wall CAVE-like VE.

## 5.1 Design

Performance data are obtained using extensive built-in graphics statistics gathering features provided by the OpenGL Performer™ toolkit [6, 56]. This scene graph based software toolkit is designed to help optimize applications and discover bottlenecks running on SGI® supported platforms. Initial computation times for each of the three methods are recorded using the SGI high-resolution *syssgi* hardware clock with sub-microsecond accuracy and accessible through the OpenGL Performer API<sup>1</sup>. Although the Points representation is included in the performance comparisons, it is not suitable for actual implementation in our application since the points are not all the same approximate distance from the viewer. OpenGL points are rendered to a specific “point size” that always use the same number of pixels on the display regardless of the proximity of the viewer, making them change in size relative to surrounding geometry depending on the viewer location. OpenGL points may be applicable in other situations where the particles are all viewed from approximately the same distance.

The test configurations were taken from the 10/23/1995 08:18 time step of the Ocean-side dataset and were chosen to investigate the limitations of the three algorithms in the following scenarios:

---

<sup>1</sup>This is much more precise than the commonly used real-time clock that only has an accuracy of 1-20 milliseconds, depending on the hardware platform.

1. Shallow Region A Larger Area (SRALA): A  $12 \times 21$  point shallow water region that maximizes the amount of texture memory used and includes both dense and sparse regions of particles. Fewer layers were rendered to lessen the effects of blending. Methods which use primitives for individual particles would do less work in sparse regions. Machine A was chosen for this purpose since it has the largest amount of texture memory and the most advanced SGI graphics pipeline (see Table 5.1). This region contains 252 grid locations per  $z$  direction layer, and tests were run from 1 to 8 layers. The slice resolution chosen was  $64 \times 64$ .
2. Shallow Region B Dense Particles (SRBDP): A  $6 \times 22$  point shallow water region containing dense concentrations of particles over the full 31 layers of the dataset for 132 grid locations per  $z$  direction layer. The slice resolution of  $16 \times 16$  in this configuration maximizes the number of glyphs and the blending of layers during rendering. Since the application is designed for the VE, Machine B is the testbed for this scenario. Machine B is directly connected to the VE, as shown in Table 5.1. Data was collected for layers 1 through 8, then every fourth layer through 31.
3. Shallow Region B Changing Resolutions (SRBCR): The same shallow water region on Machine B, but studying the effects of increasing slice resolution on rendering for 3 layers. Data was collected for resolutions of  $16 \times 16$  through  $128 \times 128$ .

Each test case was run 5 times and the times were averaged. Since OpenGL has the requirement that the length and width of texture images must be a power of 2, the slice resolutions were chosen accordingly [78]. For details on the Oceanside dataset and the test configurations, see Appendix A.

Table 5.1 Machine Configurations for Benchmark Tests.

	Machine A	Machine B
Type	Onyx 2	Onyx 2
Graphics	Infinite Reality 3	Infinite Reality
Num Processors	4	8
RAM (GB)	4	4
Texture Memory (MB)	512	128
Usage	High-end Desktop	CAVE-like VE

## 5.2 Results

The frame rate comparison in Figure 5.1 shows that the SCT algorithm executes at 66 frames per second (*fps*) for up to 5 layers of the shallow water region, then decreases to 33 *fps* for layers 6 and 7. This occurs because logic in the runtime portion of the OpenGL Performer API attempts to match the frame rate of the scene rendered to the video refresh rate [6]. For Machine A SRALA, this rate is 66 Hz. Once the frame rate drops below 12 *fps*, the rate is not affected by the video refresh rate, and is based simply on the number of times the scene can be rendered during a second.

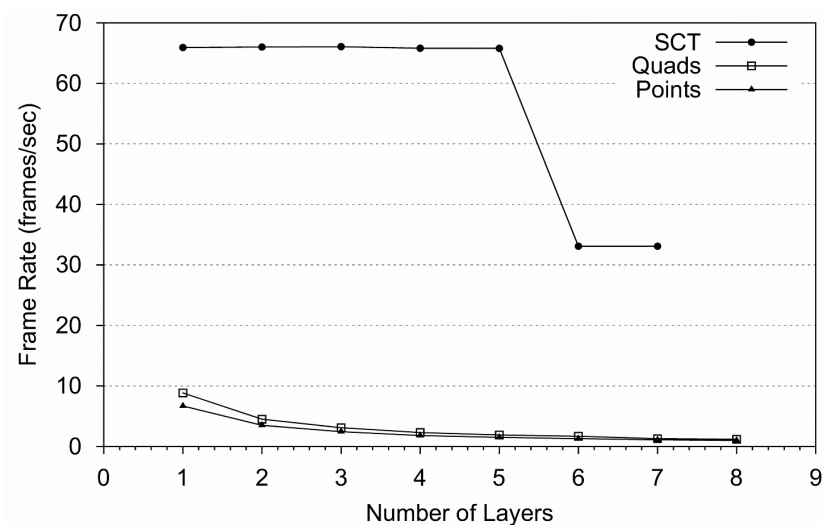


Figure 5.1 Frame Rate vs. Number of Layers for Machine A SRALA.

As shown in Figure 5.1, the Quads algorithm rendered the first layer of the configuration at just under 9 *fps*, and the Points algorithm at around 7 *fps*. Note that the Quads

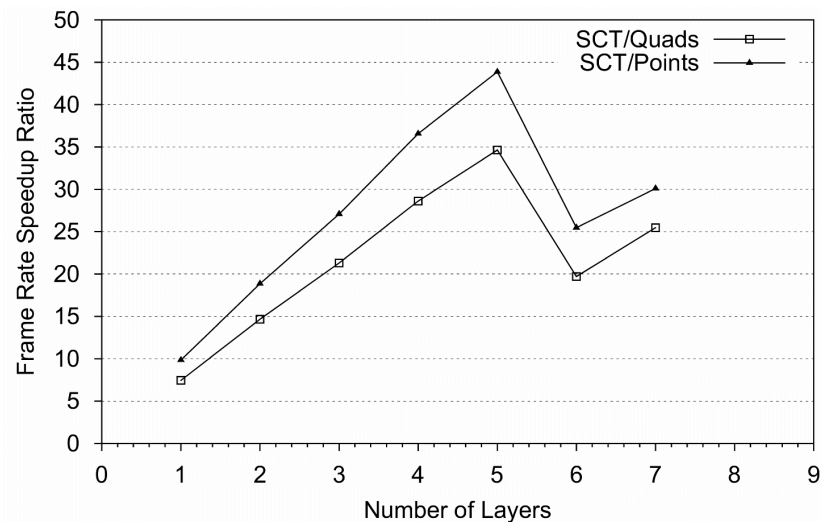


Figure 5.2 Frame Rate Speedup Ratio vs. Number of Layers for Machine A SRALA.

method is generally faster than Points since the Infinite Reality graphics pipeline is optimized for triangles,<sup>2</sup> and the pipeline must do extra work to draw each point to the point size specified in the Points algorithm. In contrast to the SCT algorithm, neither the Quads nor Points methods could produce acceptable frame rates for two or more layers.

The results can also be shown in terms of a frame rate speedup ratio of SCT vs. Quads or Points, which can be computed in terms of  $fps_{SCT}/fps_{Other}$ . In Figure 5.2, the frame rate speedup ratio for SCT vs. Quads varies from 7 to just under 35, with higher speedups occurring when the Quads method bogs down the graphics pipeline when trying to render more layers. For SCT vs. Points, the frame rate speedup ratio varies from 10 to 44.

Another perspective can be seen in Figure 5.3 and Figure 5.4. This series of runs was performed in the VE configuration on Machine B for the shallow water region SRBDP.

<sup>2</sup>A quadrilateral is internally split into 2 triangles.

Figure 5.3 shows frame rate vs. number of layers for the SCT, Quads, and Points algorithms for a low slice resolution of  $16 \times 16$ . In this case, the frame rate for all methods is considerably affected by the amount of blending required for the large number of glyphs displayed in a vertical column. The Quads and Points algorithms can maintain a frame rate above 10 *fps* for up to 5 layers. At 8 layers, a frame rate of around 6 *fps* is still navigable in the VE, but difficult. The SCT algorithm starts as high as 48 *fps* for 1 layer, stays above 10 *fps* for up to 10 layers, and 6 *fps* for up to 16 layers. At a slice resolution of  $16 \times 16$ , each layer adds about 2 MB of texture memory, and Machine B has enough to view all 31 layers. The end result is that the SCT algorithm is still up to 2 times faster than Quads or Points in cases where the texture memory is not filled to capacity, but where there may be many glyphs to display (see Figure 5.4).

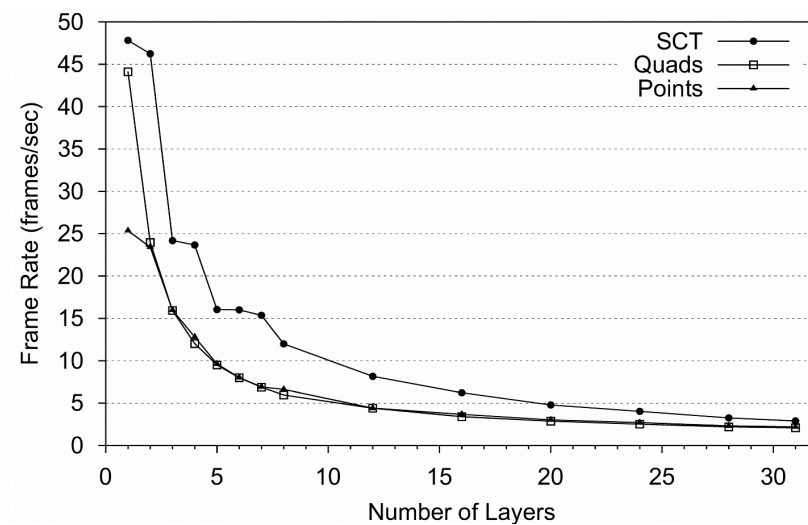


Figure 5.3 Frame Rate vs. Number of Layers for Machine B SRBDP.

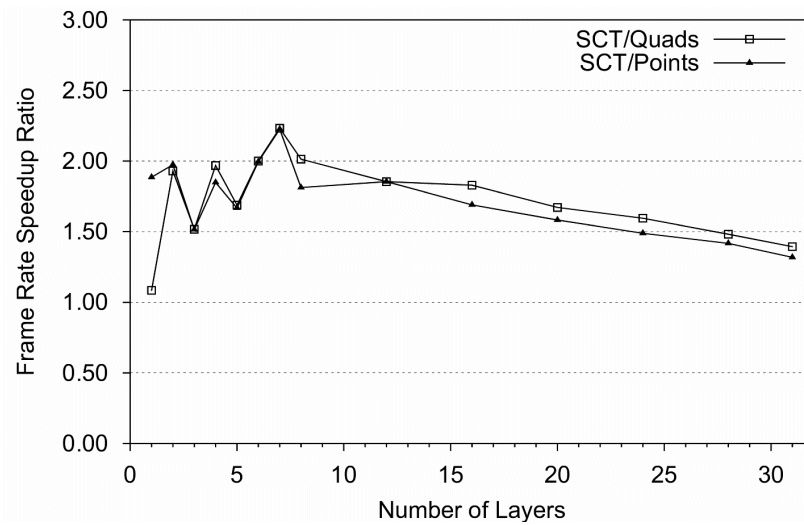


Figure 5.4 Frame Rate Speedup vs. Number of Layers for Machine B SRBDP.

Figure 5.5 shows the same VE shallow water region configuration SRBCR for 3 layers at differing slice resolutions of  $16 \times 16$  through  $128 \times 128$ . The Quads and Points algorithms can maintain a frame rate of 16 *fps* at  $16 \times 16$ , but only 4 to 5 *fps* at  $32 \times 32$ . In contrast, the SCT algorithm can maintain a frame rate of 24 *fps* up to a resolution of  $64 \times 64$ . In other words, the SCT algorithm can display 4 to 16 times the number of particles at a faster frame rate than the other two algorithms (for this particular case). In cases where there are very few particles in a particular bin, the SCT algorithm is more likely to be able to represent those particles with a higher resolution than is possible with the other algorithms. The numbers of glyphs computed for each bin at each resolution for this configuration are shown in Table 5.2<sup>3</sup>. Note that bin 7 is not represented at the  $16 \times 16$  resolution, but is

<sup>3</sup>For this particular dataset, the consolidation scheme resulted in values for only seven of the bins. Other datasets could have values in all of the bins, representing more of the larger size particles.

represented at  $32 \times 32$  and higher. This indicates that with a higher slice resolution, the SCT algorithm can display values in a greater range than the Quads or Points methods at an acceptable frame rate. This capability allows more detail information to be shown because of the larger pool of particles that can be displayed at one time, and improves with increasing slice resolution.

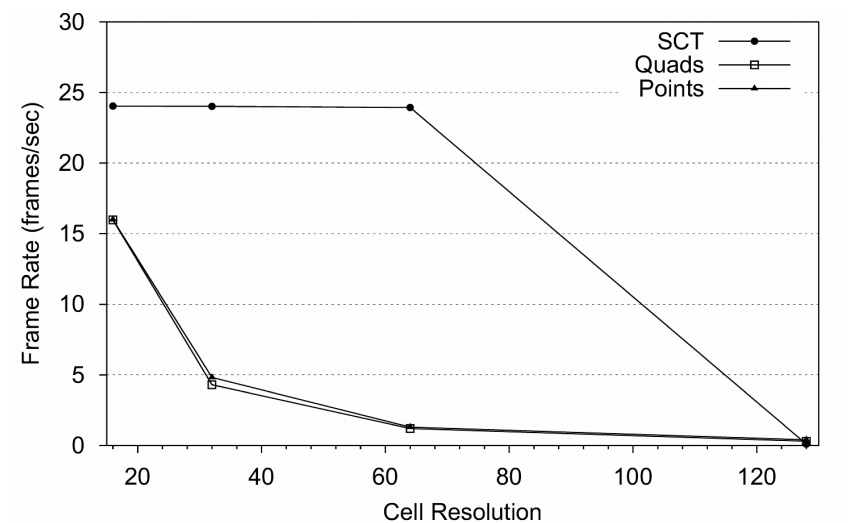


Figure 5.5 Frame Rate vs. Slice Resolution for Machine B SRBCR.

It is useful to note that frame rate comparisons do not tell the whole story. Although the SCT algorithm can achieve a higher frame rate than either Points or Quads, it does so at the expense of more memory and startup processing time to synthesize the texture. Figure 5.6 shows the startup times for execution of all three algorithms. The startup time is defined to be the amount of time it takes for the application to complete the geometry that will be rendered for each visualization method. For the SCT method this includes the time



Table 5.2 Number of Actual Consolidated Glyphs Used in Volume for Machine B SRBCR.

Bin	16x16	32x32	64x64	128x128
1	12,302	49,212	196,885	787,618
2	18,088	72,463	289,876	1,159,530
3	5,100	20,345	81,392	325,642
4	4,713	18,840	75,332	301,350
5	1,663	6,522	26,171	104,574
6	404	2,110	8,771	35,073
7	0	73	524	2,342
Total	42,270	169,565	678,951	2,716,130
PPG	6,181,820,000	1,541,040,000	384,867,000	96,205,100

to synthesize the textures, as well as the time to complete the triangle fan geometry for all of the requested grid point locations. For the Points and Quads methods, it is the amount of time it takes to complete the color-mapped geometry primitives for all of the requested grid point locations. The time required per layer varies linearly with all three methods, although the slope for the SCT algorithm is much steeper (6.20 sec/layer for SCT, 0.67 sec/layer for Quads, and 0.53 sec/layer for Points). This slope can be converted to a general slope of seconds required per megabyte of memory: SCT requires 0.10 sec/MB, Quads requires 0.06 sec/MB, and Points requires 0.18 sec/MB. This may seem counterintuitive, but in reality all pixels in the SCT texture must be assigned values, even if they do not represent actual glyphs for particles (in which case they would be transparent). The Quads and Points algorithms only use memory for the actual glyphs rendered, whereas the SCT algorithm uses much more memory to synthesize and store the textures (see Figure 5.7). The fact that the Quads algorithm takes less time per megabyte than the Points is due to the

similar amount of time it takes for both methods to locate the glyphs, with only slightly more work required to place four closely spaced points for a quadrilateral than a single point. Therefore, the Quads algorithm requires more memory, but the time per MB is less. Figure 5.8 confirms the additional time required for the SCT algorithm: it is approximately 9.4 times slower than the Quads, and 11.7 times slower than the Points.

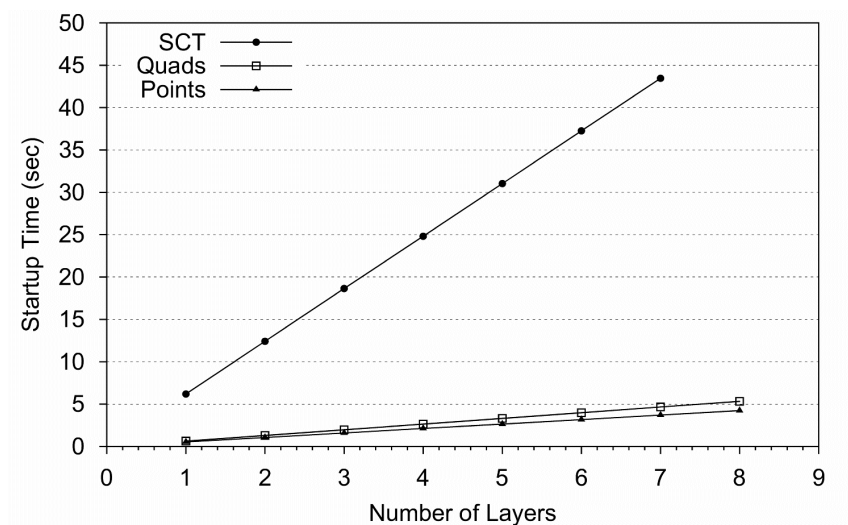


Figure 5.6 Startup Time vs. Number of Layers for Machine A SRALA.

One goal of this study was to determine the limitations of the SCT algorithm, and Machine A was used for this purpose. There was only one case where the SCT algorithm did not render the visualization, and this occurred when it could not complete the 8 layer configuration because a process maximum shared memory limit of 500 MB was exceeded (see Figure 5.1). This was due to an OpenGL Performer memory mapping problem during

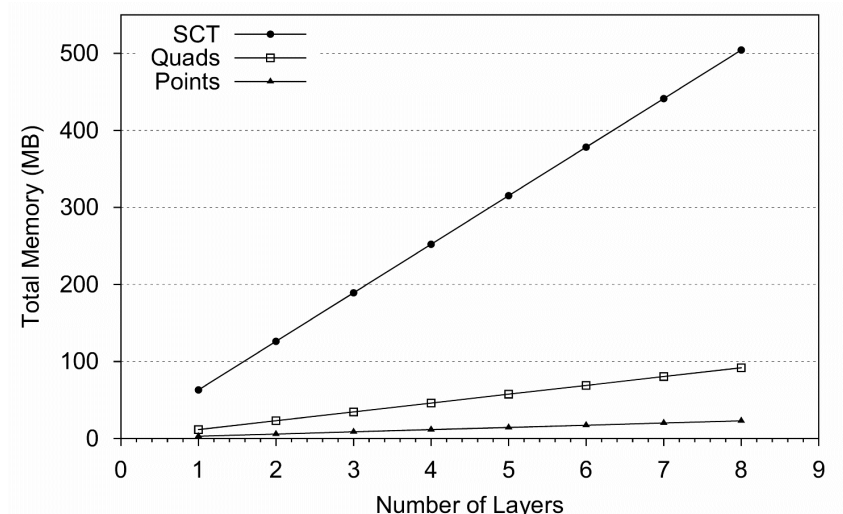


Figure 5.7 Total Memory vs. Number of Layers for Machine A SRALA.

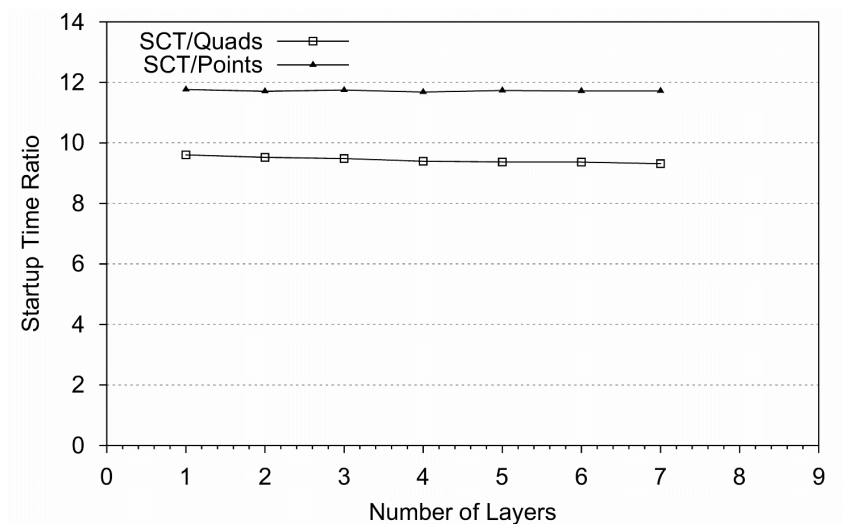


Figure 5.8 Startup Time Speedup Ratio vs. Number of Layers for Machine A SRALA.

the attempted allocation of about 500 MB of texture memory, as indicated in Figure 5.7 and documented in the release notes [58].

The SCT algorithm has been shown to take considerably more memory and startup time than either of the other two methods. However, both aspects can be easily justified as reasonable for the increased frame rate during scene rendering. Texture memory is available in ever increasing amounts on new computers expressly for this purpose [53], and massive amounts of main memory are utilized to reduce file access latencies. At the point where the texture is computed, there is only color and transparency assigned based on bin type for each glyph. This portion could easily be split by cell and partitioned among several processors as described in Section 6.1.

## CHAPTER VI

### CONCLUSIONS

This research makes several contributions in the visualization of multiple related scalar fields as applied to sedimentation data. The new SCT algorithm was developed that provides an excellent indication of “how much” sediment concentration is present within a cell, based on the number of particles of each grain size present. The SCT method complements the point detail view that directly shows SSC values by grain size on a  $\log_{10}$  color scale. This gives the viewer a better indication for the types of sediment present and the amounts that may affect visibility.

The SCT method has certain characteristics that could be applied for visual feature detection and identification while browsing sedimentation datasets. This allows the viewer to quickly get relative amounts of basic information within a short time. To quantitatively measure the SCT method for browsing, a user study was performed to compare it with the new glyph-based Wedges visualization method that also incorporates state-of-the-art perceptual characteristics.

This is expressed in the form of two formal (paired) hypotheses:

$HT_0$ : There is no significant difference in the amount of time it takes to complete a browsing task between the two methods over different size areas.

$HT_A$ : It takes significantly less time to complete a browsing task using the SCT method vs. using the Wedges method over different size areas.

$HC_0$ : There is no significant difference in the correctness of the result during the completion of a browsing task between the two methods over different size areas.

$HC_A$ : There is a significant difference in the correctness of the result during the completion of a browsing task between the two methods over different size areas.

Data was gathered for 50 subjects performing two browsing tasks. In Task 1, the subject was asked to find the single color cell as the feature detection requirement. In Task 2, the subject selected whether a checkerboard pattern was present, which satisfied the requirement for feature identification.

Statistical analysis proved that the SCT method can be used for feature detection and identification for several size areas (regions) from multiple sedimentation datasets. For Task 1, the null hypothesis  $HT_0$  was rejected and  $HT_A$  was accepted. It took significantly less time for subjects to complete the task using the SCT method than using the Wedges method. Additionally, the null hypothesis  $HC_0$  was accepted and  $HC_A$  was rejected. There was no significant difference in the correctness of the result during the completion of a browsing task between the two methods over different size areas. Differences in accuracy were attributable to changes in *Area*, not *Method*. For Task 2, the null hypothesis  $HT_0$  was rejected, and  $HT_A$  was accepted. It took significantly less time for subjects to complete the task using the SCT method than using the Wedges method. The null hypothesis  $HC_0$  was also rejected, and  $HC_A$  was accepted. Subjects using the SCT method were

significantly more accurate than when using the Wedges method over different size areas. Differences in accuracy were attributable to both changes in *Method* and *Area*.

In another study the interactive performance of the SCT method was compared with two glyph-based representations: OpenGL points and quadrilaterals. Performance statistics showed the SCT method to have an increase in rendering speed of up to 44 times faster than the other methods, depending on the volume to be displayed and the host system. For a given frame rate, performance data showed that the SCT algorithm can display from 4 to 16 times the amount of information of the Quads or Points algorithms at a faster frame rate in the VE.

The SCT method has been successfully applied to oceanographic sedimentation data with up to sixteen scalar values per grid point. Scientists can use the SCT method to help understand the physical processes involving sediment transport in complex coastal environments. The method may be applied to other problem domains such as aerosol transport and climate modeling. Future publications will describe its use in the visualization of dust aerosol transport in global circulation models [11, 12, 13, 16, 61].

## 6.1 Future Work

Straightforward enhancements to the SCT algorithm include adding a variable size glyph, parallelizing the texture synthesis portion of the algorithm, and extending the method for time-varying data. Implementing a variable size glyph (such as  $3 \times 3$  or  $4 \times 5$ ) is complicated by the OpenGL optimization requirement that the length and width of a texture

image be a power of 2 [78]. The leftover pixels computed during the texture synthesis stage would need to be randomly distributed and made transparent. This would allow better utilization of the pixels in the texture and more bins to be represented.

The parallelization of the texture synthesis portion of the SCT algorithm can be accomplished by partitioning the total cells to be textured among available processors on the host and neighboring computers. For instance, the longest startup time for the SCT algorithm was just under 45 seconds for 1,764 cells of the shallow water region. If the task was simply split among 20 processors, then each one would compute the texture for approximately 88 cells. Even with the added overhead of communication and other process loads, it is reasonable to expect that the overall startup time of the SCT algorithm could be reduced to less than 5 seconds.

Extending the SCT algorithm for time-varying data requires that the bin information for each glyph be saved along with the texture for the current time step, in order to compute the differences in the texture for the next time step. The same texture memory can be used and only glyph locations within the texture that must change are affected.

More future work involves performing user studies emphasizing other perceptual aspects of the SCT and Wedges methods.



## REFERENCES

- [1] "AERONET: Aerosol Robotic Network," <http://aeronet.gsfc.nasa.gov>.
- [2] "Battlespace Atmospheric and Cloud Impacts on Military Operations (BACIMO) Conference," 2003, <http://www.nrlmry.navy.mil/bacimo.html>.
- [3] R. A. Crawfis, *New Techniques of the Scientific Visualization of Three-Dimensional Multi-Variate and Vector Fields*, doctoral dissertation, Lawrence Livermore National Laboratory, University of California, Livermore, CA, October 1995.
- [4] C. Cruz-Neira, D. J. Sandin, and T. A. DeFanti, "Surround-Screen Projection-Based Virtual Reality: The Design and Implementation of the CAVE," *SIGGRAPH 93 Conference Proceedings*, J. T. Kajiya, ed. August 1993, Annual Conference Series, pp. 135–142, ACM SIGGRAPH, Addison Wesley, ISBN 0-89791-601-8.
- [5] W. de Leeuw and R. van Liere, "Comparing LIC and Spot Noise," *Proceedings Visualization '98*. 1998, pp. 359–365, IEEE Computer Society Press.
- [6] G. Eckel, *IRIS Performer Programmer's Guide*, Silicon Graphics, Inc., Document Number 007-1680-040.
- [7] J. A. Ferwerda, "Psychometrics 101: How to Design, Conduct, and Analyze Perceptual Experiments in Computer Graphics," ACM SIGGRAPH 2002 Course, July 2002.
- [8] A. P. Field, *Discovering Statistics Using SPSS for Windows: Advanced Techniques for the Beginner*, London: Sage, 2000.
- [9] J. Fredsoe and R. Deigaard, *Mechanics of Coastal Sediment Transport*, Advanced Series on Ocean Engineering. World Scientific Publishing Company, River Edge, NJ, 1992.
- [10] G. D. Garson, *Guide to Writing Empirical Papers, Theses, and Dissertations*, Marcel Dekker, Inc., 270 Madison Avenue, New York, NY 10016, 2002.
- [11] P. Ginoux, M. Chin, I. Tegen, J. M. Prospero, B. Holben, O. Dubovik, and S.-J. Lin, "Sources and Distributions of Dust Aerosols Simulated With the GOCART Model," *Journal of Geophysical Research*, vol. 106, no. D17, September 16 2001, pp. 20,255–20,273.

- [12] “NASA Goddard Institute for Space Studies,” <http://www.giss.nasa.gov/research>.
- [13] “NASA Goddard Institute for Space Studies,” <http://www.giss.nasa.gov/data/dust>.
- [14] S. M. Glenn and W. D. Grant, “A suspended sediment correction for combined wave and current flows,” *J. Geophys. Res.*, vol. 92, 1987, pp. 8244–8246.
- [15] A. M. Graziano and M. L. Raulin, *Research Methods: A Process of Inquiry*, 4th edition, Allyn and Bacon, 160 Gould Street, Needham Heights, MA 02494, 2000.
- [16] R. J. Griffin, D. Dabdub, M. J. Kleeman, M. P. Fraser, G. R. Cass, and J. H. Seinfeld, “Secondary Organic Aerosol: III. Urban/Regional Scale Model of Size- and Composition-Resolved Aerosols,” *Journal of Geophysical Research*, vol. 107, no. D17, 2002.
- [17] R. Grzeszczuk, C. Henn, and R. Yagel, “Advanced Geometric Techniques for Ray Casting Volumes,” *SIGGRAPH '98 Course Notes*. ACM SIGGRAPH, July 1998, ACM SIGGRAPH.
- [18] J. Hansen, M. Sato, and I. Tegen, “Anomalous Atmospheric Absorption? Or Aerosols,” [http://www.giss.nasa.gov/research/intro/hansen\\_06/](http://www.giss.nasa.gov/research/intro/hansen_06/), August 1999.
- [19] C. G. Healey, “Choosing Effective Colours for Data Visualization,” *Proceedings Visualization '96*, San Francisco, CA, October 1996, IEEE Computer Society and ACM SIGGRAPH, pp. 263–270, IEEE Computer Society Press and ACM.
- [20] C. G. Healey, K. S. Booth, and J. T. Enns, “High-Speed Visual Estimation Using Preattentive Processing,” *ACM Transactions on Human-Computer Interaction*, vol. 3, no. 2, 1996, pp. 107–135.
- [21] C. G. Healey and J. T. Enns, “Building Perceptual Textures to Visualize Multidimensional Datasets,” *Proceedings Visualization '98*, D. Ebert, H. Rushmeier, and H. Hagen, eds., Research Triangle Park, NC, October 1998, pp. 111–18, IEEE Computer Society Press and ACM.
- [22] C. G. Healey and J. T. Enns, “Perception and Painting: A Search for Effective, Engaging Visualizations,” *IEEE Computer Graphics and Applications*, March–April 2002, pp. 10–15.
- [23] W. Heidrich, R. Westermann, H.-P. Seidel, and T. Ertl, “Applications of Pixel Textures in Visualization and Realistic Image Synthesis,” *ACM Symposium on Interactive 3D Graphics*. April 1999, pp. 127–134, ACM.
- [24] L. Hong and A. E. Kaufman, “Fast Projection-Based Ray-Casting Algorithm for Rendering Curvilinear Volumes,” *IEEE Transactions on Visualization and Computer Graphics*, vol. 5, no. 4, October–December 1999, pp. 322–332.

- [25] D. C. Howell, *Statistical Methods for Psychology*, Duxbury, Thompson Learning™, Pacific Grove, CA, 2002.
- [26] V. Interrante, “Conveying the 3D Shape of Smoothly Curving Transparent Surfaces via Texture,” *IEEE Transactions on Visualization and Computer Graphics*, vol. 3, no. 2, April-June 1997, pp. 98–117.
- [27] B. Jobard, G. Erlebacher, and M. Hussaini, “Hardware-Accelerated Texture Advection for Unsteady Flow Visualization,” *Proceedings Visualization '00*. 2000, pp. 155–161, IEEE Computer Society Press and ACM.
- [28] B. Jobard and W. Lefer, “The Motion Map: Efficient Computation of Steady Flow Animations,” *Proceedings Visualization '97*. 1997, pp. 323–328, IEEE Computer Society Press and ACM.
- [29] A. Kaufman, ed., *Volume Visualization*, IEEE Computer Society Press, Los Alamitos, CA, 1991.
- [30] T. R. Keen, *Coupled Sediment Dynamics and Optics*, <http://www7320.nrlssc.navy.mil/csdo/>.
- [31] T. R. Keen and S. M. Glenn, “Resuspension and Advection of Sediment During Hurricane Andrew on the Louisiana Continental Shelf,” *5th Int. Conf. Estuarine and Coastal Model., Proc.*, Alexandria, Virginia, 1998, pp. 481–494.
- [32] T. R. Keen, R. J. Vickery, P. Flynn, R. H. Stavn, and W. McBride, “Scientific Visualization of Sediment Dynamics in the Bottom Boundary Layer,” *7th Int. Conf. Estuarine and Coastal Model., Proc.*, St. Pete Beach, Florida, November 2001.
- [33] D. A. Keim, “Information Visualization and Visual Data Mining,” *IEEE Transactions on Visualization and Computer Graphics*, vol. 8, no. 1, January-March 2002, pp. 1–8.
- [34] R. M. Kirby and D. H. Laidlaw, “Visualizing Multivalued Data from 2D Incompressible Flows Using Concepts from Painting,” *Proceedings Visualization '99*. October 1999, pp. 333–339, 540, IEEE Computer Society Press and ACM.
- [35] W. C. Krumbein, “Size Frequency Distributions of sediments and the Normal Phi Curve,” *Journal of Sedimentary Petrology*, vol. 8, no. 3, 1938, pp. 84–90.
- [36] F. Kuester, R. Bruckschen, B. Hamann, and K. I. Joy, “Visualization of Particle Traces in Virtual Environments,” *Proceedings of the ACM Symposium on Virtual Reality Software and Technology*, Baniff, Alberta, Canada, 2001, pp. 151–157, ACM Press.
- [37] D. H. Laidlaw, “Loose, Artistic ”Textures” for Visualization,” *IEEE Computer Graphics and Applications*, vol. 21, no. 2, March-April 2001, pp. 6–9.

- [38] H. Levkowitz, “Color Icons: Merging Color and Texture Perception for Integrated Visualization of Multiple Parameters,” *Proceedings Visualization '91*. 1991, pp. 164–170, IEEE Computer Society Press and ACM.
- [39] H. Levkowitz, *Color Theory and Modeling for Computer Graphics, Visualization, and Multimedia Applications*, Kluwer Academic Publishers, 1997.
- [40] M. Levoy, “Display of Surfaces from Volume Data,” *IEEE Computer Graphics and Applications*, vol. 8, no. 3, May 1988, pp. 29–37.
- [41] R. Lowry, “Concepts and Applications of Inferential Statistics,” Web Textbook, <http://faculty.vassar.edu/lowry/webtext.html>.
- [42] E. B. Lum and K.-L. Ma, “Interactivity is the Key to Expressive Visualization,” *ACM SIGGRAPH Computer Graphics*, vol. 36, no. 3, August 2002, pp. 5–9.
- [43] A. Mahesh, V. P. Walden, and S. G. Warren, “Ground-Based Infrared Remote Sensing of Cloud Properties Over the Antarctic Plateau. Part II: Cloud Optical Depths and Particle Sizes,” *Journal of Applied Meteorology*, vol. 40, no. 7, July 2001, pp. 1279–1294.
- [44] N. Max and B. Becker, “Flow Visualization Using Moving Textures,” *Proceedings of ICASE/LaRC Symposium on Visualizing Time Varying Data*, D. Banks, T. Crockett, and S. Katy, eds. 1996, vol. 3321, pp. 77–87, NASA Conference Publication.
- [45] N. Max, R. Crawfis, and B. Becker, “Applications of Texture Mapping to Volume and Flow Visualization,” *Graphicon 95*, 1995.
- [46] N. Max, P. Williams, and C. Silva, “Approximate Volume Rendering for Curvilinear and Unstructured Grids by Hardware-Assisted Polyhedron Projection,” *International Journal of Imaging Systems and Technology*, vol. 11, no. 1, 2000, pp. 53–61.
- [47] M. Meißner, J. Huang, D. Bartz, K. Mueller, and R. Crawfis, “A Practical Evaluation of Popular Volume Rendering Algorithms,” *Proceedings Volume Visualization and Graphics Symposium 2000*, S. N. Spencer, ed., New York, NY, October 2000, pp. 81–90, ACM SIGGRAPH, ISBN 1-58113-308-1.
- [48] J. S. Montrym, D. R. Baum, D. L. Dignam, and C. J. Migdal, “Infinite Reality: a Real-Time Graphics System,” *SIGGRAPH 97 Conference Proceedings*, J. T. Whitted, ed. August 1997, Annual Conference Series, pp. 293–302, ACM SIGGRAPH, Addison Wesley, ISBN 0-89791-896-7.
- [49] P. Nielsen, *Coastal Bottom Boundary Layers and Sediment Transport*, vol. 4 of *Advanced Series on Ocean Engineering*, World Scientific Publishing Company, River Edge, NJ, 1992.

- [50] H. O. Pfannkuch and R. Paulson, *Grain Size Distribution and Hydraulic Properties*, <http://hydrate.eas.gatech.edu/eas4420/soilscsclass.htm>.
- [51] N. A. Phillips, “A Coordinate System Having Some Special Advantages for Numerical Forecasting,” *Journal of Applied Meteorology*, 1957.
- [52] P. J. Rajlich, *An Object-Oriented Approach to Developing Visualization Tools Portable Across Desktop and Virtual Environments*, Master’s thesis, University of Illinois at Urbana-Champaign, 1998, 57 pages, <http://monet.astro.uiuc.edu/~prajlich/T>.
- [53] C. Rezk-Salama, K. Engel, M. Bauer, G. Greiner, and T. Ertl, “Interactive Volume Rendering on Standard PC Graphics Hardware Using Multi-Textures and Multi-Stage Rasterization,” *SIGGRAPH/Eurographics Workshop on Graphics Hardware Conference Proceedings*, Interlaken, Switzerland, August 2000, pp. 109–118, ACM SIGGRAPH, Addison Wesley.
- [54] C. Rezk-Salama, P. Hastreiter, C. Teitzel, and T. Ertl, “Interactive Exploration of Volume Line Integral Convolution Based on 3D Texture Mapping,” *Proceedings Visualization '99*, October 1999, pp. 233–240, IEEE Computer Society Press and ACM.
- [55] A. J. Ridgwell, “Dust in the Earth System: The Biogeochemical Linking of Land, Air, and Sea,” *Philosophical Transactions of the Royal Society A*, vol. 360, 2002, pp. 2905–2924.
- [56] J. Rohlf and J. Helman, “IRIS Performer: A High Performance Multiprocessing Toolkit for Real-Time 3D Graphics,” *SIGGRAPH 94 Conference Proceedings*, A. S. Glassner, ed. 1994, Annual Conference Series, pp. 381–394, ACM SIGGRAPH, Addison-Wesley, ISBN 0-89791-667-0.
- [57] W. Schroeder, K. Martin, and W. Lorensen, *The Visualization Toolkit, An Object-Oriented Approach to 3D Graphics*, 2nd edition, Prentice-Hall PTR, Upper Saddle River, NJ 07458, 1998, ISBN 0-13-954694-4.
- [58] *OpenGL Performer Version 2.5 Release Notes*, SGI, <http://www.sgi.com/software/performer>.
- [59] B. G. Tabachnick and L. S. Fidell, *Using Multivariate Statistics*, 4th edition, Allyn and Bacon, 160 Gould Street, Needham Heights, MA 02494, 2001.
- [60] R. Taylor, “Visualizing Multiple Fields on the Same Surface,” *IEEE Computer Graphics and Applications*, vol. 22, no. 3, May-June 2002, pp. 6–9.

- [61] I. Tegen and A. A. Lacis, "Modeling of Particle Size Distribution and Its Influence on the Radiative Properties of Mineral Dust Aerosol," *Journal of Geophysical Research*, vol. 101, no. D14, August 27 1996, pp. 19237–19244.
- [62] E. R. Tufte, *Envisioning Information*, Graphics Press, Cheshire, CT, 1990.
- [63] E. R. Tufte, *Visual Explanations*, Graphics Press, Cheshire, CT, 1997.
- [64] E. R. Tufte, *The Visual Display of Quantitative Information*, 2nd edition, Graphics Press, Cheshire, CT, 2001.
- [65] J. W. Tukey, *Exploratory Data Analysis*, Addison-Wesley, Reading, MA, 1977.
- [66] R. J. Vickery, "Information Visualization of Multiple Scalar Fields using Virtual Reality," Mississippi State University Institutional Review Board for the Protection of Human Subjects, December 2002, Docket #02-308.
- [67] R. J. Vickery, R. J. Brou, D. W. Carruth, T. R. Keen, R. J. Moorhead, and S. M. Doane, "Usability Issues in the Development of an Immersive System for Visualization of 5D Sedimentation Models," *9th International Conference on Human-Computer Interaction, Poster Sessions: Abridged Proceedings*. Human-Computer Interaction International, August 2001, pp. 62–64, Lawrence Erlbaum and Associates.
- [68] R. J. Vickery, T. R. Keen, R. J. Moorhead, R. J. Brou, D. W. Carruth, and S. M. Doane, "Volume Visualization of 5D Sedimentation Models," *Visualization and Data Analysis 2002*, R. F. Erbacher, P. C. Chen, M. Groehn, J. C. Roberts, and C. M. Wittenbrink, eds., San Jose, CA, January 2002, vol. 4665 of *Proceedings of SPIE*, pp. 165–176.
- [69] R. J. Vickery, T. R. Keen, R. J. Moorhead, J. Meyer, R. J. Brou, A. M. Noble, J. P. Martin, and S. M. Doane, "Rendering Particles for 5D Scalar Fields in a Virtual Environment: The Need for Speed," *High Performance Computing Symposium*, Orlando, FL, March 2003.
- [70] R. J. Vickery, T. R. Keen, R. J. Moorhead, J. Meyer, R. J. Brou, A. M. Noble, J. P. Martin, and S. M. Doane, "Interactive Poster: Effects of Relative Particle Sizing and Bin Consolidation Enhancements to a 5D Volume Visualization Algorithm," *Visualization 2002 DVD*, Boston, MA, October 2002, IEEE Computer Society Press and ACM.
- [71] C. Ware, *Information Visualization: Perception for Design*, Morgan Kaufmann, San Francisco, 2000.
- [72] C. Ware and W. Knight, "Using Visual Texture for Information Display," *ACM Transactions on Graphics*, vol. 14, no. 1, January 1995, pp. 3–20.



- [73] R. Washington, M. Todd, N. J. Middleton, and A. S. Goudie, “Dust-Storm Source Areas Determined by the Total Ozone Monitoring Spectrometer and Surface Observations,” *Annals of the Association of American Geographers*, vol. 93, no. 2, 2003, pp. 297–313.
- [74] B. Watson, A. Friedman, and A. McGaffey, “Using Naming Time to Evaluate Quality Predictors for Model Simplification,” *ACM CHI Conference*, 2000.
- [75] R. Wegenkittl, H. Löffelmann, and E. Gröller, “Visualizing the Behavior of Higher Dimensional Dynamical Systems,” *Proceedings Visualization '97*, 1997, pp. 119–125, IEEE Computer Society Press and ACM.
- [76] C. Weigle, W. Emigh, G. Liu, R. M. Taylor II, J. T. Enns, and C. G. Healey, “Oriented Sliver Textures: A Technique for Local Value Estimation of Multiple Scalar Fields,” *Proc. Graphics Interface 2000*, 2000, pp. 163–170.
- [77] P. C. Wong and R. D. Bergeron, “30 Years of Multidimensional Multivariate Visualization,” *Scientific Visualization: Overviews, Methodologies, and Techniques*, G. M. Nielson, H. Hagen, and H. Müller, eds., IEEE Computer Society, Los Alamitos, CA, 1997, chapter 1, pp. 3–34.
- [78] M. Woo, J. L. Neider, T. R. Davis, and D. R. Shreiner, *OpenGL Programming Guide, Third Edition*, Addison-Wesley, Reading, Mass., 1999.
- [79] G. Wyszecki and W. S. Stiles, *Color Science: Concepts and Methods, Quantitative Data and Formulae*, John Wiley and Sons, New York, 1982.
- [80] S. B. Ziegeler, *Using Virtual Environments to Visualize Atmospheric Data: Can It Improve a Meteorologist’s Potential to Analyze the Information?*, master’s thesis, Mississippi State University, May 2002.

## APPENDIX A

### DATASET AND TEST CASE INFORMATION

The datasets used in this study were provided courtesy of Dr. Timothy Keen from the Naval Research Lab at Stennis Space Center, Mississippi. The datasets represent a wide range of weather conditions, locations, and sediment classes. The detailed descriptions are given in Table 3.1. Geographic location information for each dataset is given in Figure A.1 through Figure A.6. Each map outlines the index information for the dataset along with longitude and latitude coordinates.



Figure A.1 Louisiana Coast Hurricane Andrew Dataset Location.



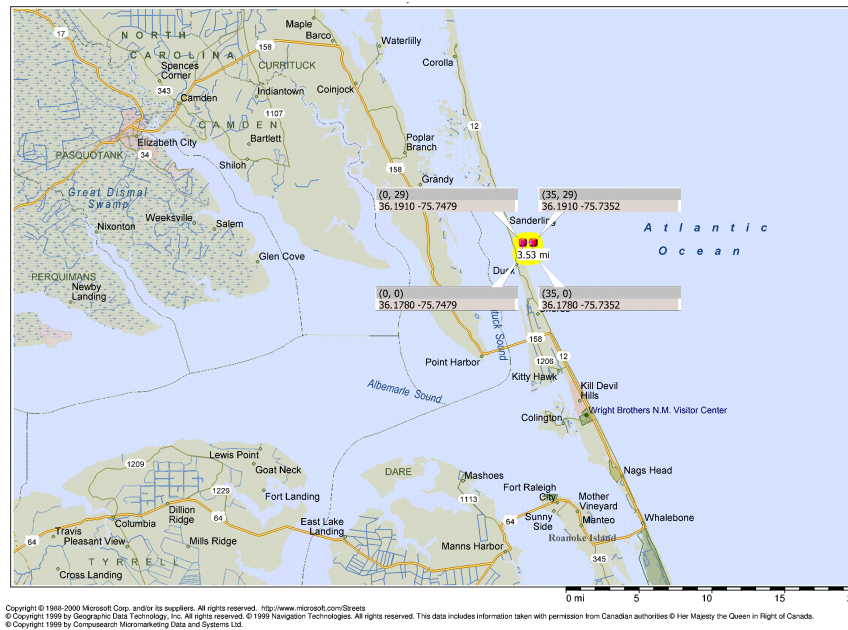


Figure A.2 Duck, North Carolina Dataset Location.

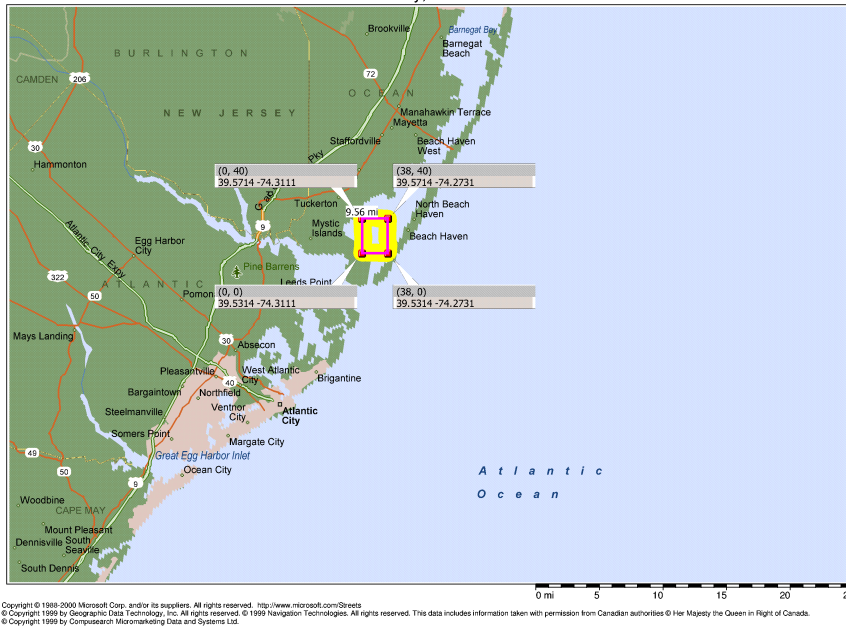


Figure A.3 Great Bay, New Jersey Dataset Location.

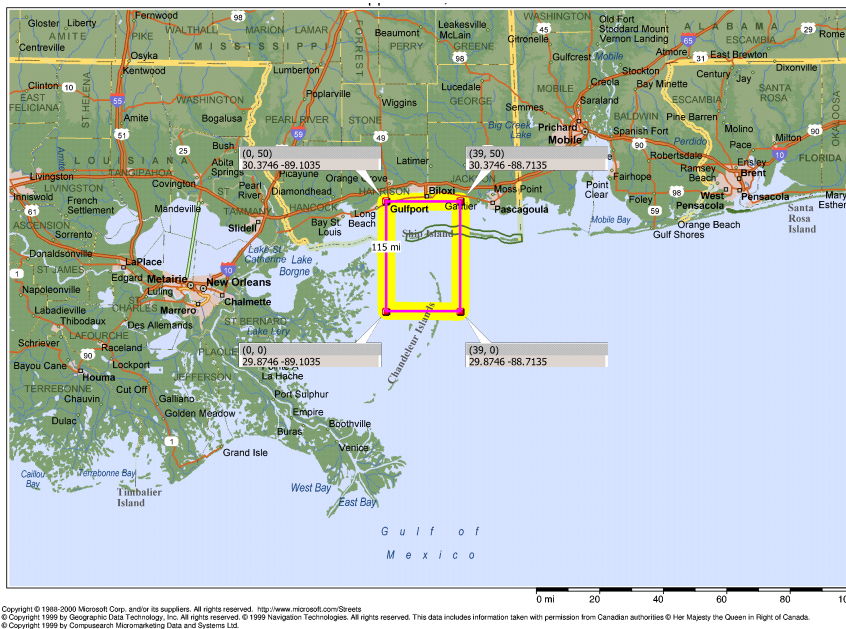


Figure A.4 Mississippi Sound MSB Dataset Location.

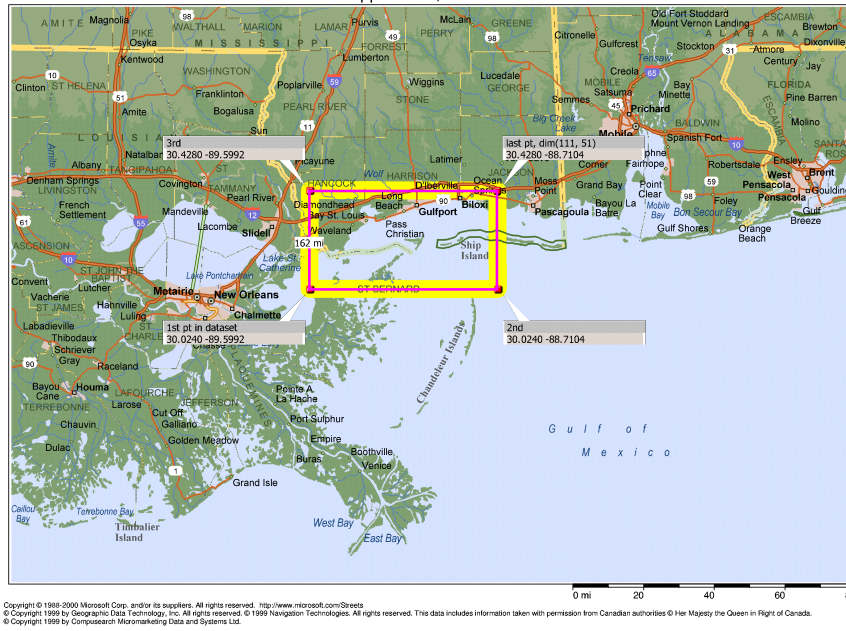


Figure A.5 Mississippi Sound Hurricane Camille Dataset Location.

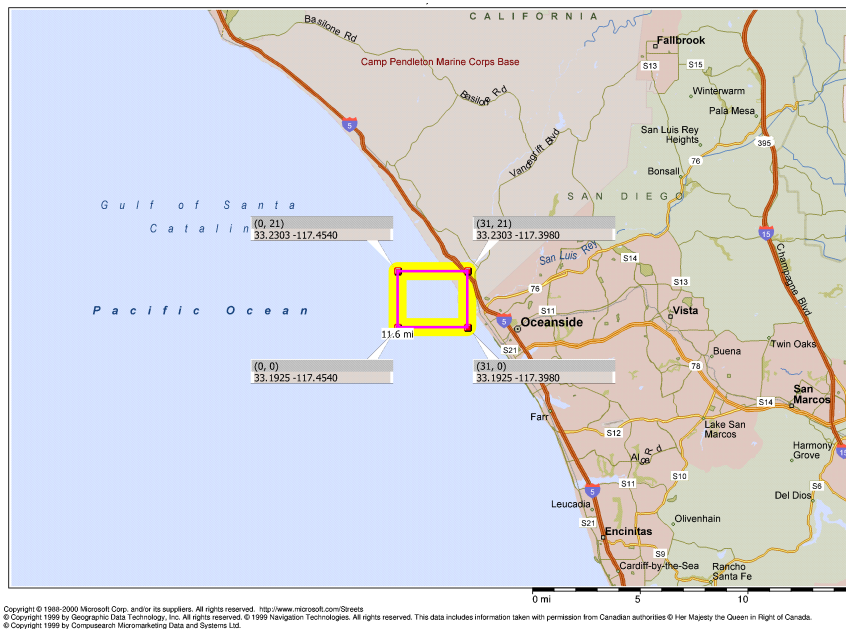


Figure A.6 Oceanside, California Dataset Location.

The following summary output was generated by the application for each dataset, and includes dimensions and ranges for variables computed, especially pertaining to the SSC variable.

-----  
 Andrew Dataset Summary  
 -----

NUMBER OF HEADERS: 83  
 NUMBER OF RECORDS: 635  
 IM: 355  
 JM: 262  
 LEVELS: 31

NUMBER OF SEDIMENT CLASSES: 20

GRAIN SIZE	PHI	CATEGORY
2.363000e-06	8.725165e+00	clay - mix w a little silt
3.460000e-06	8.175012e+00	clay - mix w a little silt
5.066000e-06	7.624937e+00	silt - very fine
7.417000e-06	7.074949e+00	silt - very fine
1.086000e-05	6.524832e+00	silt - fine
1.590000e-05	5.974829e+00	silt - medium
2.328000e-05	5.424765e+00	silt - medium
3.408000e-05	4.874931e+00	silt - coarse
4.989000e-05	4.325105e+00	silt - coarse
7.305000e-05	3.774972e+00	sand - very fine
1.069000e-04	3.225666e+00	sand - very fine
1.566000e-04	2.674844e+00	sand - fine
2.293000e-04	2.124692e+00	sand - fine
3.356000e-04	1.575185e+00	sand - medium
4.914000e-04	1.025030e+00	sand - medium
7.195000e-04	4.749334e-01	sand - coarse
1.053000e-03	-7.450542e-02	sand - very coarse
1.542000e-03	-6.248027e-01	sand - very coarse
2.258000e-03	-1.175045e+00	gravel - granule
3.306000e-03	-1.725087e+00	gravel - granule

DATA LONG DIMENSION: 74  
 DATA LAT DIMENSION: 51  
 DATA LONG MIN VALUE: -93.02272034  
 DATA LONG MAX VALUE: -89.37271881  
 DATA LAT MIN VALUE: 27.89660072  
 DATA LAT MAX VALUE: 30.39660072

format: min minidx mini minj mink mintstep max maxidx maxi maxj maxk maxtstep  
 sssp  
 AvgMinMaxSsc 0.000000e+00 2.244836e-01  
 AvgSscWtMethod 3  
 MinMaxAvgSsc 0.000000e+00 0 0 0 0 0 4.274262e+00 6289 73 33 1 0  
 MinMaxSscOverall 0.000000e+00 0 0 0 0 0 1.016401e+00 6215 73 32 1 0  
 MinSscOverallNonZero 5.007414e-09 54678 66 24 14 22  
 MinLog10SscOverallNonZero -8.300386e+00  
 MinMaxParticleContribOverall 0.000000e+00 0 0 0 0 0 1.310044e+10 6289 73 33 1 0  
 MinParticleContribOverallNonZero 2.000047e+00 36332 72 31 9 15  
 MinMaxParticleContribPerSlice 0.000000e+00 0 0 0 0 0 2.931145e+10 6289 73 33 1 0  
 MinParticleContribPerSliceNonZero 9.715678e-02 84099 35 14 22 24  
 MinSsc[grsz]  
 0.000000e+00 0 0 0 0 0  
 0.000000e+00 0 0 0 0 0  
 0.000000e+00 0 0 0 0 0  
 0.000000e+00 0 0 0 0 0

```

0.000000e+00 0 0 0 0 0
0.000000e+00 0 0 0 0 0
0.000000e+00 0 0 0 0 0
0.000000e+00 0 0 0 0 0
0.000000e+00 0 0 0 0 0
0.000000e+00 0 0 0 0 0
0.000000e+00 0 0 0 0 0
0.000000e+00 0 0 0 0 0
0.000000e+00 0 0 0 0 0
0.000000e+00 0 0 0 0 0
0.000000e+00 0 0 0 0 0
0.000000e+00 0 0 0 0 0
0.000000e+00 0 0 0 0 0
0.000000e+00 0 0 0 0 0
0.000000e+00 0 0 0 0 0
0.000000e+00 0 0 0 0 0
0.000000e+00 0 0 0 0 0
MinSscNonZero[grsz]
1.000000e+10 0 0 0 0 0
1.000000e+10 0 0 0 0 0
1.000000e+10 0 0 0 0 0
1.000000e+10 0 0 0 0 0
1.000000e+10 0 0 0 0 0
1.000000e+10 0 0 0 0 0
5.009377e-09 92193 63 21 24 25
5.012344e-09 27507 53 14 7 21
5.013983e-09 28294 26 25 7 15
5.009114e-09 4919 35 15 1 23
5.007767e-09 81416 16 29 21 24
5.007649e-09 54428 38 21 14 22
5.007414e-09 54678 66 24 14 22
5.009166e-09 114304 48 14 30 21
5.007737e-09 69465 53 20 18 20
5.008014e-09 61468 48 14 16 17
1.000000e+10 0 0 0 0 0
1.000000e+10 0 0 0 0 0
1.000000e+10 0 0 0 0 0
1.000000e+10 0 0 0 0 0
1.000000e+10 0 0 0 0 0
MaxSsc[grsz]
0.000000e+00 1 1 0 0 0
0.000000e+00 1 1 0 0 0
0.000000e+00 1 1 0 0 0
0.000000e+00 1 1 0 0 0
0.000000e+00 1 1 0 0 0
3.283576e-02 5301 47 20 1 24
2.293397e-01 6289 73 33 1 0
4.989535e-01 6289 73 33 1 0
8.442191e-01 6215 73 32 1 0
1.016401e+00 6215 73 32 1 0
9.107118e-01 6215 73 32 1 0
6.072913e-01 6215 73 32 1 0
2.443435e-01 6215 73 32 1 0
7.675255e-02 4936 52 15 1 21
2.882402e-02 4784 48 13 1 20
0.000000e+00 1 1 0 0 0
0.000000e+00 1 1 0 0 0
0.000000e+00 1 1 0 0 0
0.000000e+00 1 1 0 0 0
0.000000e+00 1 1 0 0 0
MinParticleContrib[grsz]
0.000000e+00 0 0 0 0 0
0.000000e+00 0 0 0 0 0
0.000000e+00 0 0 0 0 0
0.000000e+00 0 0 0 0 0

```

```

0.000000e+00  0  0  0  0  0
0.000000e+00  0  0  0  0  0
0.000000e+00  0  0  0  0  0
0.000000e+00  0  0  0  0  0
0.000000e+00  0  0  0  0  0
0.000000e+00  0  0  0  0  0
0.000000e+00  0  0  0  0  0
0.000000e+00  0  0  0  0  0
0.000000e+00  0  0  0  0  0
0.000000e+00  0  0  0  0  0
0.000000e+00  0  0  0  0  0
0.000000e+00  0  0  0  0  0
0.000000e+00  0  0  0  0  0
0.000000e+00  0  0  0  0  0
0.000000e+00  0  0  0  0  0
0.000000e+00  0  0  0  0  0
0.000000e+00  0  0  0  0  0
MinParticleContribNonZero[grsz]
1.000000e+10  0  0  0  0  0
1.000000e+10  0  0  0  0  0
1.000000e+10  0  0  0  0  0
1.000000e+10  0  0  0  0  0
1.000000e+10  0  0  0  0  0
8.981481e+02  92193  63  21  24  25
2.863172e+02  27507  53  14  7  21
9.129346e+01  28294  26  25  7  15
2.907206e+01  4919  35  15  1  23
9.258462e+00  81416  16  29  21  24
2.954312e+00  54428  38  21  14  22
2.001437e+00  84043  53  13  22  15
2.000364e+00  24739  23  28  6  26
2.000047e+00  36332  72  31  9  15
2.000462e+00  54222  54  18  14  19
1.000000e+10  0  0  0  0  0
1.000000e+10  0  0  0  0  0
1.000000e+10  0  0  0  0  0
1.000000e+10  0  0  0  0  0
1.000000e+10  0  0  0  0  0
MaxParticleContrib[grsz]
0.000000e+00  1  1  0  0  0
0.000000e+00  1  1  0  0  0
0.000000e+00  1  1  0  0  0
0.000000e+00  1  1  0  0  0
0.000000e+00  1  1  0  0  0
5.887234e+09  5301  47  20  1  24
1.310044e+10  6289  73  33  1  0
9.084830e+09  6289  73  33  1  0
4.899708e+09  6215  73  32  1  0
1.879144e+09  6215  73  32  1  0
5.372833e+08  6215  73  32  1  0
1.139665e+08  6215  73  32  1  0
1.460643e+07  6215  73  32  1  0
1.463465e+06  4936  52  15  1  21
1.750671e+05  4784  48  13  1  20
0.000000e+00  1  1  0  0  0
0.000000e+00  1  1  0  0  0
0.000000e+00  1  1  0  0  0
0.000000e+00  1  1  0  0  0
0.000000e+00  1  1  0  0  0
FindMinMaxOverAllTimeSteps 1

```

-----  
 Duck10 Dataset Summary  
 -----

NUMBER OF HEADERS: 73  
 NUMBER OF RECORDS: 325  
 IM: 36  
 JM: 30  
 LEVELS: 31

NUMBER OF SEDIMENT CLASSES: 10

GRAIN SIZE	PHI	CATEGORY
2.860000e-06	8.449769e+00	clay - mix w a little silt
6.130000e-06	7.349897e+00	silt - very fine
1.314000e-05	6.249891e+00	silt - fine
2.816000e-05	5.150209e+00	silt - medium
6.037000e-05	4.050024e+00	silt - coarse
1.294000e-04	2.950091e+00	sand - fine
2.774000e-04	1.849960e+00	sand - medium
5.946000e-04	7.500087e-01	sand - coarse
1.275000e-03	-3.504973e-01	sand - very coarse
2.732000e-03	-1.449958e+00	gravel - granule

DATA LONG DIMENSION: 36

DATA LAT DIMENSION: 30

DATA LONG MIN VALUE: -75.74790192

DATA LONG MAX VALUE: -75.73519897

DATA LAT MIN VALUE: 36.17800140

DATA LAT MAX VALUE: 36.19100189

format: min minidx mini minj mink mintstep max maxidx maxi maxj maxk maxtstep  
 sssp

AvgMinMaxSsc 0.000000e+00 1.259039e+03

AvgSscWtMethod 3

MinMaxAvgSsc 0.000000e+00 0 0 0 0 0 1.077421e+04 9803 35 37 1 2

MinMaxSscOverall 0.000000e+00 0 0 0 0 0 1.077150e+04 9803 35 37 1 2

MinSscOverallNonZero 2.650000e-09 69138 96 10 12 2

MinLog10SscOverallNonZero -8.576755e+00

MinMaxParticleContribOverall 0.000000e+00 0 0 0 0 0 9.435249e+14 6245 29 5 1 1

MinParticleContribOverallNonZero 2.000170e+00 19188 96 19 3 1

MinMaxParticleContribPerSlice 0.000000e+00 0 0 0 0 0 9.437270e+14 6245 29 5 1 1

MinParticleContribPerSliceNonZero 8.552703e+01 72074 35 37 12 2

MinSsc[grsz]

0.000000e+00 0 0 0 0 0

0.000000e+00 0 0 0 0 0

0.000000e+00 0 0 0 0 0

0.000000e+00 0 0 0 0 0

0.000000e+00 0 0 0 0 0

0.000000e+00 0 0 0 0 0

0.000000e+00 0 0 0 0 0

0.000000e+00 0 0 0 0 0

0.000000e+00 0 0 0 0 0

0.000000e+00 0 0 0 0 0

MinSscNonZero[grsz]

1.487915e-05 180253 100 42 31 2

4.082900e-06 168757 37 41 29 2

5.300973e-06 83173 34 35 14 2

2.650000e-09 72074 35 37 12 2

2.650000e-09 69138 96 10 12 2

2.650000e-09 155177 110 20 27 2

2.650024e-06 157019 65 37 27 1

2.650133e-06 119389 64 4 21 1

2.650659e-06 13096 109 15 2 1

2.651213e-06 29697 60 12 5 0

MaxSsc[grsz]



```

3.062640e+01 6245 29 5 1 1
1.187202e+02 6360 33 6 1 0
1.941673e+02 11191 91 49 1 0
1.077150e+04 9803 35 37 1 2
9.119921e+02 7927 46 20 1 2
3.172982e+02 8873 104 28 1 0
1.705867e+02 7454 17 16 1 1
5.466570e+01 8237 23 23 1 0
4.669865e+00 8265 51 23 1 2
1.616517e+01 8265 51 23 1 2
MinParticleContrib[grsz]
0.000000e+00 0 0 0 0 0
0.000000e+00 0 0 0 0 0
0.000000e+00 0 0 0 0 0
0.000000e+00 0 0 0 0 0
0.000000e+00 0 0 0 0 0
0.000000e+00 0 0 0 0 0
0.000000e+00 0 0 0 0 0
0.000000e+00 0 0 0 0 0
0.000000e+00 0 0 0 0 0
0.000000e+00 0 0 0 0 0
0.000000e+00 0 0 0 0 0
0.000000e+00 0 0 0 0 0
MinParticleContribNonZero[grsz]
4.583905e+08 180253 100 42 31 2
1.277447e+07 168757 37 41 29 2
1.683934e+06 83173 34 35 14 2
8.552703e+01 72074 35 37 12 2
8.680363e+00 69138 96 10 12 2
3.473439e+00 143855 110 20 25 2
8.947177e+01 157019 65 37 27 1
9.085493e+00 119389 64 4 21 1
2.000732e+00 68694 96 6 12 0
2.000170e+00 19188 96 19 3 1
MaxParticleContrib[grsz]
9.435249e+14 6245 29 5 1 1
3.714485e+14 6360 33 6 1 0
6.168017e+13 11191 91 49 1 0
3.476432e+14 9803 35 37 1 2
2.987329e+12 7927 46 20 1 2
1.055408e+11 8873 104 28 1 0
5.759454e+09 7454 17 16 1 1
1.874113e+08 8237 23 23 1 0
1.623788e+06 8265 51 23 1 2
5.713388e+05 8265 51 23 1 2
FindMinMaxOverAllTimeSteps 1

```

-----  
Duck20 Dataset Summary  
-----

```

NUMBER OF HEADERS: 83
NUMBER OF RECORDS: 635
IM: 36
JM: 30
LEVELS: 31
NUMBER OF SEDIMENT CLASSES: 20

```

GRAIN SIZE	PHI	CATEGORY
2.363000e-06	8.725165e+00	clay - mix w a little silt
3.460000e-06	8.175012e+00	clay - mix w a little silt
5.066000e-06	7.624937e+00	silt - very fine
7.417000e-06	7.074949e+00	silt - very fine
1.086000e-05	6.524832e+00	silt - fine
1.590000e-05	5.974829e+00	silt - medium
2.328000e-05	5.424765e+00	silt - medium







```

4.900066e+03 6564 12 2 6 31
1.563512e+03 19092 12 20 17 14
4.973317e+02 24172 16 11 22 22
1.584167e+02 21670 34 1 20 13
5.053048e+01 15993 9 24 14 0
1.609700e+01 12482 26 16 11 9
5.128052e+00 7726 22 4 7 7
2.000286e+00 5457 21 1 5 11
2.004049e+00 5450 14 1 5 10
2.008665e+00 1132 16 1 1 10
1.000000e+10 0 0 0 0 0
MaxParticleContrib[grsz]
0.000000e+00 1 1 0 0 0
0.000000e+00 1 1 0 0 0
0.000000e+00 1 1 0 0 0
1.334817e+15 1194 6 3 1 22
7.607858e+14 2063 11 27 1 20
6.752111e+13 1875 3 22 1 10
2.013089e+13 1977 33 24 1 21
1.216374e+13 1223 35 3 1 23
1.598137e+12 1977 33 24 1 21
3.618617e+11 1448 8 10 1 18
7.089113e+10 1304 8 6 1 15
1.103330e+10 1523 11 12 1 17
5.734393e+09 1593 9 14 1 17
4.999025e+08 1191 3 3 1 24
7.526900e+08 1230 6 4 1 27
5.381173e+08 1230 6 4 1 27
1.706378e+05 2128 4 29 1 8
1.159412e+04 2092 4 28 1 8
4.754906e+02 1084 4 0 1 16
0.000000e+00 1 1 0 0 0
FindMinMaxOverAllTimeSteps 1
format: min minidx mini minj mink mintstep max maxidx maxi maxj maxx maxtstep
findoveralltstep
wd -1.287500e+01 35 35 0 0 0 1.000000e+00 33480 0 0 31 0 0

```

-----  
Great Bay Dataset Summary  
-----

```

NUMBER OF HEADERS: 83
NUMBER OF RECORDS: 635
IM: 177
JM: 198
LEVELS: 31
NUMBER OF SEDIMENT CLASSES: 20

```

GRAIN SIZE	PHI	CATEGORY
2.363000e-06	8.725165e+00	clay - mix w a little silt
3.460000e-06	8.175012e+00	clay - mix w a little silt
5.066000e-06	7.624937e+00	silt - very fine
7.417000e-06	7.074949e+00	silt - very fine
1.086000e-05	6.524832e+00	silt - fine
1.590000e-05	5.974829e+00	silt - medium
2.328000e-05	5.424765e+00	silt - medium
3.408000e-05	4.874931e+00	silt - coarse
4.989000e-05	4.325105e+00	silt - coarse
7.305000e-05	3.774972e+00	sand - very fine
1.069000e-04	3.225666e+00	sand - very fine
1.566000e-04	2.674844e+00	sand - fine
2.293000e-04	2.124692e+00	sand - fine
3.356000e-04	1.575185e+00	sand - medium
4.914000e-04	1.025030e+00	sand - medium





```

1.000000e+10  0  0  0  0  0
1.000000e+10  0  0  0  0  0
1.000000e+10  0  0  0  0  0
MaxParticleContrib[grsz]
0.000000e+00  1  1  0  0  0
0.000000e+00  1  1  0  0  0
0.000000e+00  1  1  0  0  0
0.000000e+00  1  1  0  0  0
0.000000e+00  1  1  0  0  0
0.000000e+00  1  1  0  0  0
7.904907e+11  2037  9  11  1  27
3.167867e+11  2484  27  22  1  26
2.613858e+11  1996  7  10  1  14
5.316466e+10  1736  20  3  1  28
3.763765e+10  2002  13  10  1  9
2.642167e+10  1785  30  4  1  22
5.473431e+10  2109  3  13  1  10
7.371370e+08  2223  0  16  1  21
4.566156e+07  2223  0  16  1  21
1.125730e+06  2563  28  24  1  8
0.000000e+00  1  1  0  0  0
0.000000e+00  1  1  0  0  0
0.000000e+00  1  1  0  0  0
0.000000e+00  1  1  0  0  0
0.000000e+00  1  1  0  0  0
0.000000e+00  1  1  0  0  0
FindMinMaxOverAllTimeSteps 1

```

-----  
MSB Dataset Summary  
-----

```

NUMBER OF HEADERS: 78
NUMBER OF RECORDS: 480
IM: 182
JM: 139
LEVELS: 31
NUMBER OF SEDIMENT CLASSES: 15

```

GRAIN SIZE	PHI	CATEGORY
2.518000e-06	8.633506e+00	clay - mix w a little silt
4.187000e-06	7.899867e+00	silt - very fine
6.960000e-06	7.166697e+00	silt - very fine
1.157000e-05	6.433467e+00	silt - fine
1.924000e-05	5.699747e+00	silt - medium
3.198000e-05	4.966686e+00	silt - coarse
5.317000e-05	4.233244e+00	silt - coarse
8.839000e-05	3.499973e+00	sand - very fine
1.469000e-04	2.767094e+00	sand - fine
2.443000e-04	2.033274e+00	sand - fine
4.061000e-04	1.300093e+00	sand - medium
6.752000e-04	5.666132e-01	sand - coarse
1.122000e-03	-1.660727e-01	sand - very coarse
1.866000e-03	-8.999490e-01	sand - very coarse
3.102000e-03	-1.633199e+00	gravel - granule

```

DATA LONG DIMENSION: 40
DATA LAT DIMENSION: 51
DATA LONG MIN VALUE: -89.10350037
DATA LONG MAX VALUE: -88.71350098
DATA LAT MIN VALUE: 29.87459946
DATA LAT MAX VALUE: 30.37459946

```

```

format: min minidx mini minj mink mintstep  max maxidx maxi maxj maxk maxtstep
sssp
AvgMinMaxSsc 0.000000e+00 4.608286e-04
AvgSscWtMethod 3

```

```

MinMaxAvgSsc 0.000000e+00 0 0 0 0 0 6.071728e-03 2191 31 3 1 30
MinMaxSscOverall 0.000000e+00 0 0 0 0 0 2.755421e-03 2191 31 3 1 30
MinSscOverallNonZero 5.220599e-08 15828 28 38 7 30
MinLog10SscOverallNonZero -7.282279e+00
MinMaxParticleContribOverall 0.000000e+00 0 0 0 0 0 7.366708e+07 2194 34 3 1 31
MinParticleContribOverallNonZero 1.190312e+01 38832 32 1 19 28
MinMaxParticleContribPerSlice 0.000000e+00 0 0 0 0 0 9.238215e+07 2242 2 5 1 29
MinParticleContribPerSliceNonZero 1.190312e+01 38832 32 1 19 28
MinSsc[grsz]
0.000000e+00 0 0 0 0 0
0.000000e+00 0 0 0 0 0
0.000000e+00 0 0 0 0 0
0.000000e+00 0 0 0 0 0
0.000000e+00 0 0 0 0 0
0.000000e+00 0 0 0 0 0
0.000000e+00 0 0 0 0 0
0.000000e+00 0 0 0 0 0
0.000000e+00 0 0 0 0 0
0.000000e+00 0 0 0 0 0
0.000000e+00 0 0 0 0 0
0.000000e+00 0 0 0 0 0
0.000000e+00 0 0 0 0 0
0.000000e+00 0 0 0 0 0
0.000000e+00 0 0 0 0 0
0.000000e+00 0 0 0 0 0
0.000000e+00 0 0 0 0 0
0.000000e+00 0 0 0 0 0
0.000000e+00 0 0 0 0 0
MinSscNonZero[grsz]
1.000000e+10 0 0 0 0 0
1.000000e+10 0 0 0 0 0
1.000000e+10 0 0 0 0 0
5.226741e-08 23542 22 27 11 30
5.221120e-08 55830 30 18 27 30
5.231188e-08 37431 31 17 18 29
5.220599e-08 15828 28 38 7 30
5.256037e-08 63270 30 0 31 26
5.235650e-08 38832 32 1 19 28
1.000000e+10 0 0 0 0 0
1.000000e+10 0 0 0 0 0
1.000000e+10 0 0 0 0 0
1.000000e+10 0 0 0 0 0
1.000000e+10 0 0 0 0 0
1.000000e+10 0 0 0 0 0
1.000000e+10 0 0 0 0 0
MaxSsc[grsz]
0.000000e+00 1 1 0 0 0
0.000000e+00 1 1 0 0 0
0.000000e+00 1 1 0 0 0
1.583135e-04 2194 34 3 1 31
2.418346e-04 2074 34 0 1 30
6.046703e-04 2073 33 0 1 30
2.176035e-03 2191 31 3 1 30
2.755421e-03 2191 31 3 1 30
9.761535e-04 2511 31 11 1 30
0.000000e+00 1 1 0 0 0
0.000000e+00 1 1 0 0 0
0.000000e+00 1 1 0 0 0
0.000000e+00 1 1 0 0 0
0.000000e+00 1 1 0 0 0
0.000000e+00 1 1 0 0 0
0.000000e+00 1 1 0 0 0
0.000000e+00 1 1 0 0 0
MinParticleContrib[grsz]
0.000000e+00 0 0 0 0 0
0.000000e+00 0 0 0 0 0
0.000000e+00 0 0 0 0 0
0.000000e+00 0 0 0 0 0
0.000000e+00 0 0 0 0 0
0.000000e+00 0 0 0 0 0
0.000000e+00 0 0 0 0 0
0.000000e+00 0 0 0 0 0
0.000000e+00 0 0 0 0 0
0.000000e+00 0 0 0 0 0

```

```

0.000000e+00  0  0  0  0  0
0.000000e+00  0  0  0  0  0
0.000000e+00  0  0  0  0  0
0.000000e+00  0  0  0  0  0
0.000000e+00  0  0  0  0  0
0.000000e+00  0  0  0  0  0
0.000000e+00  0  0  0  0  0
0.000000e+00  0  0  0  0  0
0.000000e+00  0  0  0  0  0
0.000000e+00  0  0  0  0  0
MinParticleContribNonZero[grsz]
1.000000e+10  0  0  0  0  0
1.000000e+10  0  0  0  0  0
1.000000e+10  0  0  0  0  0
2.432128e+04  23542  22  27  11  30
5.283284e+03  55830  30  18  27  30
1.152711e+03  37431  31  17  18  29
2.503087e+02  15828  28  38  7  30
5.485353e+01  63270  30  0  31  26
1.190312e+01  38832  32  1  19  28
1.000000e+10  0  0  0  0  0
1.000000e+10  0  0  0  0  0
1.000000e+10  0  0  0  0  0
1.000000e+10  0  0  0  0  0
1.000000e+10  0  0  0  0  0
1.000000e+10  0  0  0  0  0
1.000000e+10  0  0  0  0  0
MaxParticleContrib[grsz]
0.000000e+00  1  1  0  0  0
0.000000e+00  1  1  0  0  0
0.000000e+00  1  1  0  0  0
7.366708e+07  2194  34  3  1  31
2.447139e+07  2074  34  0  1  30
1.332413e+07  2073  33  0  1  30
1.043330e+07  2191  31  3  1  30
2.875638e+06  2191  31  3  1  30
2.219260e+05  2511  31  11  1  30
0.000000e+00  1  1  0  0  0
0.000000e+00  1  1  0  0  0
0.000000e+00  1  1  0  0  0
0.000000e+00  1  1  0  0  0
0.000000e+00  1  1  0  0  0
0.000000e+00  1  1  0  0  0
FindMinMaxOverAllTimeSteps 1

```

-----  
Mississippi Sound Dataset Summary  
-----

NUMBER OF HEADERS: 73  
NUMBER OF RECORDS: 325  
IM: 286  
JM: 210  
LEVELS: 31

NUMBER OF SEDIMENT CLASSES: 10

GRAIN SIZE	PHI	CATEGORY
2.860000e-06	8.449769e+00	clay - mix w a little silt
6.130000e-06	7.349897e+00	silt - very fine
1.314000e-05	6.249891e+00	silt - fine
2.816000e-05	5.150209e+00	silt - medium
6.037000e-05	4.050024e+00	silt - coarse
1.294000e-04	2.950091e+00	sand - fine
2.774000e-04	1.849960e+00	sand - medium
5.946000e-04	7.500087e-01	sand - coarse
1.275000e-03	-3.504973e-01	sand - very coarse



2.732000e-03 -1.449958e+00 gravel - granule  
 DATA LONG DIMENSION: 111  
 DATA LAT DIMENSION: 51  
 DATA LONG MIN VALUE: -89.59923553  
 DATA LONG MAX VALUE: -88.71044159  
 DATA LAT MIN VALUE: 30.02396011  
 DATA LAT MAX VALUE: 30.42795944

format: min minidx mini minj mink mintstep max maxidx maxi maxj maxk maxtstep  
 sssp  
 AvgMinMaxSsc 0.000000e+00 1.259039e+03  
 AvgSscWtMethod 3  
 MinMaxAvgSsc 0.000000e+00 0 0 0 0 0 1.077421e+04 9803 35 37 1 2  
 MinMaxSscOverall 0.000000e+00 0 0 0 0 0 1.077150e+04 9803 35 37 1 2  
 MinSscOverallNonZero 2.650000e-09 69138 96 10 12 2  
 MinLog10SscOverallNonZero -8.576755e+00  
 MinMaxParticleContribOverall 0.000000e+00 0 0 0 0 0 9.435249e+14 6245 29 5 1 1  
 MinParticleContribOverallNonZero 2.000170e+00 19188 96 19 3 1  
 MinMaxParticleContribPerSlice 0.000000e+00 0 0 0 0 0 9.437270e+14 6245 29 5 1 1  
 MinParticleContribPerSliceNonZero 8.552703e+01 72074 35 37 12 2  
 MinSsc[grsz]  
 0.000000e+00 0 0 0 0 0  
 0.000000e+00 0 0 0 0 0  
 0.000000e+00 0 0 0 0 0  
 0.000000e+00 0 0 0 0 0  
 0.000000e+00 0 0 0 0 0  
 0.000000e+00 0 0 0 0 0  
 0.000000e+00 0 0 0 0 0  
 0.000000e+00 0 0 0 0 0  
 0.000000e+00 0 0 0 0 0  
 0.000000e+00 0 0 0 0 0  
 MinSscNonZero[grsz]  
 1.487915e-05 180253 100 42 31 2  
 4.082900e-06 168757 37 41 29 2  
 5.300973e-06 83173 34 35 14 2  
 2.650000e-09 72074 35 37 12 2  
 2.650000e-09 69138 96 10 12 2  
 2.650000e-09 155177 110 20 27 2  
 2.650024e-06 157019 65 37 27 1  
 2.650133e-06 119389 64 4 21 1  
 2.650659e-06 13096 109 15 2 1  
 2.651213e-06 29697 60 12 5 0  
 MaxSsc[grsz]  
 3.062640e+01 6245 29 5 1 1  
 1.187202e+02 6360 33 6 1 0  
 1.941673e+02 11191 91 49 1 0  
 1.077150e+04 9803 35 37 1 2  
 9.119921e+02 7927 46 20 1 2  
 3.172982e+02 8873 104 28 1 0  
 1.705867e+02 7454 17 16 1 1  
 5.466570e+01 8237 23 23 1 0  
 4.669865e+00 8265 51 23 1 2  
 1.616517e+01 8265 51 23 1 2  
 MinParticleContrib[grsz]  
 0.000000e+00 0 0 0 0 0  
 0.000000e+00 0 0 0 0 0  
 0.000000e+00 0 0 0 0 0  
 0.000000e+00 0 0 0 0 0  
 0.000000e+00 0 0 0 0 0  
 0.000000e+00 0 0 0 0 0  
 0.000000e+00 0 0 0 0 0  
 0.000000e+00 0 0 0 0 0  
 0.000000e+00 0 0 0 0 0  
 0.000000e+00 0 0 0 0 0

```

0.000000e+00  0  0  0  0  0
MinParticleContribNonZero[grsz]
4.583905e+08  180253  100  42  31  2
1.277447e+07  168757  37  41  29  2
1.683934e+06  83173  34  35  14  2
8.552703e+01  72074  35  37  12  2
8.680363e+00  69138  96  10  12  2
3.473439e+00  143855  110  20  25  2
8.947177e+01  157019  65  37  27  1
9.085493e+00  119389  64  4  21  1
2.000732e+00  68694  96  6  12  0
2.000170e+00  19188  96  19  3  1
MaxParticleContrib[grsz]
9.435249e+14  6245  29  5  1  1
3.714485e+14  6360  33  6  1  0
6.168017e+13  11191  91  49  1  0
3.476432e+14  9803  35  37  1  2
2.987329e+12  7927  46  20  1  2
1.055408e+11  8873  104  28  1  0
5.759454e+09  7454  17  16  1  1
1.874113e+08  8237  23  23  1  0
1.623788e+06  8265  51  23  1  2
5.713388e+05  8265  51  23  1  2
FindMinMaxOverAllTimeSteps 1

```

```

-----
Oceanside Dataset Description With Variables (netCDF version)
-----

```

```

NUMBER OF HEADERS =    64
NUMBER OF RECORDS =    46
IM =    36
JM =    30
LEVELS =    31
Z HEIGHT ABOVE BED (M):
0.1854E-02
0.2940E-02
0.4662E-02
0.7392E-02
0.1172E-01
0.1859E-01
0.2947E-01
0.4673E-01
0.7410E-01
0.1175E+00
0.1863E+00
0.2026E+00
0.2204E+00
0.2397E+00
0.2607E+00
0.2836E+00
0.3084E+00
0.3355E+00
0.3649E+00
0.3969E+00
0.4316E+00
0.4695E+00
0.5106E+00
0.5554E+00
0.6041E+00
0.6570E+00
0.7146E+00
0.7772E+00

```

```

0.8453E+00
0.9194E+00
0.1000E+01
NUMBER OF SEDIMENT CLASSES =      1-20
SIZE CLASS MID POINTS (M): (will have up to 20 entries here)
0.8839E-04
VARIABLES:
LONGITUDE
LATITUDE
WD: WATER DEPTH
UB: E-W BOTTOM CURRENT
VB: N-S BOTTOM CURRENT
WO: WAVE ORBITAL
WC: WAVE CURRENT
KBC
KB
KBRP
KBST
USTARC
USTARCW
URUW
DW
RH: RIPPLE HEIGHT
RL: RIPPLE LENGTH
ISSC: INTEG. SUSPENDED SEDIMENT CONC. (KG/M^2)
RSD: RESUSPENSION DEPTH (M)
ALD: ACTIVE LAYER DEPTH (M)
RWD: REWORKING DEPTH (M)
NBTL: NEAR-BED TRANSPORT LAYER (M)
SPECTRAL SUSPENDED SEDIMENT PROFILES (KG/M^3)
CONCENTRATION (KG/M^3): CLASS      1  LEVEL      1
through
CONCENTRATION (KG/M^3): CLASS      1  LEVEL     31

```

-----  
Oceanside Dataset Summary  
-----

```

NUMBER OF HEADERS: 83
NUMBER OF RECORDS: 635
IM: 32
JM: 22
LEVELS: 31

```

NUMBER OF SEDIMENT CLASSES: 20

GRAIN SIZE	PHI	CATEGORY
2.363000e-06	8.725165e+00	clay - mix w a little silt
3.460000e-06	8.175012e+00	clay - mix w a little silt
5.066000e-06	7.624937e+00	silt - very fine
7.417000e-06	7.074949e+00	silt - very fine
1.086000e-05	6.524832e+00	silt - fine
1.590000e-05	5.974829e+00	silt - medium
2.328000e-05	5.424765e+00	silt - medium
3.408000e-05	4.874931e+00	silt - coarse
4.989000e-05	4.325105e+00	silt - coarse
7.305000e-05	3.774972e+00	sand - very fine
1.069000e-04	3.225666e+00	sand - very fine
1.566000e-04	2.674844e+00	sand - fine
2.293000e-04	2.124692e+00	sand - fine
3.356000e-04	1.575185e+00	sand - medium
4.914000e-04	1.025030e+00	sand - medium
7.195000e-04	4.749334e-01	sand - coarse
1.053000e-03	-7.450542e-02	sand - very coarse
1.542000e-03	-6.248027e-01	sand - very coarse





```

MaxParticleContrib[grsz]
1.529269e+12 797 29 2 1 8
1.314182e+12 797 29 2 1 8
9.924484e+11 797 29 2 1 8
6.573443e+11 797 29 2 1 8
3.816865e+11 797 29 2 1 8
1.946176e+11 797 29 2 1 8
8.736376e+10 797 29 2 1 8
3.476684e+10 797 29 2 1 8
1.432854e+10 1214 30 15 1 6
9.836793e+09 1333 21 19 1 5
7.575587e+09 1302 22 18 1 8
2.070442e+09 1303 23 18 1 8
1.171629e+08 797 29 2 1 8
2.391342e+07 862 30 4 1 8
3.002595e+06 862 30 4 1 8
2.919900e+05 862 30 4 1 8
0.000000e+00 1 1 0 0 0
0.000000e+00 1 1 0 0 0
0.000000e+00 1 1 0 0 0
0.000000e+00 1 1 0 0 0
FindMinMaxOverAllTimeSteps 1

```

For a description of each test case used for the actual experiment of the user study described in Chapter 4, see Table A.1. This table gives the index locations and area sizes for each of the test cases. The quadrant location of the cell on the front wall of the CAVE is also given in terms of Upper Left (UL), Upper Right (UR), Lower Left (LL), and Lower Right (LR). The test cases included for the user study training and examples are presented in Table A.2 and Table A.3.

Table A.1 User Study Test Cases: Main Experiment.

**ACTUAL**

Task1 - Find the single color cell Z Scale = 1

XY Area	Color	N	Dataset	Run	Test Case	Time Step	Front Wall Position								Quadrant Location	
							I Low	I High	J Low	J High	UL	UR	LL	LR		
small 4x4	green	1	mssnd	22	9	0	84	87	1	4				1	LL Quad, corner	
med 7x7	green	1	mssnd	22	8	0	18	24	6	12				1	LR Quad	
large 10x10	green	1	mssnd	22	2	2	9	18	9	18	1				UL Quad, 2nd row middle	
small 4x4	red	1	msb	16	1	30	31	34	9	12		1			UR Quad, top row	
med 7x7	red	1	duck10	20	2	9	19	25	16	22	1	1			UL or UR Quad, mid region	
large 10x10	red	1	mssnd	22	7	2	95	104	2	11				1	LR Quad, bottom row	
small 4x4	blue	1	gbay	23	3	9	30	33	3	6		1			UR Quad	
med 7x7	blue	1	duck10	20	1	22	3	9	1	7			1		LL Quad, bottom row, 2nd cell	
large 10x10	blue	1	mssnd	22	5	2	52	61	12	21			1		LL Quad, middle left edge	
Total		9									Totals	2	3	3	2	9

Task2 - Identify whether checkerboard pattern is present

XY Area	Pattern	N	Dataset	Run	Test Case	Time Step	I Low	I High	J Low	J High
small 4x4	check	1	duck20	31	2	23	10	13	15	18
med 7x7	check	1	andrew	30	1	23	25	31	19	25
large 10x10	check	1	andrew	26	1	24	23	32	19	28
small 4x4	none	1	andrew	30	2	22	55	58	19	22
med 7x7	none	1	duck20	31	1	16	12	18	4	10
large 10x10	none	1	duck20	25	2	23	10	19	8	17
Total		6								

Table A.2 User Study Test Cases: Training.

**TRAINING**

Task1 - Find the single color cell Z Scale = 1

XY Area	Color	N	Dataset	Run	Test Case	Time Step	Front Wall Position								Quadrant Location	
							I Low	I High	J Low	J High	UL	UR	LL	LR		
med 7x7	green	1	mssnd	24	4	1	28	34	6	12				1	LR Quad, corner	
small 4x4	red	1	gbay	23	4	7	24	27	2	5				1	LR Quad, or UL Quad for red	
large 10x10	blue	1	mssnd	22	10	1	50	59	28	37						
Total		3									Totals	0	0	0	2	2

Task2 - Identify whether checkerboard pattern is present

XY Area	Pattern	N	Dataset	Run	Test Case	Time Step	I Low	I High	J Low	J High
large 10x10	check	1	andrew	26	14	22	30	39	16	25
large 10x10	none	1	duck20	28	6	22	24	33	19	28
Total		2								

Table A.3 User Study Test Cases: Examples.

**EXAMPLES**

Task1 - Find the single color cell      Z Scale = 1

XY Area	Color	N	Dataset	Run	Test Case	Time Step	Front Wall Position								Quadrant Location	
							I Low	I High	J Low	J High	UL	UR	LL	LR		
med 7x7	green	1	mssnd	29	3	1	13	19	13	19		1				UL Quad UR Quad
large 10x10	red	1	mssnd	24	2	0	89	98	7	16	1					
small 4x4	blue	1	gbay	23	1	8	20	23	35	38		1				
Total		3									Totals	1	2	0	0	3

Task2 - Identify whether checkerboard pattern is present

XY Area	Pattern	N	Dataset	Run	Test Case	Time Step	I Low	I High	J Low	J High
large 10x10	check	1	andrew	26	2	25	20	29	21	30
large 10x10	none	1	duck20	28	4	16	24	33	1	10
Total		2								



The test cases for the performance study described in Chapter 5 were all taken from the Oceanside dataset, time step 5, dated 10/23/1995 08:18. This time step contained a good range of sedimentation classes for the desired configurations. The specific test case details are given in Table A.4.

Table A.4 Performance Study Test Cases.

Num	Description	I Low	I High	J Low	J High	Layers	Points Per Layer	Resolutions
1	Shallow Region A	20	31	1	21	1-8	252	64x64
2	Shallow Region B	26	31	0	21	1-31	132	16x16
3	Shallow Region B	26	31	0	21	1-3	132	16x16, 32x32, 64x64, 128x128

For copyright permission information on the maps included in this appendix see <http://www.microsoft.com/permission/copyrgt/cop-img.htm#Maps>. An excerpt from the web page is shown in Figure A.7.

## Permission: Use of Images

### **MAPS FROM: Microsoft Streets & Trips (version 2000 & 2001)**

Please note that Microsoft is contractually limited by third party content providers as to the quantity of maps and the type of use permitted by end-users. End users of these mapping products are currently restricted to redistribution of no more than 1000 copies of maps from Microsoft Streets & Trips provided that you do not sell or sublicense such reproduced maps. You must retain, and not delete or alter, any and all legal notices contained with the maps, including, but not limited to, copyright notices. These restrictions apply to all forms of distribution, including web site distribution. Provided that you follow the guidelines outlined here, no further written permission is required or necessary.

For Microsoft Streets and Trips version 2002, please refer to the End User License Agreement, *specifically, Section 1, Grant of License, Permitted Use of Maps.*

For information on how to add Streets & Trips maps to web sites please see <http://www.microsoft.com/streets/>.

If you wish to distribute a quantity of maps in excess of 1000 from Streets & Trips, you will need to acquire an additional license for every 1000 maps created. For more information on licensing restrictions please review the End User License Agreement (EULA) agreed to when installing the product.

<http://www.microsoft.com/permission/copyrgt/cop-img.htm> 10/6/2003

Figure A.7 Microsoft Copyright Permission for Maps.

## APPENDIX B

### DISTRIBUTION NORMALIZATION PROCESS

This Appendix describes the detailed steps taken to normalize the distributions for 18 Task 1 cases as shown in Table 4.2, and 12 Task 2 cases in Table 4.3. In the literature, cases are often called treatments or conditions [15]. In order to use parametric statistical methods, such as MANOVA, the distributions for each case must be considered normal distributions [8, 59]. The distributions can be tested for normality at the .05 significance level using SPSS Explore options. The distributions that fail can be adjusted using several accepted approaches until they pass the normality test. The results of MANOVA testing are valid with respect to the modified distributions, and the changes made with appropriate justifications are stated in the results.

The *Time* distributions tended to have most of the values to the left of the mean but also trailing off to extremely long values as shown in Figure B.1 for Task 1 (the Task 2 distributions are similar). This means that the median was considerably less than the mean, because the few long *Time* values shifted the mean to the right in the distribution. The resulting statistics for *Time* are shown in Table B.1 for Task 1 and Table B.2 for Task 2. The extremely long values are considered outliers, but to include as many of them as possible, a transformation can be used. A common transformation that is done for these

types of distributions is a  $\log_{10}$  transformation [59]. This was done as a first step for both Task 1 and Task 2 data. This tends to bring outliers closer to the mean.

The remaining outliers can be handled by either deletion or modification. In practice, both approaches are used [59]. When examining the distributions based on subject, it was found that one subject in particular tended to have extremely long *Time* values for almost all cases. Deleting this subject improved the normality tests for almost all distributions in both tasks, so the final analysis was done without this subject, leaving 49 total. Other extreme outliers were adjusted individually until problem distributions could pass the SPSS normality tests. In SPSS, outliers are identified in Stem-and-Leaf plots, as well as Box plots. The criteria for determination is based on a concept known as “Tukey’s Hinges” [59, 65]. In this approach a value that is outside a range defined by  $1.5 * \text{InterquartileRange}$  is considered to be an outlier, where the *InterquartileRange* is the range of the middle 50% of the observations [25]. A value outside more than  $3 * \text{InterquartileRange}$  is considered to be an extreme. Both outliers and extremes cause distributions to not be normal. In this case, all outliers and extremes in the transformed distributions that were the result of extremely long *Time* values were set to  $1.5 * \text{InterquartileRange}$ . This has the effect of setting a maximum time cutoff for each case. This improved all of the distributions considerably, but for a few cases there were too many responses at extreme values for them to be considered normal. For Task 1, Case 13, three additional outliers were set to the original distribution average value. For Task 2, Case 1, two extremes were adjusted in this manner, and for Case 5, seven extremes

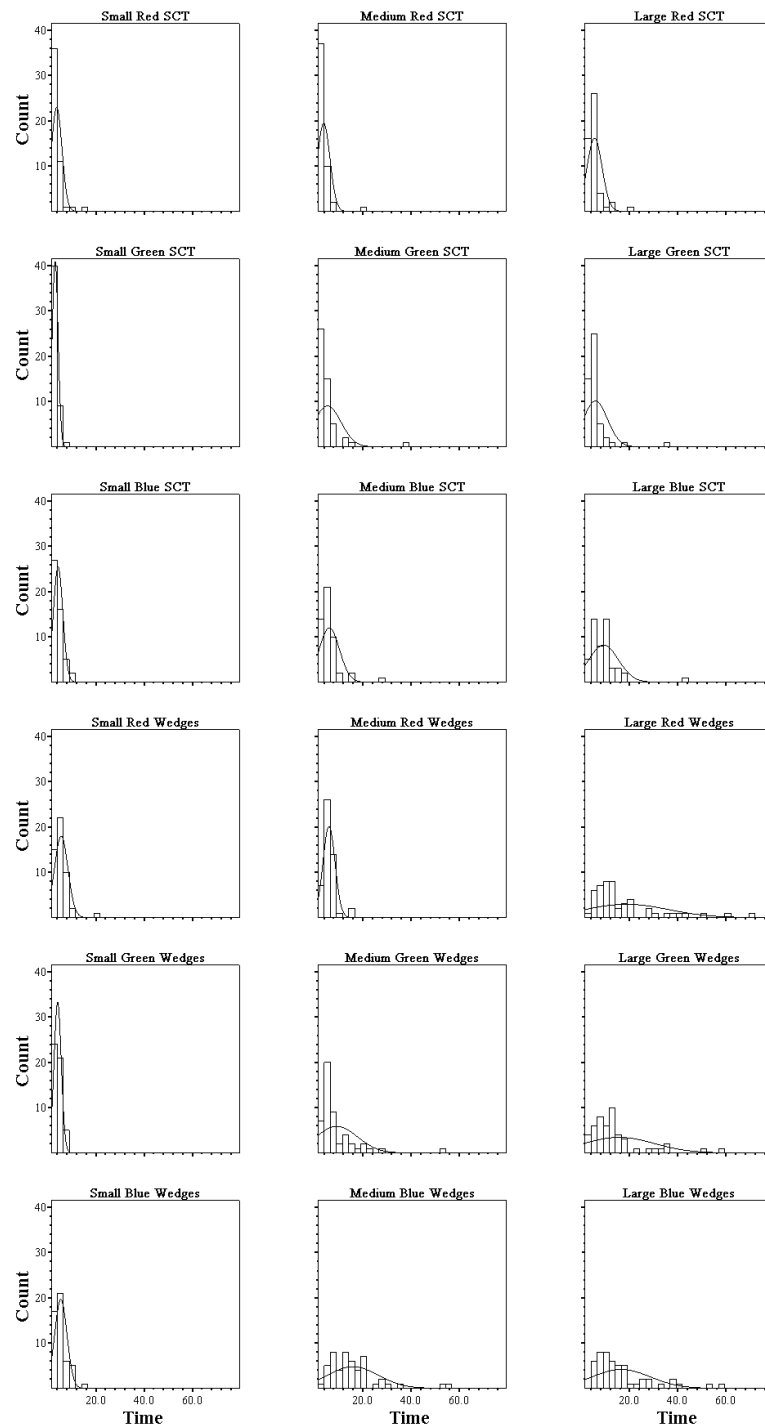


Figure B.1 Histogram frequency distribution of *Time* by *Case* for Task 1.

Table B.1 Task 1 Original *Time* Statistics for 50 Users.

Method	Case	Mean	Median	Minimum	Maximum	Range	Std. Deviation
SCT	0	3.8063	3.2215	1.7896	15.5484	13.7588	2.1814
	1	3.1547	2.7670	1.6267	8.3260	6.6993	1.2276
	2	4.3870	3.9432	1.9940	10.9747	8.9807	1.9708
	3	3.8524	3.1587	1.8030	19.3629	17.5600	2.5849
	4	5.4443	4.0080	1.8820	38.5335	36.6515	5.5639
	5	6.1642	5.1923	2.2299	28.9226	26.6927	4.1913
	6	5.4910	4.7529	2.6346	21.1337	18.4991	3.1083
	7	5.8496	4.5849	2.2472	35.1964	32.9493	4.9848
	8	9.2327	7.6478	2.5878	42.7253	40.1375	6.1442
	Total	5.2647	4.1559	1.6267	42.7253	41.0986	4.2367
Wedges	9	5.6721	5.0519	2.1427	19.3153	17.1726	2.7937
	10	4.1966	4.1438	1.5429	8.0943	6.5514	1.5073
	11	5.5145	4.7319	2.3408	16.2941	13.9533	2.5597
	12	6.0415	5.9506	2.3702	15.3135	12.9433	2.4958
	13	9.2704	6.0058	3.0744	54.3291	51.2547	8.5602
	14	15.9589	13.3533	3.7868	56.5748	52.7880	10.5654
	15	18.7573	12.9114	3.9005	79.5767	75.6762	17.1547
	16	15.5960	11.8464	2.7738	77.7254	74.9516	14.6138
	17	16.5303	12.7588	4.2340	58.8520	54.6180	12.0706
	Total	10.8375	6.9089	1.5429	79.5767	78.0338	11.1312

Table B.2 Task 2 Original *Time* Statistics for 50 Users.

Method	Case Num	Mean	Median	Minimum	Maximum	Range	Std. Deviation
SCT	0	5.1579	3.7280	1.2874	41.1388	39.8514	6.1612
	1	5.2600	3.4085	1.3547	28.5080	27.1533	5.5237
	2	6.6295	4.2160	1.4086	47.8371	46.4285	8.3639
	3	5.1771	4.2556	1.0266	21.2747	20.2482	4.0808
	4	4.2163	2.0976	.8311	52.3659	51.5348	8.1817
	5	4.0963	2.0962	1.1448	29.5091	28.3643	5.0247
	Total		5.0895	3.2509	.8311	52.3659	51.5348
Wedges	6	12.9628	8.9303	3.3346	44.2446	40.9100	9.7502
	7	17.4513	14.0501	4.2619	69.3921	65.1302	12.5091
	8	23.0070	17.7897	1.5353	89.0945	87.5592	17.0964
	9	11.6170	8.7338	2.6231	32.3384	29.7153	7.7175
	10	12.8856	9.1698	1.5622	60.4133	58.8511	12.6338
	11	18.0176	13.0816	2.7317	87.4020	84.6703	16.0400
	Total		15.9902	11.8332	1.5353	89.0945	87.5592

were adjusted. For these cases, the median was considerably smaller than the mean and the average times of the original distributions were under five seconds. The resulting adjusted *Time* statistics for each of the distributions are shown in Table B.3 for Task 1 and Table B.4 for Task 2.

When the *Homogeneity of Variance* assumption is violated, SPSS computes corrected values for the significance tests of within-subjects effects. Since all of the corrected values were highly significant, the conservative Greenhouse-Geisser corrected values were reported and used for interpretation. Additionally the Bonferroni method was chosen to control Type I pooled error rates in the results generated for pairwise comparisons [8]. Since the cumulative error rate multiplies with the number of comparisons, this means

Table B.3 Task 1 Adjusted *Time* Statistics for 49 Users.

Method	Case	Mean	Median	Minimum	Maximum	Range	Std. Deviation
SCT	0	3.5279	3.1981	1.7896	7.3127	5.5231	1.2488
	1	3.1207	2.7563	1.6267	7.4865	5.8598	1.1648
	2	4.3901	3.8932	1.9940	10.9747	8.9807	1.9911
	3	3.5358	3.0619	1.8030	7.0993	5.2964	1.3063
	4	4.5277	3.9747	1.8820	10.1505	8.2686	2.1434
	5	5.6721	5.1687	2.2299	14.6484	12.4185	2.5291
	6	5.0008	4.7460	2.6346	9.3008	6.6662	1.6372
	7	5.1555	4.5408	2.2471	12.1214	9.8742	2.2955
	8	8.8427	7.1996	2.5878	25.4700	22.8822	4.5203
	Total	4.8637	4.1186	1.6267	25.4700	23.8433	2.8019
Wedges	9	5.3937	4.9866	2.1427	10.5471	8.4044	2.0026
	10	4.1862	4.0869	1.5429	8.0943	6.5514	1.5212
	11	5.2945	4.6697	2.3408	10.1227	7.7819	2.0539
	12	5.8270	5.8718	2.3702	13.7388	11.3686	2.0225
	13	7.3271	5.9306	3.0744	21.4295	18.3551	3.8515
	14	16.1131	13.4346	3.7868	56.5748	52.7880	10.6179
	15	18.8247	13.0474	3.9005	76.0526	72.1520	17.0518
	16	14.3281	11.7742	2.7738	57.5321	54.7583	11.6599
	17	16.6346	12.9757	4.2340	57.2688	53.0349	12.0436
	Total	10.4366	6.8265	1.5429	76.0526	74.5097	10.4330



Table B.4 Task 2 Adjusted *Time* Statistics for 49 Users.

Method	Case	Mean	Median	Minimum	Maximum	Range	Std. Deviation
SCT	0	4.2905	3.6605	1.2874	16.3733	15.0859	2.6606
	1	4.0746	3.3497	1.3547	12.4484	11.0937	2.6168
	2	5.6195	4.1547	1.4086	32.4138	31.0052	4.9662
	3	4.8548	4.2166	1.0265	21.2747	20.2482	3.4201
	4	2.5263	2.0935	.8311	6.8294	5.9983	1.4378
	5	2.4384	2.0635	1.1448	5.1415	3.9967	1.0540
	Total	3.9674	3.0668	.8311	32.4138	31.5826	3.1788
Wedges	6	12.5488	8.7064	3.3346	44.2446	40.9100	9.3966
	7	17.3589	13.8161	4.2619	69.3921	65.1302	12.6215
	8	22.8851	17.5810	1.5353	89.0945	87.5592	17.2516
	9	11.4395	8.3888	2.6231	32.3384	29.7153	7.6937
	10	12.5288	8.9938	1.5622	60.4133	58.8511	12.5076
	11	18.0033	12.7422	2.7317	87.4020	84.6703	16.2059
	Total	15.7941	11.5302	1.5353	89.0945	87.5592	13.5654

that the overall desired error rate is divided by the number of comparisons to ensure that the cumulative error rate remains below the desired error rate (either 0.01 or 0.05).

## APPENDIX C

### ACCURACY INFORMATION

This Appendix describes the detailed steps taken to assign the values to the *Correct* variable. The distributions of subject intersections with the front wall of the CAVE are shown in Figure C.1. The test cases are separated by method in the first two columns, with all 50 subject responses in each plot, and the control distribution in the third column, with 20 responses covering the entire range acceptable in each plot. Subject responses outside 1.5 times the acceptable control range for the  $x$  and  $z$  directions were marked incorrect.

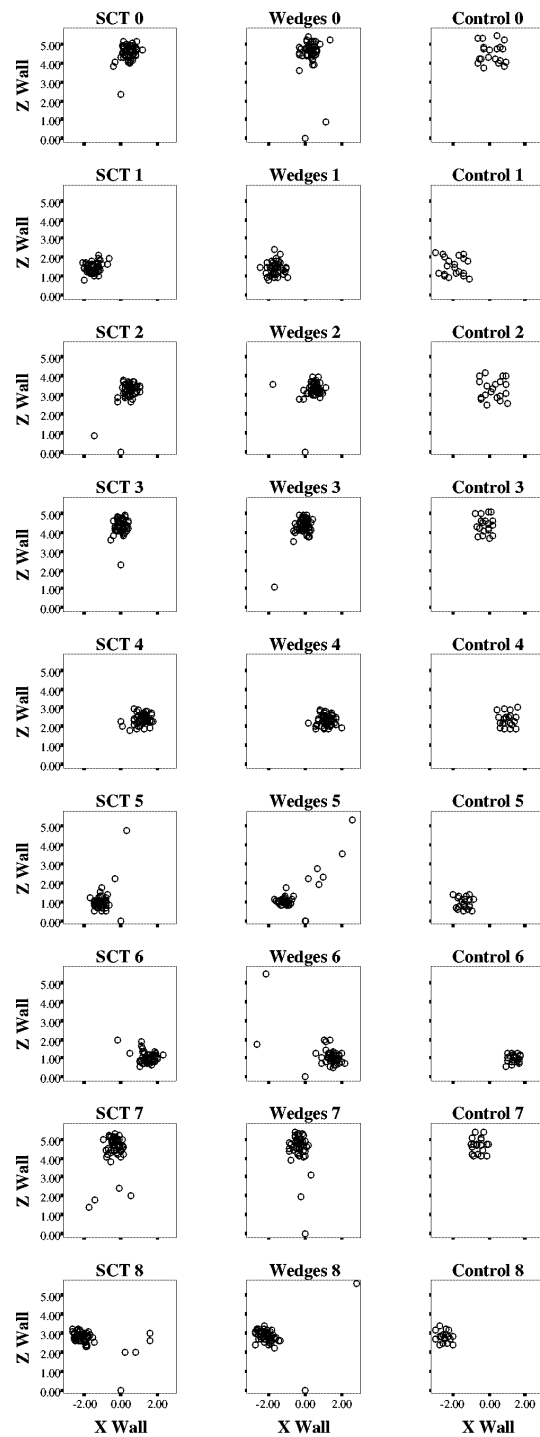


Figure C.1 Accuracy Distributions for Task 1.

## APPENDIX D

### SUMMARY STATISTICS

Additional graphs from the user study analysis are included for *Color*, *Pattern*, and combination effects. Many of these are not significant results, but are included for completeness. The detailed SPSS generated MANOVA results are included in Appendix E.

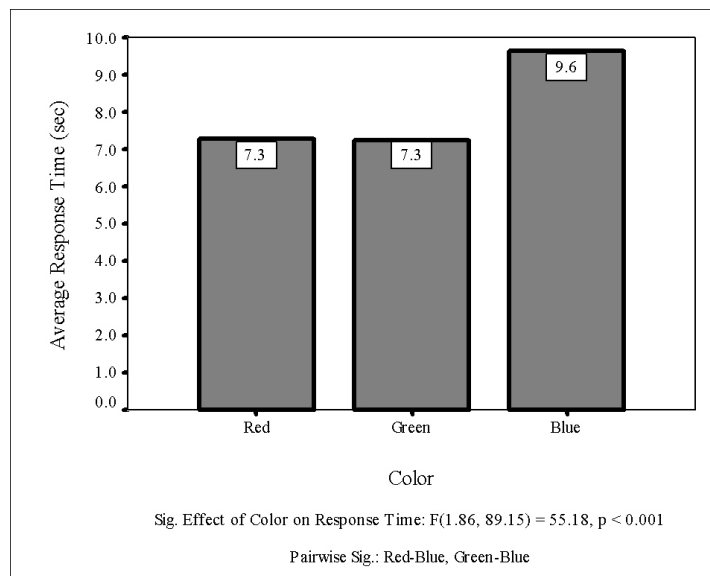


Figure D.1 Task 1 *Time* vs. *Color* for 50 subjects.

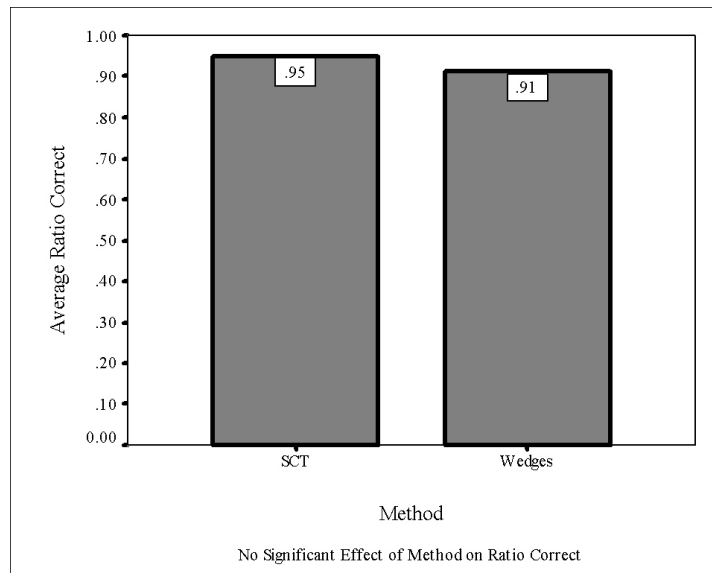


Figure D.2 Task 1 *Correct* vs. *Method* for 50 subjects.

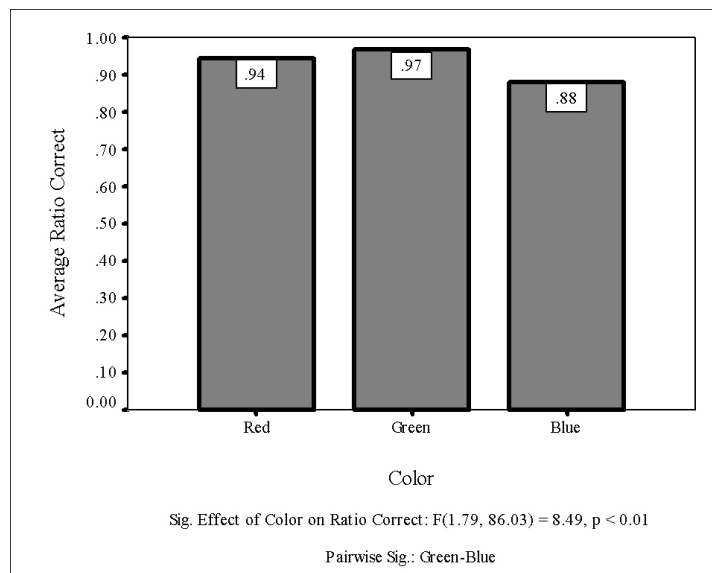


Figure D.3 Task 1 *Correct* vs. *Color* for 50 subjects.

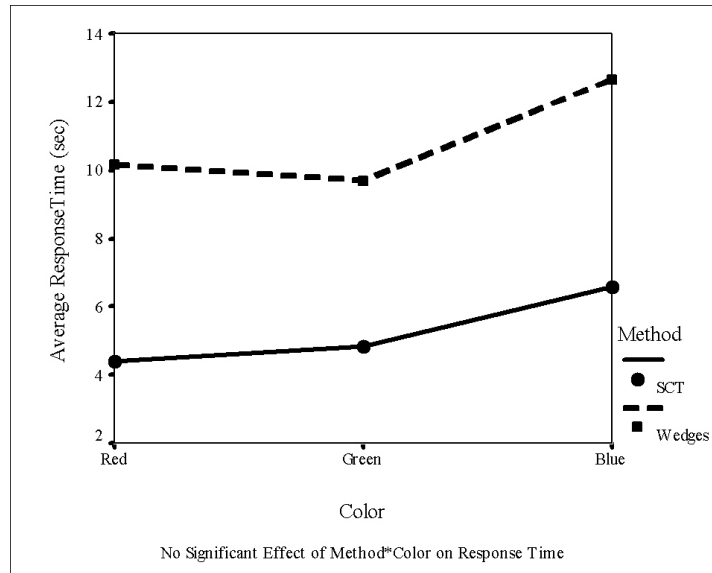


Figure D.4 Task 1 *Time vs. Color* by *Method* for 50 subjects.

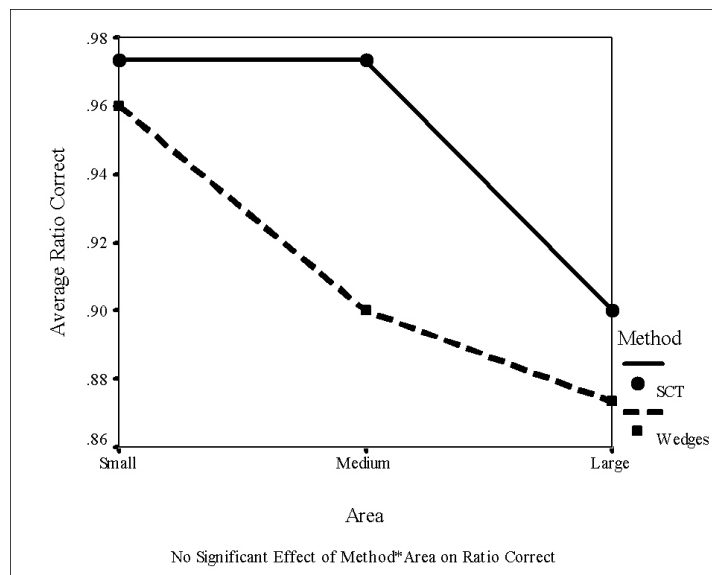


Figure D.5 Task 1 *Correct vs. Area* by *Method* for 50 subjects.

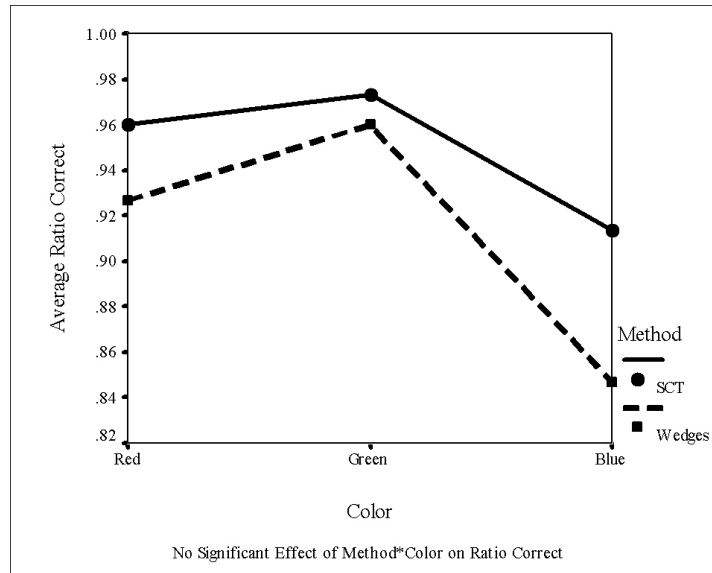


Figure D.6 Task 1 *Correct* vs. *Color* by *Method* for 50 subjects.

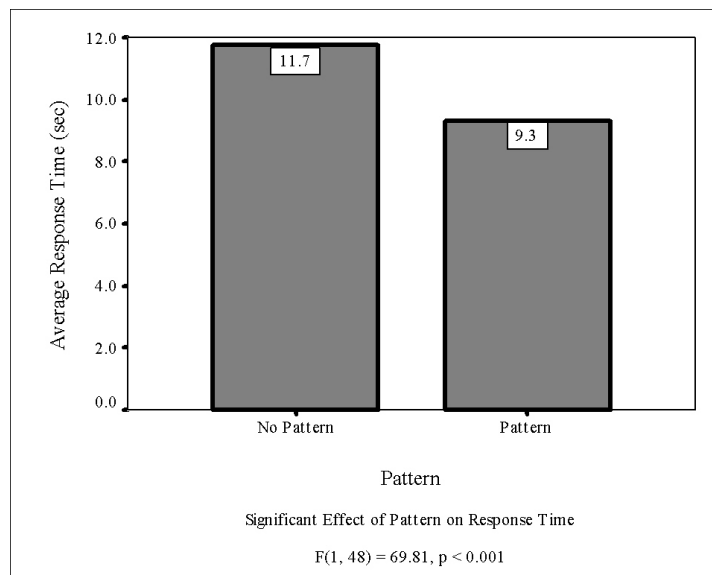


Figure D.7 Task 2 *Time* vs. *Pattern* for 50 subjects.

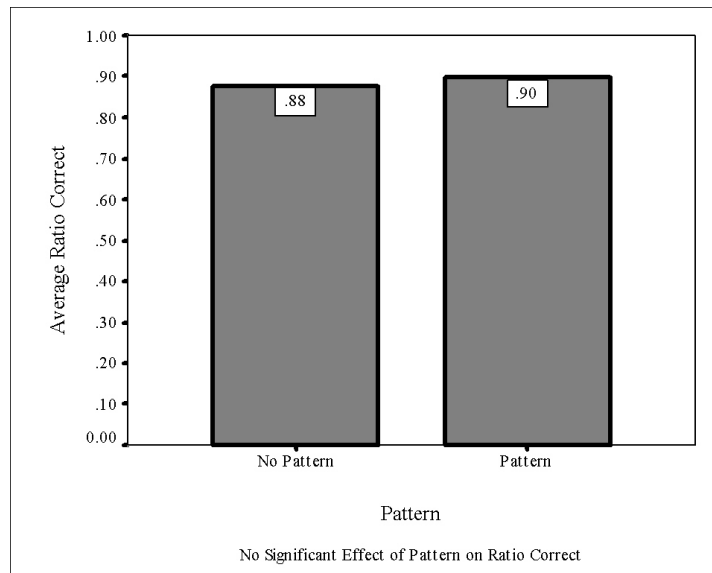


Figure D.8 Task 2 *Correct* vs. *Pattern* for 50 subjects.

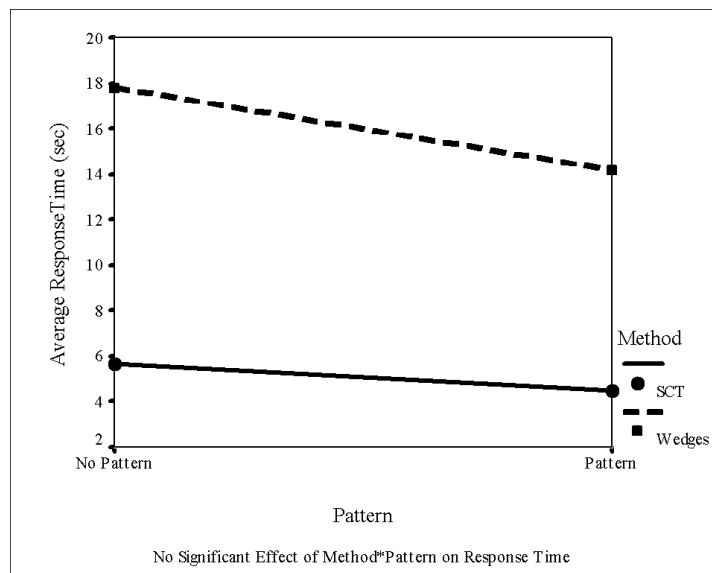


Figure D.9 Task 2 *Time* vs. *Pattern* by *Method* for 50 subjects.



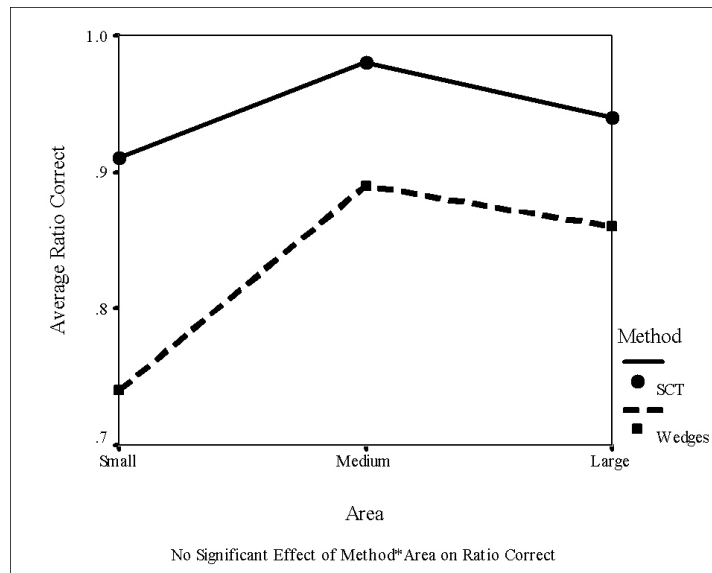


Figure D.10 Task 2 *Correct vs. Area* by *Method* for 50 subjects.

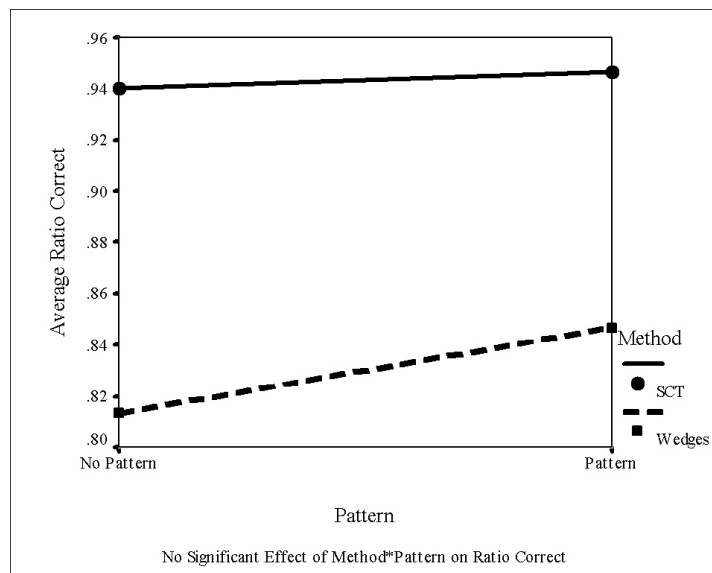


Figure D.11 Task 2 *Correct vs. Pattern* by *Method* for 50 subjects.

## APPENDIX E

### SPSS OUTPUT

Task 1 and Task 2 MANOVA results are reported for 49 users using  $\log_{10}(Time)$  with outliers adjusted as described in Appendix B. The Pooled error adjustment method is the conservative Bonferroni method with power and confidence intervals computed for  $\alpha < 0.01$ .

Note that for the Task 1 univariate effect of *Area*, the *Correct* observed power was 0.944 at  $\alpha < 0.05$ . For the Task 1 univariate effect of *Color*, the *Correct* observed power was 0.946 at  $\alpha < 0.05$ . For the Task1 univariate effect of *Method \* Area \* Color*, the *Correct* observed power was 0.826 at  $\alpha < 0.05$ . For the Task 2 univariate effect of *Area*, the *Time* observed power was 0.964 at  $\alpha < 0.05$ . For the Task 2 univariate effect of *Area*, the *Correct* observed power was 0.895 at  $\alpha < 0.05$ . Values of power above 0.8 are considered adequate for research [10], although Field recommends a value above 0.9 [8].

U49 TASK 1 MANOVA OF LOG(TIME) AND CORRECT WITH OUTLIERS ADJUSTED, ALPHA = 0.01, RUN ON 030924 AT 8:07 PM  
 data file: u49-t1-var-logt-out-adj-comb-correct-030924-01.sav  
 same as first one, but with alpha = .01

```
GLM
  tl.0.0.0 tl.0.0.1 tl.0.0.2 tl.0.1.0 tl.0.1.1 tl.0.1.2 tl.0.2.0 tl.0.2.1
  tl.0.2.2 tl.1.0.0 tl.1.0.1 tl.1.0.2 tl.1.1.0 tl.1.1.1 tl.1.1.2 tl.1.2.0
  tl.1.2.1 tl.1.2.2 r.0.0.0 r.0.0.1 r.0.0.2 r.0.1.0 r.0.1.1 r.0.1.2 r.0.2.0
  r.0.2.1 r.0.2.2 r.1.0.0 r.1.0.1 r.1.0.2 r.1.1.0 r.1.1.1 r.1.1.2 r.1.2.0
  r.1.2.1 r.1.2.2
  /WSFACTOR = method 2 Polynomial area 3 Polynomial color 3 Polynomial
  /MEASURE = time correct
  /METHOD = SSTYPE(3)
  /PLOT = PROFILE( area*method color*method area*method*color )
  /EMMEANS = TABLES(OVERALL)
  /EMMEANS = TABLES(method) COMPARE ADJ(BONFERRONI)
  /EMMEANS = TABLES(area) COMPARE ADJ(BONFERRONI)
  /EMMEANS = TABLES(color) COMPARE ADJ(BONFERRONI)
  /EMMEANS = TABLES(method*area)
  /EMMEANS = TABLES(method*color)
  /EMMEANS = TABLES(area*color)
  /EMMEANS = TABLES(method*area*color)
  /PRINT = DESCRIPTIVE ETASQ OPOWER
  /PLOT = RESIDUALS
  /CRITERIA = ALPHA(.01)
  /WSDESIGN = method area color method*area method*color area*color method
  *area*color .
```

**General Linear Model**

**Warnings**

The residual plot for R.0.0.1: Correct? is not produced because its residual variance is zero.  
 The residual plot for R.0.1.1: Correct? is not produced because its residual variance is zero.  
 The residual plot for R.1.0.1: Correct? is not produced because its residual variance is zero.  
 The residual plot for R.1.1.0: Correct? is not produced because its residual variance is zero.  
 The residual plot for R.1.1.1: Correct? is not produced because its residual variance is zero.

**Within-Subjects Factors**

Measure	METHOD	AREA	COLOR	Dependent Variable	
TIME	1	1	1	TL.0.0.0	
			2	TL.0.0.1	
			3	TL.0.0.2	
		2	1	1	TL.0.1.0
				2	TL.0.1.1
				3	TL.0.1.2
		3	1	1	TL.0.2.0
				2	TL.0.2.1
				3	TL.0.2.2
	2	1	1	TL.1.0.0	
			2	TL.1.0.1	
			3	TL.1.0.2	
		2	1	1	TL.1.1.0
				2	TL.1.1.1
				3	TL.1.1.2
		3	1	1	TL.1.2.0
				2	TL.1.2.1
				3	TL.1.2.2
CORRECT	1	1	1	R.0.0.0	
			2	R.0.0.1	
			3	R.0.0.2	
		2	1	1	R.0.1.0
				2	R.0.1.1
				3	R.0.1.2
		3	1	1	R.0.2.0
				2	R.0.2.1
				3	R.0.2.2
	2	1	1	R.1.0.0	
			2	R.1.0.1	
			3	R.1.0.2	
		2	1	1	R.1.1.0
				2	R.1.1.1
				3	R.1.1.2
		3	1	1	R.1.2.0
				2	R.1.2.1
				3	R.1.2.2

Descriptive Statistics

	Mean	Std. Deviation	N
TL.0.0.0	.5244817	.13933930	49
TL.0.0.1	.4699380	.14130107	49
TL.0.0.2	.6055938	.17502045	49
TL.0.1.0	.5218381	.15141625	49
TL.0.1.1	.6159864	.18189255	49
TL.0.1.2	.7187527	.17201483	49
TL.0.2.0	.6783475	.13341366	49
TL.0.2.1	.6748851	.17962928	49
TL.0.2.2	.8957459	.21238776	49
TL.1.0.0	.7026529	.16227240	49
TL.1.0.1	.5956520	.15170339	49
TL.1.0.2	.6932080	.16415925	49
TL.1.1.0	.7413710	.14680429	49
TL.1.1.1	.8185530	.19418222	49
TL.1.1.2	1.1333244	.25185409	49
TL.1.2.0	1.1442765	.32432668	49
TL.1.2.1	1.0439820	.31178213	49
TL.1.2.2	1.1303494	.27639399	49
R.0.0.0: Correct?	.98	.143	49
R.0.0.1: Correct?	1.00	.000	49
R.0.0.2: Correct?	.96	.200	49
R.0.1.0: Correct?	.98	.143	49
R.0.1.1: Correct?	1.00	.000	49
R.0.1.2: Correct?	.96	.200	49
R.0.2.0: Correct?	.92	.277	49
R.0.2.1: Correct?	.92	.277	49
R.0.2.2: Correct?	.88	.331	49
R.1.0.0: Correct?	.96	.200	49
R.1.0.1: Correct?	1.00	.000	49
R.1.0.2: Correct?	.96	.200	49
R.1.1.0: Correct?	1.00	.000	49
R.1.1.1: Correct?	1.00	.000	49
R.1.1.2: Correct?	.73	.446	49
R.1.2.0: Correct?	.88	.331	49
R.1.2.1: Correct?	.90	.306	49
R.1.2.2: Correct?	.90	.306	49

Multivariate Tests<sup>a</sup>

Effect			Value	F	Hypothesis df	Error df	Sig.	Partial Eta Squared	Noncent. Parameter	Observed Power <sup>b</sup>
Between Subjects	Intercept	Pillai's Trace	.993	3319.372 <sup>b</sup>	2.000	47.000	.000	.993	6638.744	1.000
		Wilks' Lambda	.007	3319.372 <sup>b</sup>	2.000	47.000	.000	.993	6638.744	1.000
		Hotelling's Trace	141.250	3319.372 <sup>b</sup>	2.000	47.000	.000	.993	6638.744	1.000
		Roy's Largest Root	141.250	3319.372 <sup>b</sup>	2.000	47.000	.000	.993	6638.744	1.000
Within Subjects	METHOD	Pillai's Trace	.873	161.202 <sup>b</sup>	2.000	47.000	.000	.873	322.404	1.000
		Wilks' Lambda	.127	161.202 <sup>b</sup>	2.000	47.000	.000	.873	322.404	1.000
		Hotelling's Trace	6.860	161.202 <sup>b</sup>	2.000	47.000	.000	.873	322.404	1.000
		Roy's Largest Root	6.860	161.202 <sup>b</sup>	2.000	47.000	.000	.873	322.404	1.000
	AREA	Pillai's Trace	.923	135.363 <sup>b</sup>	4.000	45.000	.000	.923	541.454	1.000
		Wilks' Lambda	.077	135.363 <sup>b</sup>	4.000	45.000	.000	.923	541.454	1.000
		Hotelling's Trace	12.032	135.363 <sup>b</sup>	4.000	45.000	.000	.923	541.454	1.000
		Roy's Largest Root	12.032	135.363 <sup>b</sup>	4.000	45.000	.000	.923	541.454	1.000
	COLOR	Pillai's Trace	.677	23.630 <sup>b</sup>	4.000	45.000	.000	.677	94.520	1.000
		Wilks' Lambda	.323	23.630 <sup>b</sup>	4.000	45.000	.000	.677	94.520	1.000
		Hotelling's Trace	2.100	23.630 <sup>b</sup>	4.000	45.000	.000	.677	94.520	1.000
		Roy's Largest Root	2.100	23.630 <sup>b</sup>	4.000	45.000	.000	.677	94.520	1.000
	METHOD * AREA	Pillai's Trace	.560	14.300 <sup>b</sup>	4.000	45.000	.000	.560	57.199	1.000
		Wilks' Lambda	.440	14.300 <sup>b</sup>	4.000	45.000	.000	.560	57.199	1.000
		Hotelling's Trace	1.271	14.300 <sup>b</sup>	4.000	45.000	.000	.560	57.199	1.000
		Roy's Largest Root	1.271	14.300 <sup>b</sup>	4.000	45.000	.000	.560	57.199	1.000
	METHOD * COLOR	Pillai's Trace	.151	2.006 <sup>b</sup>	4.000	45.000	.110	.151	8.025	.301
		Wilks' Lambda	.849	2.006 <sup>b</sup>	4.000	45.000	.110	.151	8.025	.301
		Hotelling's Trace	.178	2.006 <sup>b</sup>	4.000	45.000	.110	.151	8.025	.301
		Roy's Largest Root	.178	2.006 <sup>b</sup>	4.000	45.000	.110	.151	8.025	.301
	AREA * COLOR	Pillai's Trace	.773	17.408 <sup>b</sup>	8.000	41.000	.000	.773	139.268	1.000
		Wilks' Lambda	.227	17.408 <sup>b</sup>	8.000	41.000	.000	.773	139.268	1.000
		Hotelling's Trace	3.397	17.408 <sup>b</sup>	8.000	41.000	.000	.773	139.268	1.000
		Roy's Largest Root	3.397	17.408 <sup>b</sup>	8.000	41.000	.000	.773	139.268	1.000
	METHOD * AREA * COLOR	Pillai's Trace	.590	7.362 <sup>b</sup>	8.000	41.000	.000	.590	58.895	.998
		Wilks' Lambda	.410	7.362 <sup>b</sup>	8.000	41.000	.000	.590	58.895	.998
		Hotelling's Trace	1.436	7.362 <sup>b</sup>	8.000	41.000	.000	.590	58.895	.998
		Roy's Largest Root	1.436	7.362 <sup>b</sup>	8.000	41.000	.000	.590	58.895	.998

a. Computed using alpha = .01

b. Exact statistic

c.

Design: Intercept

Within Subjects Design: METHOD+AREA+COLOR+METHOD\*AREA+METHOD\*COLOR+AREA\*COLOR+METHOD\*AREA\*COLOR

Mauchly's Test of Sphericity<sup>b</sup>

Within Subjects Effect	Measure	Mauchly's W	Approx. Chi-Square	df	Sig.	Epsilon <sup>3</sup>		
						Greenhouse-Geisser	Huynh-Feldt	Lower-bound
METHOD	TIME	1.000	.000	0	.	1.000	1.000	1.000
	CORRECT	1.000	.000	0	.	1.000	1.000	1.000
AREA	TIME	.856	7.285	2	.026	.874	.905	.500
	CORRECT	.658	19.643	2	.000	.745	.764	.500
COLOR	TIME	.923	3.755	2	.153	.929	.965	.500
	CORRECT	.884	5.792	2	.055	.896	.929	.500
METHOD * AREA	TIME	.957	2.065	2	.356	.959	.998	.500
	CORRECT	.831	8.681	2	.013	.856	.884	.500
METHOD * COLOR	TIME	.986	.683	2	.711	.986	1.000	.500
	CORRECT	.854	7.420	2	.024	.873	.903	.500
AREA * COLOR	TIME	.535	29.011	9	.001	.800	.864	.250
	CORRECT	.101	106.645	9	.000	.676	.720	.250
METHOD * AREA * COLOR	TIME	.709	15.937	9	.068	.893	.974	.250
	CORRECT	.126	96.255	9	.000	.614	.649	.250

Tests the null hypothesis that the error covariance matrix of the orthonormalized transformed dependent variables is proportional to an identity matrix.

a. May be used to adjust the degrees of freedom for the averaged tests of significance. Corrected tests are displayed in the Tests of Within-Subjects Effects table.

b.

Design: Intercept

Within Subjects Design: METHOD+AREA+COLOR+METHOD\*AREA+METHOD\*COLOR+AREA\*COLOR+METHOD\*AREA\*COLOR

## Tests of Within-Subjects Effects

Multivariate<sup>d,e</sup>

Within Subjects Effect		Value	F	Hypothesis df	Error df	Sig.	Partial Eta Squared	Noncent. Parameter	Observed Power <sup>f</sup>
METHOD	Pillai's Trace	.873	161.202 <sup>b</sup>	2.000	47.000	.000	.873	322.404	1.000
	Wilks' Lambda	.127	161.202 <sup>b</sup>	2.000	47.000	.000	.873	322.404	1.000
	Hotelling's Trace	6.860	161.202 <sup>b</sup>	2.000	47.000	.000	.873	322.404	1.000
	Roy's Largest Root	6.860	161.202 <sup>b</sup>	2.000	47.000	.000	.873	322.404	1.000
AREA	Pillai's Trace	.879	37.637	4.000	192.000	.000	.439	150.547	1.000
	Wilks' Lambda	.123	87.943 <sup>b</sup>	4.000	190.000	.000	.649	351.773	1.000
	Hotelling's Trace	7.115	167.193	4.000	188.000	.000	.781	668.773	1.000
	Roy's Largest Root	7.112	341.392 <sup>c</sup>	2.000	96.000	.000	.877	682.785	1.000
COLOR	Pillai's Trace	.543	17.892	4.000	192.000	.000	.272	71.569	1.000
	Wilks' Lambda	.459	22.619 <sup>b</sup>	4.000	190.000	.000	.323	90.478	1.000
	Hotelling's Trace	1.175	27.609	4.000	188.000	.000	.370	110.438	1.000
	Roy's Largest Root	1.171	56.218 <sup>c</sup>	2.000	96.000	.000	.539	112.436	1.000
METHOD * AREA	Pillai's Trace	.465	14.534	4.000	192.000	.000	.232	58.134	1.000
	Wilks' Lambda	.552	16.408 <sup>b</sup>	4.000	190.000	.000	.257	65.632	1.000
	Hotelling's Trace	.779	18.305	4.000	188.000	.000	.280	73.222	1.000
	Roy's Largest Root	.737	35.354 <sup>c</sup>	2.000	96.000	.000	.424	70.709	1.000
METHOD * COLOR	Pillai's Trace	.098	2.482	4.000	192.000	.045	.049	9.926	.462
	Wilks' Lambda	.904	2.467 <sup>b</sup>	4.000	190.000	.046	.049	9.868	.459
	Hotelling's Trace	.104	2.452	4.000	188.000	.047	.050	9.810	.455
	Roy's Largest Root	.075	3.585 <sup>c</sup>	2.000	96.000	.032	.069	7.169	.405
AREA * COLOR	Pillai's Trace	.261	7.216	8.000	384.000	.000	.131	57.727	1.000
	Wilks' Lambda	.746	7.550 <sup>b</sup>	8.000	382.000	.000	.137	60.403	1.000
	Hotelling's Trace	.332	7.883	8.000	380.000	.000	.142	63.068	1.000
	Roy's Largest Root	.301	14.448 <sup>c</sup>	4.000	192.000	.000	.231	57.790	1.000
METHOD * AREA * COLOR	Pillai's Trace	.246	6.744	8.000	384.000	.000	.123	53.955	1.000
	Wilks' Lambda	.754	7.226 <sup>b</sup>	8.000	382.000	.000	.131	57.812	1.000
	Hotelling's Trace	.325	7.708	8.000	380.000	.000	.140	61.664	1.000
	Roy's Largest Root	.321	15.424 <sup>c</sup>	4.000	192.000	.000	.243	61.695	1.000

a. Computed using alpha = .01

b. Exact statistic

c. The statistic is an upper bound on F that yields a lower bound on the significance level.

d.

Design: Intercept

Within Subjects Design: METHOD+AREA+COLOR+METHOD\*AREA+METHOD\*COLOR+AREA\*COLOR+METHOD\*AREA\*COLOR

e. Tests are based on averaged variables.

## Univariate Tests

Source	Measure		Type III Sum of Squares	df	Mean Square	F	Sig.	Partial Eta Squared	Noncent. Parameter	Observed Power <sup>f</sup>
METHOD	TIME	Sphericity Assumed	14.373	1	14.373	315.793	.000	.868	315.793	1.000
		Greenhouse-Geisser	14.373	1.000	14.373	315.793	.000	.868	315.793	1.000
		Huynh-Feldt	14.373	1.000	14.373	315.793	.000	.868	315.793	1.000
		Lower-bound	14.373	1.000	14.373	315.793	.000	.868	315.793	1.000

## Univariate Tests

Source	Measure		Type III Sum of Squares	df	Mean Square	F	Sig.	Partial Eta Squared	Noncent. Parameter	Observed Power <sup>a</sup>
METHOD	CORRECT	Sphericity Assumed	.192	1	.192	1.808	.185	.036	1.808	.101
		Greenhouse-Geisser	.192	1.000	.192	1.808	.185	.036	1.808	.101
		Huynh-Feldt	.192	1.000	.192	1.808	.185	.036	1.808	.101
		Lower-bound	.192	1.000	.192	1.808	.185	.036	1.808	.101
Error(METHOD)	TIME	Sphericity Assumed	2.185	48	4.551E-02					
		Greenhouse-Geisser	2.185	48.000	4.551E-02					
		Huynh-Feldt	2.185	48.000	4.551E-02					
		Lower-bound	2.185	48.000	4.551E-02					
	CORRECT	Sphericity Assumed	5.086	48	.106					
		Greenhouse-Geisser	5.086	48.000	.106					
		Huynh-Feldt	5.086	48.000	.106					
		Lower-bound	5.086	48.000	.106					
AREA	TIME	Sphericity Assumed	15.949	2	7.975	332.505	.000	.874	665.009	1.000
		Greenhouse-Geisser	15.949	1.749	9.120	332.505	.000	.874	581.516	1.000
		Huynh-Feldt	15.949	1.810	8.814	332.505	.000	.874	601.700	1.000
		Lower-bound	15.949	1.000	15.949	332.505	.000	.874	332.505	1.000
	CORRECT	Sphericity Assumed	.914	2	.457	9.682	.000	.168	19.363	.919
		Greenhouse-Geisser	.914	1.491	.613	9.682	.001	.168	14.433	.827
		Huynh-Feldt	.914	1.528	.598	9.682	.001	.168	14.790	.836
		Lower-bound	.914	1.000	.914	9.682	.003	.168	9.682	.666
Error(AREA)	TIME	Sphericity Assumed	2.302	96	2.398E-02					
		Greenhouse-Geisser	2.302	83.947	2.743E-02					
		Huynh-Feldt	2.302	86.861	2.651E-02					
		Lower-bound	2.302	48.000	4.797E-02					
	CORRECT	Sphericity Assumed	4.531	96	4.719E-02					
		Greenhouse-Geisser	4.531	71.557	6.332E-02					
		Huynh-Feldt	4.531	73.325	6.179E-02					
		Lower-bound	4.531	48.000	9.439E-02					
COLOR	TIME	Sphericity Assumed	4.554	2	2.277	55.177	.000	.535	110.353	1.000
		Greenhouse-Geisser	4.554	1.857	2.452	55.177	.000	.535	102.483	1.000
		Huynh-Feldt	4.554	1.929	2.361	55.177	.000	.535	106.438	1.000
		Lower-bound	4.554	1.000	4.554	55.177	.000	.535	55.177	1.000
	CORRECT	Sphericity Assumed	.819	2	.409	8.494	.000	.150	16.988	.871
		Greenhouse-Geisser	.819	1.792	.457	8.494	.001	.150	15.223	.834
		Huynh-Feldt	.819	1.857	.441	8.494	.001	.150	15.776	.846
		Lower-bound	.819	1.000	.819	8.494	.005	.150	8.494	.594
Error(COLOR)	TIME	Sphericity Assumed	3.962	96	4.127E-02					
		Greenhouse-Geisser	3.962	89.154	4.444E-02					
		Huynh-Feldt	3.962	92.594	4.279E-02					
		Lower-bound	3.962	48.000	8.254E-02					
	CORRECT	Sphericity Assumed	4.626	96	4.819E-02					
		Greenhouse-Geisser	4.626	86.026	5.377E-02					
		Huynh-Feldt	4.626	89.147	5.189E-02					
		Lower-bound	4.626	48.000	9.637E-02					

## Univariate Tests

Source	Measure		Type III Sum of Squares	df	Mean Square	F	Sig.	Partial Eta Squared	Noncent. Parameter	Observed Power <sup>a</sup>
METHOD * AREA	TIME	Sphericity Assumed	1.939	2	.970	33.569	.000	.412	67.138	1.000
		Greenhouse-Geisser	1.939	1,918	1.011	33.569	.000	.412	64.371	1.000
		Huynh-Feldt	1.939	1,996	.972	33.569	.000	.412	66.989	1.000
		Lower-bound	1.939	1,000	1.939	33.569	.000	.412	33.569	.999
	CORRECT	Sphericity Assumed	.166	2	8.277E-02	2.134	.124	.043	4.268	.209
		Greenhouse-Geisser	.166	1,711	9.672E-02	2.134	.132	.043	3.652	.183
		Huynh-Feldt	.166	1,768	9.361E-02	2.134	.130	.043	3.774	.188
		Lower-bound	.166	1,000	.166	2.134	.151	.043	2.134	.122
Error(METHOD*AREA)	TIME	Sphericity Assumed	2.773	96	2.888E-02					
		Greenhouse-Geisser	2.773	92,043	3.012E-02					
		Huynh-Feldt	2.773	95,787	2.895E-02					
		Lower-bound	2.773	48,000	5.776E-02					
	CORRECT	Sphericity Assumed	3.723	96	3.878E-02					
		Greenhouse-Geisser	3.723	82,146	4.533E-02					
		Huynh-Feldt	3.723	84,884	4.386E-02					
		Lower-bound	3.723	48,000	7.757E-02					
METHOD * COLOR	TIME	Sphericity Assumed	.123	2	6.164E-02	1.925	.151	.039	3.851	.182
		Greenhouse-Geisser	.123	1,972	6.252E-02	1.925	.152	.039	3.796	.180
		Huynh-Feldt	.123	2,000	6.164E-02	1.925	.151	.039	3.851	.182
		Lower-bound	.123	1,000	.123	1.925	.172	.039	1.925	.108
	CORRECT	Sphericity Assumed	.166	2	8.277E-02	2.599	.080	.051	5.199	.270
		Greenhouse-Geisser	.166	1,745	9.485E-02	2.599	.087	.051	4.536	.241
		Huynh-Feldt	.166	1,805	9.168E-02	2.599	.086	.051	4.693	.248
		Lower-bound	.166	1,000	.166	2.599	.113	.051	2.599	.154
Error(METHOD*COLOR)	TIME	Sphericity Assumed	3.073	96	3.201E-02					
		Greenhouse-Geisser	3.073	94,635	3.247E-02					
		Huynh-Feldt	3.073	96,000	3.201E-02					
		Lower-bound	3.073	48,000	6.402E-02					
	CORRECT	Sphericity Assumed	3.057	96	3.184E-02					
		Greenhouse-Geisser	3.057	83,767	3.649E-02					
		Huynh-Feldt	3.057	86,663	3.527E-02					
		Lower-bound	3.057	48,000	6.368E-02					
AREA * COLOR	TIME	Sphericity Assumed	1.837	4	.459	14.107	.000	.227	56.428	1.000
		Greenhouse-Geisser	1.837	3,201	.574	14.107	.000	.227	45.155	1.000
		Huynh-Feldt	1.837	3,456	.531	14.107	.000	.227	48.760	1.000
		Lower-bound	1.837	1,000	1.837	14.107	.000	.227	14.107	.853
	CORRECT	Sphericity Assumed	.726	4	.181	3.427	.010	.067	13.708	.660
		Greenhouse-Geisser	.726	2,704	.268	3.427	.023	.067	9.267	.493
		Huynh-Feldt	.726	2,881	.252	3.427	.020	.067	9.873	.518
		Lower-bound	.726	1,000	.726	3.427	.070	.067	3.427	.215
Error(AREA*COLOR)	TIME	Sphericity Assumed	6.251	192	3.256E-02					
		Greenhouse-Geisser	6.251	153,643	4.068E-02					
		Huynh-Feldt	6.251	165,908	3.768E-02					
		Lower-bound	6.251	48,000	.130					

## Univariate Tests

Source	Measure		Type III Sum of Squares	df	Mean Square	F	Sig.	Partial Eta Squared	Noncent. Parameter	Observed Power <sup>a</sup>	
Error(AREA*COLOR)	CORRECT	Sphericity Assumed	10.163	192	5.293E-02						
		Greenhouse-Geisser	10.163	129.789	7.831E-02						
		Huynh-Feldt	10.163	138.283	7.350E-02						
		Lower-bound	10.163	48.000	.212						
METHOD * AREA * COLOR	TIME	Sphericity Assumed	1.319	4	.330	13.322	.000	.217	53.289	1.000	
		Greenhouse-Geisser	1.319	3.573	.369	13.322	.000	.217	47.599	1.000	
		Huynh-Feldt	1.319	3.896	.339	13.322	.000	.217	51.899	1.000	
		Lower-bound	1.319	1.000	1.319	13.322	.001	.217	13.322	.828	
	CORRECT	Sphericity Assumed	.794	4	.198	4.580	.001	.087	18.321	.829	
		Greenhouse-Geisser	.794	2.454	.323	4.580	.008	.087	11.242	.623	
		Huynh-Feldt	.794	2.597	.306	4.580	.007	.087	11.893	.648	
		Lower-bound	.794	1.000	.794	4.580	.037	.087	4.580	.305	
	Error(METHOD*AREA*COLOR)	TIME	Sphericity Assumed	4.754	192	2.476E-02					
			Greenhouse-Geisser	4.754	171.499	2.772E-02					
Huynh-Feldt			4.754	186.990	2.542E-02						
Lower-bound			4.754	48.000	9.904E-02						
CORRECT		Sphericity Assumed	8.317	192	4.332E-02						
		Greenhouse-Geisser	8.317	117.814	7.060E-02						
		Huynh-Feldt	8.317	124.642	6.673E-02						
		Lower-bound	8.317	48.000	.173						

a. Computed using alpha = .01

## Tests of Within-Subjects Contrasts

Source	Measure	METHOD	AREA	COLOR	Type III Sum of Squares	df	Mean Square	F	Sig.	Partial Eta Squared	Noncent. Parameter	Observed Power <sup>a</sup>
METHOD	TIME	Linear			14.373	1	14.373	315.793	.000	.868	315.793	1.000
	CORRECT	Linear			.192	1	.192	1.808	.185	.036	1.808	.101
Error(METHOD)	TIME	Linear			2.185	48	4.551E-02					
	CORRECT	Linear			5.086	48	.106					
AREA	TIME	Linear			15.945	1	15.945	513.352	.000	.914	513.352	1.000
					4.812E-03	1	4.812E-03	.285	.596	.006	.285	.021
	CORRECT	Linear			.900	1	.900	14.313	.000	.230	14.313	.859
					1.417E-02	1	1.417E-02	.449	.506	.009	.449	.028
Error(AREA)	TIME	Linear			1.491	48	3.106E-02					
					.812	48	1.691E-02					
	CORRECT	Linear			3.017	48	6.285E-02					
					1.514	48	3.153E-02					
COLOR	TIME	Linear	Linear		3.048	1	3.048	85.865	.000	.641	85.865	1.000
			Quadratic		1.506	1	1.506	32.018	.000	.400	32.018	.998
	CORRECT	Linear	Linear		.435	1	.435	8.149	.006	.145	8.149	.571
			Quadratic		.383	1	.383	8.924	.004	.157	8.924	.621
Error(COLOR)	TIME	Linear	Linear		1.704	48	3.550E-02					
			Quadratic		2.258	48	4.704E-02					
	CORRECT	Linear	Linear		2.565	48	5.343E-02					
			Quadratic		2.061	48	4.294E-02					
METHOD * AREA	TIME	Linear	Linear		1.878	1	1.878	54.710	.000	.533	54.710	1.000
			Quadratic		6.130E-02	1	6.130E-02	2.615	.112	.052	2.615	.155



Tests of Within-Subjects Contrasts

Source	Measure	METHOD	AREA	COLOR	Type III Sum of Squares	df	Mean Square	F	Sig.	Partial Eta Squared	Noncent. Parameter	Observed Power <sup>a</sup>
METHOD * AREA	CORRECT	Linear	Linear		1.701E-03	1	1.701E-03	.032	.860	.001	.032	.011
			Quadratic		.164	1	.164	6.888	.012	.125	6.888	.483
Error(METHOD*AREA)	TIME	Linear	Linear		1.647	48	3.432E-02					
			Quadratic		1.125	48	2.344E-02					
	CORRECT	Linear	Linear		2.582	48	5.378E-02					
			Quadratic		1.142	48	2.379E-02					
METHOD * COLOR	TIME	Linear	Linear		6.570E-02	1	6.570E-02	2.208	.144	.044	2.208	.127
			Quadratic		5.757E-02	1	5.757E-02	1.680	.201	.034	1.680	.093
	CORRECT	Linear	Linear		.109	1	.109	4.267	.044	.082	4.267	.281
			Quadratic		5.669E-02	1	5.669E-02	1.485	.229	.030	1.485	.081
Error(METHOD*COLOR)	TIME	Linear	Linear		1.428	48	2.976E-02					
			Quadratic		1.645	48	3.426E-02					
	CORRECT	Linear	Linear		1.224	48	2.551E-02					
			Quadratic		1.832	48	3.817E-02					
AREA * COLOR	TIME	Linear	Linear		.106	1	.106	3.128	.083	.061	3.128	.193
			Quadratic		5.377E-04	1	5.377E-04	.012	.913	.000	.012	.010
			Quadratic	Linear		1.663	1	1.663	60.538	.000	.558	60.538
	CORRECT	Linear	Quadratic		6.681E-02	1	6.681E-02	2.722	.105	.054	2.722	.163
			Linear		.000	1	.000	.000	1.000	.000	.000	.010
			Quadratic	Linear		1.361E-02	1	1.361E-02	.316	.577	.007	.316
Error(AREA*COLOR)	TIME	Linear	Linear		.575	1	.575	8.690	.005	.153	8.690	.606
			Quadratic		.137	1	.137	5.636	.022	.105	5.636	.388
			Quadratic	Linear		1.633	48	3.402E-02				
	CORRECT	Linear	Quadratic		2.121	48	4.419E-02					
			Linear		1.319	48	2.748E-02					
			Quadratic		1.178	48	2.454E-02					
METHOD * AREA * COLOR	TIME	Linear	Linear		.121	1	.121	4.562	.038	.087	4.562	.304
			Quadratic		5.525E-03	1	5.525E-03	.198	.658	.004	.198	.017
			Quadratic	Linear		1.035	1	1.035	55.744	.000	.537	55.744
	CORRECT	Linear	Quadratic		.158	1	.158	6.060	.017	.112	6.060	.421
			Linear		1.020E-02	1	1.020E-02	.282	.598	.006	.282	.021
			Quadratic	Linear		3.401E-03	1	3.401E-03	.068	.796	.001	.068
Error(METHOD*AREA*COLOR)	TIME	Linear	Quadratic		.667	1	.667	11.636	.001	.195	11.636	.763
			Quadratic		.113	1	.113	3.848	.056	.074	3.848	.248
			Quadratic	Linear		1.277	48	2.660E-02				
	CORRECT	Linear	Quadratic		1.337	48	2.786E-02					
			Linear		.891	48	1.856E-02					
			Quadratic		1.248	48	2.601E-02					
CORRECT	Linear	Linear		1.740	48	3.625E-02						
		Quadratic		2.413	48	5.028E-02						
		Quadratic	Linear		2.750	48	5.729E-02					
CORRECT	Linear	Quadratic		1.414	48	2.947E-02						

a. Computed using alpha = .01

Tests of Between-Subjects Effects

Transformed Variable: Average

Source	Measure	Type III Sum of Squares	df	Mean Square	F	Sig.	Partial Eta Squared	Noncent. Parameter	Observed Power <sup>a</sup>
Intercept	TIME	511.601	1	511.601	2539.100	.000	.981	2539.100	1.000
	CORRECT	779.185	1	779.185	5721.049	.000	.992	5721.049	1.000
Error	TIME	9.671	48	.201					
	CORRECT	6.537	48	.136					

a. Computed using alpha = .01

## Estimated Marginal Means

### 1. Grand Mean

Measure	Mean	Std. Error	99% Confidence Interval	
			Lower Bound	Upper Bound
TIME	.762	.015	.721	.802
CORRECT	.940	.012	.907	.973

## 2. METHOD

### Estimates

Measure	METHOD	Mean	Std. Error	99% Confidence Interval	
				Lower Bound	Upper Bound
TIME	1	.634	.017	.588	.680
	2	.889	.016	.846	.933
CORRECT	1	.955	.018	.907	1.002
	2	.925	.015	.884	.966

### Pairwise Comparisons

Measure	(I) METHOD	(J) METHOD	Mean Difference (I-J)	Std. Error	Sig. <sup>a</sup>	99% Confidence Interval for Difference <sup>a</sup>	
						Lower Bound	Upper Bound
TIME	1	2	-.255 <sup>a</sup>	.014	.000	-.294	-.217
	2	1	.255 <sup>a</sup>	.014	.000	.217	.294
CORRECT	1	2	2.948E-02	.022	.185	-2.932E-02	8.828E-02
	2	1	-2.948E-02	.022	.185	-8.828E-02	2.932E-02

Based on estimated marginal means

\*. The mean difference is significant at the .01 level.

a. Adjustment for multiple comparisons: Bonferroni.

### Multivariate Tests

	Value	F	Hypothesis df	Error df	Sig.	Partial Eta Squared	Noncent. Parameter	Observed Power <sup>b</sup>
Pillai's trace	.873	161.202 <sup>b</sup>	2.000	47.000	.000	.873	322.404	1.000
Wilks' lambda	.127	161.202 <sup>b</sup>	2.000	47.000	.000	.873	322.404	1.000
Hotelling's trace	6.860	161.202 <sup>b</sup>	2.000	47.000	.000	.873	322.404	1.000
Roy's largest root	6.860	161.202 <sup>b</sup>	2.000	47.000	.000	.873	322.404	1.000

Each F tests the multivariate effect of METHOD. These tests are based on the linearly independent pairwise comparisons among the estimated marginal means.

a. Computed using alpha = .01

b. Exact statistic

## 3. AREA

## Estimates

Measure	AREA	Mean	Std. Error	99% Confidence Interval	
				Lower Bound	Upper Bound
TIME	1	.599	.017	.554	.643
	2	.758	.015	.718	.798
	3	.928	.019	.878	.978
CORRECT	1	.976	.010	.950	1.002
	2	.946	.013	.910	.981
	3	.898	.023	.837	.959

## Pairwise Comparisons

Measure	(I) AREA	(J) AREA	Mean Difference (I-J)	Std. Error	Sig. <sup>a</sup>	99% Confidence Interval for Difference <sup>a</sup>	
						Lower Bound	Upper Bound
TIME	1	2	-.160 <sup>a</sup>	.010	.000	-.191	-.128
		3	-.329 <sup>a</sup>	.015	.000	-.374	-.284
	2	1	.160 <sup>a</sup>	.010	.000	.128	.191
		3	-.170 <sup>a</sup>	.013	.000	-.210	-.129
	3	1	.329 <sup>a</sup>	.015	.000	.284	.374
		2	.170 <sup>a</sup>	.013	.000	.129	.210
CORRECT	1	2	3.061E-02	.012	.033	-5.150E-03	6.637E-02
		3	7.823E-02 <sup>a</sup>	.021	.001	1.435E-02	.142
	2	1	-3.061E-02	.012	.033	-6.637E-02	5.150E-03
		3	4.762E-02	.020	.065	-1.429E-02	.110
	3	1	-7.823E-02 <sup>a</sup>	.021	.001	-.142	-1.435E-02
		2	-4.762E-02	.020	.065	-.110	1.429E-02

Based on estimated marginal means

\*. The mean difference is significant at the .01 level.

a. Adjustment for multiple comparisons: Bonferroni.

## Multivariate Tests

	Value	F	Hypothesis df	Error df	Sig.	Partial Eta Squared	Noncent. Parameter	Observed Power <sup>b</sup>
Pillai's trace	.923	135.363 <sup>b</sup>	4,000	45,000	.000	.923	541.454	1.000
Wilks' lambda	.077	135.363 <sup>b</sup>	4,000	45,000	.000	.923	541.454	1.000
Hotelling's trace	12.032	135.363 <sup>b</sup>	4,000	45,000	.000	.923	541.454	1.000
Roy's largest root	12.032	135.363 <sup>b</sup>	4,000	45,000	.000	.923	541.454	1.000

Each F tests the multivariate effect of AREA. These tests are based on the linearly independent pairwise comparisons among the estimated marginal means.

a. Computed using alpha = .01

b. Exact statistic

## 4. COLOR

## Estimates

Measure	COLOR	Mean	Std. Error	99% Confidence Interval	
				Lower Bound	Upper Bound
TIME	1	.719	.017	.674	.763
	2	.703	.018	.655	.752
	3	.863	.019	.812	.914
CORRECT	1	.952	.015	.911	.994
	2	.969	.009	.944	.994
	3	.898	.022	.840	.956

## Pairwise Comparisons

Measure	(I) COLOR	(J) COLOR	Mean Difference (I-J)	Std. Error	Sig. <sup>a</sup>	99% Confidence Interval for Difference <sup>a</sup>	
						Lower Bound	Upper Bound
TIME	1	2	1.566E-02	.016	.958	-3.242E-02	6.374E-02
		3	-.144*	.016	.000	-.192	-9.599E-02
	2	1	-1.566E-02	.016	.958	-6.374E-02	3.242E-02
		3	-.160*	.019	.000	-.218	-.101
	3	1	.144*	.016	.000	9.599E-02	.192
		2	.160*	.019	.000	.101	.218
CORRECT	1	2	-1.701E-02	.015	.766	-6.266E-02	2.864E-02
		3	5.442E-02	.019	.019	-4.474E-03	.113
	2	1	1.701E-02	.015	.766	-2.864E-02	6.266E-02
		3	7.143E-02*	.020	.003	9.524E-03	.133
	3	1	-5.442E-02	.019	.019	-.113	4.474E-03
		2	-7.143E-02*	.020	.003	-.133	-9.524E-03

Based on estimated marginal means

\*. The mean difference is significant at the .01 level.

a. Adjustment for multiple comparisons: Bonferroni.

## Multivariate Tests

	Value	F <sup>a</sup>	Hypothesis df	Error df	Sig.	Partial Eta Squared	Noncent. Parameter	Observed Power <sup>b</sup>
Pillai's trace	.677	23.630 <sup>b</sup>	4.000	45.000	.000	.677	94.520	1.000
Wilks' lambda	.323	23.630 <sup>b</sup>	4.000	45.000	.000	.677	94.520	1.000
Hotelling's trace	2.100	23.630 <sup>b</sup>	4.000	45.000	.000	.677	94.520	1.000
Roy's largest root	2.100	23.630 <sup>b</sup>	4.000	45.000	.000	.677	94.520	1.000

Each F tests the multivariate effect of COLOR. These tests are based on the linearly independent pairwise comparisons among the estimated marginal means.

a. Computed using alpha = .01

b. Exact statistic

## 5. METHOD \* AREA

Measure	METHOD	AREA	Mean	Std. Error	99% Confidence Interval	
					Lower Bound	Upper Bound
TIME	1	1	.533	.019	.483	.583
		2	.619	.019	.568	.670
		3	.750	.019	.699	.800
	2	1	.664	.017	.619	.709
		2	.898	.018	.848	.947
		3	1.106	.027	1.034	1.178
CORRECT	1	1	.980	.015	.939	1.020
		2	.980	.015	.939	1.020
		3	.905	.031	.822	.987
	2	1	.973	.013	.937	1.008
		2	.912	.021	.855	.969
		3	.891	.028	.816	.967

## 6. METHOD \* COLOR

Measure	METHOD	COLOR	Mean	Std. Error	99% Confidence Interval		
					Lower Bound	Upper Bound	
TIME	1	1	.575	.017	.529	.621	
		2	.587	.018	.538	.636	
		3	.740	.022	.681	.799	
	2	1	.863	.022	.803	.923	
		2	.819	.024	.756	.883	
		3	.986	.022	.925	1.046	
	CORRECT	1	1	.959	.023	.897	1.021
			2	.973	.013	.937	1.008
			3	.932	.027	.858	1.006
2		1	.946	.018	.898	.993	
		2	.966	.015	.927	1.005	
		3	.864	.027	.791	.937	

## 7. AREA \* COLOR

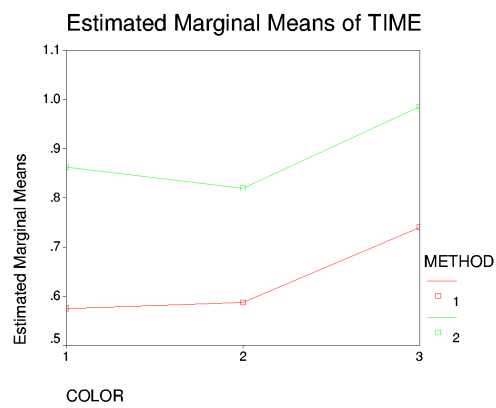
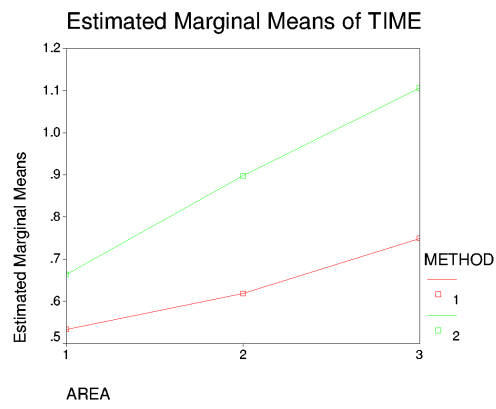
Measure	AREA	COLOR	Mean	Std. Error	99% Confidence Interval	
					Lower Bound	Upper Bound
TIME	1	1	.614	.018	.564	.663
		2	.533	.018	.484	.582
		3	.649	.020	.597	.702
	2	1	.632	.017	.587	.676
		2	.717	.021	.661	.774
		3	.926	.022	.866	.986
	3	1	.911	.028	.837	.986
		2	.859	.030	.780	.939
		3	1.013	.028	.938	1.088
CORRECT	1	1	.969	.017	.923	1.016
		2	1.000	.000	1.000	1.000
		3	.959	.020	.906	1.012
	2	1	.990	.010	.962	1.017
		2	1.000	.000	1.000	1.000
		3	.847	.036	.750	.944
	3	1	.898	.036	.802	.994
		2	.908	.028	.833	.983
		3	.888	.036	.790	.986

## 8. METHOD \* AREA \* COLOR

Measure	METHOD	AREA	COLOR	Mean	Std. Error	99% Confidence Interval		
						Lower Bound	Upper Bound	
TIME	1	1	1	.524	.020	.471	.578	
			2	.470	.020	.416	.524	
			3	.606	.025	.539	.673	
		2	1	.522	.022	.464	.580	
			2	.616	.026	.546	.686	
			3	.719	.025	.653	.785	
		3	1	.678	.019	.627	.729	
			2	.675	.026	.606	.744	
			3	.896	.030	.814	.977	
	2	1	1	.703	.023	.640	.765	
			2	.596	.022	.538	.654	
			3	.693	.023	.630	.756	
		2	1	.741	.021	.685	.798	
			2	.819	.028	.744	.893	
			3	1.133	.036	1.037	1.230	
		3	1	1.144	.046	1.020	1.269	
			2	1.044	.045	.925	1.163	
			3	1.130	.039	1.024	1.236	
	CORRECT	1	1	1	.980	.020	.925	1.034
				2	1.000	.000	1.000	1.000
				3	.959	.029	.883	1.036
			2	1	.980	.020	.925	1.034
				2	1.000	.000	1.000	1.000
				3	.959	.029	.883	1.036
			3	1	.918	.040	.812	1.024
				2	.918	.040	.812	1.024
				3	.878	.047	.751	1.004
2		1	1	.959	.029	.883	1.036	
			2	1.000	.000	1.000	1.000	
			3	.959	.029	.883	1.036	
		2	1	1.000	.000	1.000	1.000	
			2	1.000	.000	1.000	1.000	
			3	.735	.064	.564	.906	
		3	1	.878	.047	.751	1.004	
			2	.898	.044	.781	1.015	
			3	.898	.044	.781	1.015	

### Profile Plots

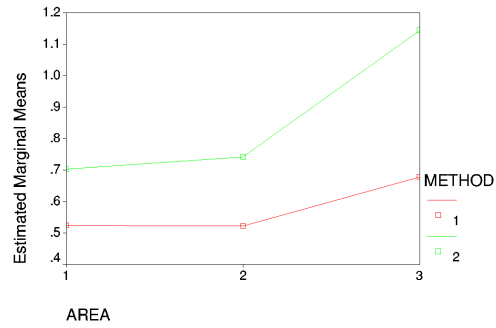
TIME



## AREA \* METHOD \* COLOR

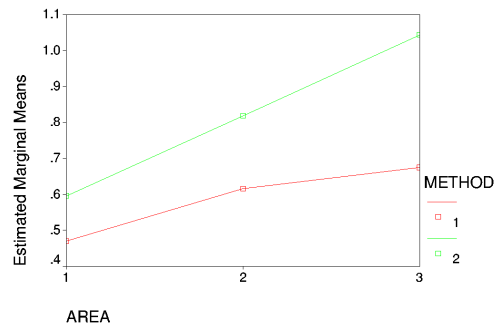
Estimated Marginal Means of TIME

At COLOR = 1



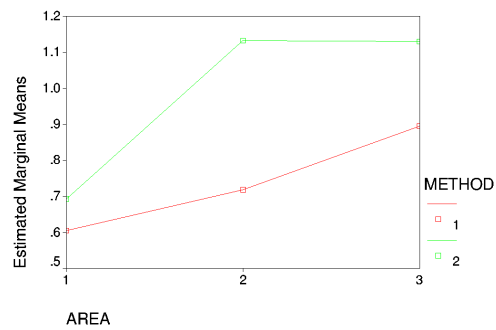
Estimated Marginal Means of TIME

At COLOR = 2

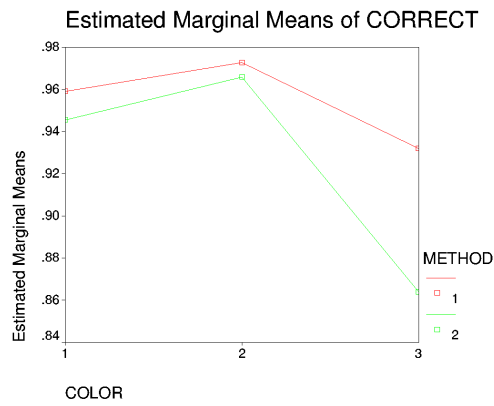
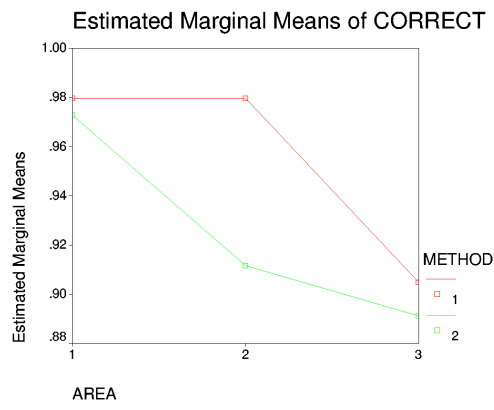


Estimated Marginal Means of TIME

At COLOR = 3

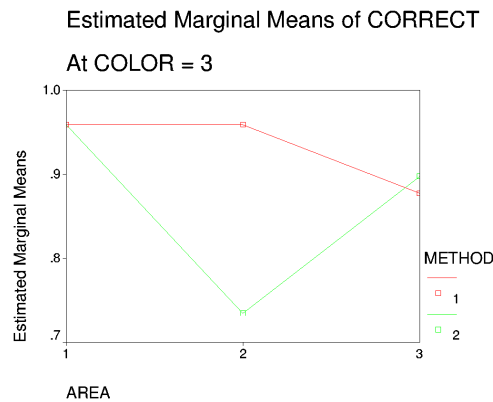
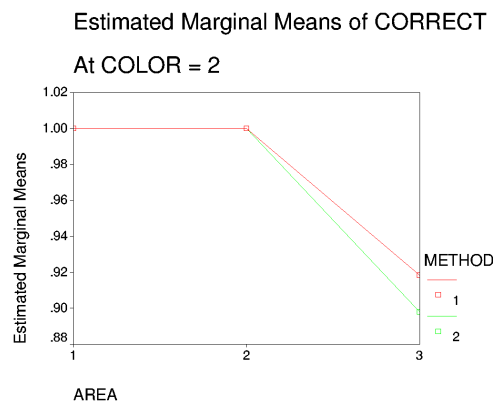
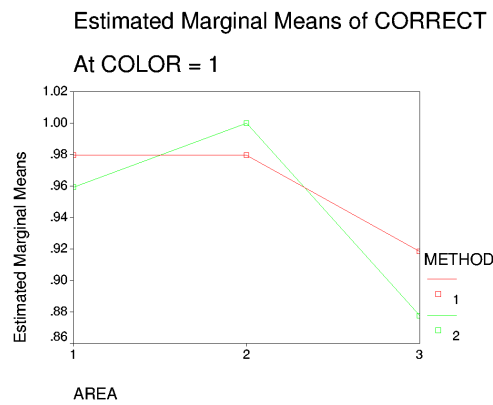


**CORRECT**





## AREA \* METHOD \* COLOR



The Task 2 pairwise comparison of small to large areas indicated a nonsignificant result which would have been significant in the analysis using strictly *Time*. This is because some values of *Time* were less than one second, resulting in  $\log_{10}(Time)$  values less than zero. When differences between distributions are taken that contain zero, generally

the result is nonsignificant because values tend to cancel out. If the distribution had been shifted slightly to all positive values, then the result would have been significant as in the MANOVA for *Time*. Therefore this pairwise comparison is indicated as significant in the analysis.

U49 TASK 2 MANOVA OF LOG(TIME) AND CORRECT WITH OUTLIERS ADJUSTED, ALPHA = 0.01, RUN ON 030924 AT 9:22 PM  
data file: u49-t2-var-log-out-adj-comb-correct-030924-01.sav  
same as first one, but with alpha = .01

```
GLM
  d.0.0.0 d.0.0.1 d.0.1.0 d.0.1.1 d.0.2.0 d.0.2.1 d.1.0.0 d.1.0.1
  d.1.1.0 d.1.1.1 d.1.2.0 d.1.2.1 r.0.0.0 r.0.0.1 r.0.1.0 r.0.1.1 r.0.2.0
  r.0.2.1 r.1.0.0 r.1.0.1 r.1.1.0 r.1.1.1 r.1.2.0 r.1.2.1
  /WSFACTOR = method 2 Polynomial pattern 2 Polynomial area 3 Polynomial
  /MEASURE = time correct
  /METHOD = SSTYPE(3)
  /PLOT = PROFILE( area*method pattern*method area*method*pattern )
  /EMMEANS = TABLES(OVERALL)
  /EMMEANS = TABLES(method) COMPARE ADJ(BONFERRONI)
  /EMMEANS = TABLES(pattern) COMPARE ADJ(BONFERRONI)
  /EMMEANS = TABLES(area) COMPARE ADJ(BONFERRONI)
  /EMMEANS = TABLES(method*pattern)
  /EMMEANS = TABLES(method*area)
  /EMMEANS = TABLES(pattern*area)
  /EMMEANS = TABLES(method*pattern*area)
  /PRINT = DESCRIPTIVE ETASQ OPOWER
  /PLOT = RESIDUALS
  /CRITERIA = ALPHA(.01)
  /WSDESIGN = method pattern area method*pattern method*area pattern*area
  method*pattern*area .
```

### General Linear Model

#### Warnings

The residual plot for R.0.0.1: Correct? is not produced because its residual variance is zero.

#### Within-Subjects Factors

Measure	METHOD	PATTERN	AREA	Dependent Variable	
TIME	1	1	1	TL.0.0.0	
			2	TL.0.0.1	
			3	TL.0.1.0	
	2	1	1	TL.0.1.1	
			2	TL.0.2.0	
			3	TL.0.2.1	
		2	1	TL.1.0.0	
			2	TL.1.0.1	
			3	TL.1.1.0	
	2	1	1	TL.1.1.1	
			2	TL.1.2.0	
			3	TL.1.2.1	
CORRECT		1	1	1	R.0.0.0
				2	R.0.0.1
				3	R.0.1.0
	2	1	1	R.0.1.1	
			2	R.0.2.0	
			3	R.0.2.1	
		2	1	R.1.0.0	
			2	R.1.0.1	
			3	R.1.1.0	
	2	1	R.1.1.1		
		2	R.1.2.0		
		3	R.1.2.1		

## Descriptive Statistics

	Mean	Std. Deviation	N
TL.0.0.0	.5693062	.23097480	49
TL.0.0.1	.5418831	.23623745	49
TL.0.1.0	.6437373	.29297724	49
TL.0.1.1	.6000650	.27668519	49
TL.0.2.0	.3488296	.20915588	49
TL.0.2.1	.3531471	.16835574	49
TL.1.0.0	1.0000966	.28683164	49
TL.1.0.1	1.1493278	.27832117	49
TL.1.1.0	1.2548179	.31424823	49
TL.1.1.1	.9692784	.28118124	49
TL.1.2.0	.9450452	.35770841	49
TL.1.2.1	1.1013005	.37500843	49
R.0.0.0: Correct?	.96	.200	49
R.0.0.1: Correct?	1.00	.000	49
R.0.1.0: Correct?	.92	.277	49
R.0.1.1: Correct?	.88	.331	49
R.0.2.0: Correct?	.98	.143	49
R.0.2.1: Correct?	.98	.143	49
R.1.0.0: Correct?	.78	.422	49
R.1.0.1: Correct?	.84	.373	49
R.1.1.0: Correct?	.88	.331	49
R.1.1.1: Correct?	.71	.456	49
R.1.2.0: Correct?	.96	.200	49
R.1.2.1: Correct?	.88	.331	49

Multivariate Tests<sup>a</sup>

Effect			Value	F	Hypothesis df	Error df	Sig.	Partial Eta Squared	Noncent. Parameter	Observed Power <sup>b</sup>
Between Subjects	Intercept	Pillai's Trace	.992	2950.813 <sup>b</sup>	2.000	47.000	.000	.992	5901.626	1.000
		Wilks' Lambda	.008	2950.813 <sup>b</sup>	2.000	47.000	.000	.992	5901.626	1.000
		Hotelling's Trace	125.567	2950.813 <sup>b</sup>	2.000	47.000	.000	.992	5901.626	1.000
		Roy's Largest Root	125.567	2950.813 <sup>b</sup>	2.000	47.000	.000	.992	5901.626	1.000
Within Subjects	METHOD	Pillai's Trace	.867	153.667 <sup>b</sup>	2.000	47.000	.000	.867	307.334	1.000
		Wilks' Lambda	.133	153.667 <sup>b</sup>	2.000	47.000	.000	.867	307.334	1.000
		Hotelling's Trace	6.539	153.667 <sup>b</sup>	2.000	47.000	.000	.867	307.334	1.000
		Roy's Largest Root	6.539	153.667 <sup>b</sup>	2.000	47.000	.000	.867	307.334	1.000
	PATTERN	Pillai's Trace	.598	34.962 <sup>b</sup>	2.000	47.000	.000	.598	69.923	1.000
		Wilks' Lambda	.402	34.962 <sup>b</sup>	2.000	47.000	.000	.598	69.923	1.000
		Hotelling's Trace	1.488	34.962 <sup>b</sup>	2.000	47.000	.000	.598	69.923	1.000
		Roy's Largest Root	1.488	34.962 <sup>b</sup>	2.000	47.000	.000	.598	69.923	1.000
	AREA	Pillai's Trace	.506	11.511 <sup>b</sup>	4.000	45.000	.000	.506	46.043	.998
		Wilks' Lambda	.494	11.511 <sup>b</sup>	4.000	45.000	.000	.506	46.043	.998
		Hotelling's Trace	1.023	11.511 <sup>b</sup>	4.000	45.000	.000	.506	46.043	.998
		Roy's Largest Root	1.023	11.511 <sup>b</sup>	4.000	45.000	.000	.506	46.043	.998
	METHOD * PATTERN	Pillai's Trace	.014	.346 <sup>b</sup>	2.000	47.000	.710	.014	.691	.027
		Wilks' Lambda	.986	.346 <sup>b</sup>	2.000	47.000	.710	.014	.691	.027
		Hotelling's Trace	.015	.346 <sup>b</sup>	2.000	47.000	.710	.014	.691	.027
		Roy's Largest Root	.015	.346 <sup>b</sup>	2.000	47.000	.710	.014	.691	.027
	METHOD * AREA	Pillai's Trace	.653	21.182 <sup>b</sup>	4.000	45.000	.000	.653	84.727	1.000
		Wilks' Lambda	.347	21.182 <sup>b</sup>	4.000	45.000	.000	.653	84.727	1.000
		Hotelling's Trace	1.883	21.182 <sup>b</sup>	4.000	45.000	.000	.653	84.727	1.000
		Roy's Largest Root	1.883	21.182 <sup>b</sup>	4.000	45.000	.000	.653	84.727	1.000
	PATTERN * AREA	Pillai's Trace	.487	10.668 <sup>b</sup>	4.000	45.000	.000	.487	42.672	.997
		Wilks' Lambda	.513	10.668 <sup>b</sup>	4.000	45.000	.000	.487	42.672	.997
		Hotelling's Trace	.948	10.668 <sup>b</sup>	4.000	45.000	.000	.487	42.672	.997
		Roy's Largest Root	.948	10.668 <sup>b</sup>	4.000	45.000	.000	.487	42.672	.997
	METHOD * PATTERN * AREA	Pillai's Trace	.223	3.232 <sup>b</sup>	4.000	45.000	.021	.223	12.926	.553
		Wilks' Lambda	.777	3.232 <sup>b</sup>	4.000	45.000	.021	.223	12.926	.553
		Hotelling's Trace	.287	3.232 <sup>b</sup>	4.000	45.000	.021	.223	12.926	.553
		Roy's Largest Root	.287	3.232 <sup>b</sup>	4.000	45.000	.021	.223	12.926	.553

a. Computed using alpha = .01

b. Exact statistic

c.

Design: Intercept

Within Subjects Design: METHOD+PATTERN+AREA+METHOD\*PATTERN+METHOD\*AREA+PATTERN\*AREA+METHOD\*PATTERN\*AREA

Mauchly's Test of Sphericity<sup>b</sup>

Within Subjects Effect	Measure	Mauchly's W	Approx. Chi-Square	df	Sig.	Epsilon <sup>a</sup>		
						Greenhouse-Geisser	Huynh-Feldt	Lower-bound
METHOD	TIME	1.000	.000	0	.	1.000	1.000	1.000
	CORRECT	1.000	.000	0	.	1.000	1.000	1.000
PATTERN	TIME	1.000	.000	0	.	1.000	1.000	1.000
	CORRECT	1.000	.000	0	.	1.000	1.000	1.000
AREA	TIME	.751	13.460	2	.001	.801	.824	.500
	CORRECT	.674	18.525	2	.000	.754	.773	.500
METHOD * PATTERN	TIME	1.000	.000	0	.	1.000	1.000	1.000
	CORRECT	1.000	.000	0	.	1.000	1.000	1.000
METHOD * AREA	TIME	.988	.579	2	.749	.988	1.000	.500
	CORRECT	.818	9.435	2	.009	.846	.874	.500
PATTERN * AREA	TIME	.978	1.031	2	.597	.979	1.000	.500
	CORRECT	.855	7.339	2	.025	.874	.904	.500
METHOD * PATTERN * AREA	TIME	.949	2.447	2	.294	.952	.990	.500
	CORRECT	.955	2.176	2	.337	.957	.996	.500

Tests the null hypothesis that the error covariance matrix of the orthonormalized transformed dependent variables is proportional to an identity matrix.

a. May be used to adjust the degrees of freedom for the averaged tests of significance. Corrected tests are displayed in the Tests of Within-Subjects Effects table.

b.

Design: Intercept

Within Subjects Design: METHOD+PATTERN+AREA+METHOD\*PATTERN+METHOD\*AREA+PATTERN\*AREA+METHOD\*PATTERN\*AREA

Tests of Within-Subjects Effects

Multivariate<sup>a,c</sup>

Within Subjects Effect		Value	F	Hypothesis df	Error df	Sig.	Partial Eta Squared	Noncent. Parameter	Observed Power <sup>d</sup>
METHOD	Pillai's Trace	.867	153.667 <sup>b</sup>	2.000	47.000	.000	.867	307.334	1.000
	Wilks' Lambda	.133	153.667 <sup>b</sup>	2.000	47.000	.000	.867	307.334	1.000
	Hotelling's Trace	6.539	153.667 <sup>b</sup>	2.000	47.000	.000	.867	307.334	1.000
	Roy's Largest Root	6.539	153.667 <sup>b</sup>	2.000	47.000	.000	.867	307.334	1.000
PATTERN	Pillai's Trace	.598	34.962 <sup>b</sup>	2.000	47.000	.000	.598	69.923	1.000
	Wilks' Lambda	.402	34.962 <sup>b</sup>	2.000	47.000	.000	.598	69.923	1.000
	Hotelling's Trace	1.488	34.962 <sup>b</sup>	2.000	47.000	.000	.598	69.923	1.000
	Roy's Largest Root	1.488	34.962 <sup>b</sup>	2.000	47.000	.000	.598	69.923	1.000
AREA	Pillai's Trace	.326	9.347	4.000	192.000	.000	.163	37.389	.996
	Wilks' Lambda	.700	9.275 <sup>b</sup>	4.000	190.000	.000	.163	37.099	.996
	Hotelling's Trace	.392	9.201	4.000	188.000	.000	.164	36.806	.996
	Roy's Largest Root	.231	11.090 <sup>c</sup>	2.000	96.000	.000	.188	22.180	.955
METHOD * PATTERN	Pillai's Trace	.014	.346 <sup>b</sup>	2.000	47.000	.710	.014	.691	.027
	Wilks' Lambda	.986	.346 <sup>b</sup>	2.000	47.000	.710	.014	.691	.027
	Hotelling's Trace	.015	.346 <sup>b</sup>	2.000	47.000	.710	.014	.691	.027
	Roy's Largest Root	.015	.346 <sup>b</sup>	2.000	47.000	.710	.014	.691	.027
METHOD * AREA	Pillai's Trace	.433	13.275	4.000	192.000	.000	.217	53.102	1.000
	Wilks' Lambda	.567	15.591 <sup>b</sup>	4.000	190.000	.000	.247	62.363	1.000
	Hotelling's Trace	.764	17.953	4.000	188.000	.000	.276	71.811	1.000
	Roy's Largest Root	.764	36.654 <sup>c</sup>	2.000	96.000	.000	.433	73.308	1.000
PATTERN * AREA	Pillai's Trace	.353	10.290	4.000	192.000	.000	.177	41.161	.999
	Wilks' Lambda	.648	11.490 <sup>b</sup>	4.000	190.000	.000	.195	45.959	1.000
	Hotelling's Trace	.540	12.691	4.000	188.000	.000	.213	50.763	1.000
	Roy's Largest Root	.536	25.720 <sup>c</sup>	2.000	96.000	.000	.349	51.440	1.000
METHOD * PATTERN * AREA	Pillai's Trace	.111	2.812	4.000	192.000	.027	.055	11.248	.536
	Wilks' Lambda	.891	2.812 <sup>b</sup>	4.000	190.000	.027	.056	11.248	.536
	Hotelling's Trace	.120	2.811	4.000	188.000	.027	.056	11.245	.536
	Roy's Largest Root	.096	4.604 <sup>c</sup>	2.000	96.000	.012	.088	9.208	.539

a. Computed using alpha = .01

b. Exact statistic

c. The statistic is an upper bound on F that yields a lower bound on the significance level.

d. Design: Intercept

Within Subjects Design:

METHOD+PATTERN+AREA+METHOD\*PATTERN+METHOD\*AREA+PATTERN\*AREA+METHOD\*PATTERN\*AREA

e. Tests are based on averaged variables.

Univariate Tests

Source	Measure		Type III Sum of Squares	df	Mean Square	F	Sig.	Partial Eta Squared	Noncent. Parameter	Observed Power <sup>d</sup>
METHOD	TIME	Sphericity Assumed	46.179	1	46.179	303.762	.000	.864	303.762	1.000
		Greenhouse-Geisser	46.179	1.000	46.179	303.762	.000	.864	303.762	1.000
		Huynh-Feldt	46.179	1.000	46.179	303.762	.000	.864	303.762	1.000
		Lower-bound	46.179	1.000	46.179	303.762	.000	.864	303.762	1.000

## Univariate Tests

Source	Measure		Type III Sum of Squares	df	Mean Square	F	Sig.	Partial Eta Squared	Noncent. Parameter	Observed Power <sup>a</sup>
METHOD	CORRECT	Sphericity Assumed	1.852	1	1.852	18.150	.000	.274	18.150	.938
		Greenhouse-Geisser	1.852	1.000	1.852	18.150	.000	.274	18.150	.938
		Huynh-Feldt	1.852	1.000	1.852	18.150	.000	.274	18.150	.938
		Lower-bound	1.852	1.000	1.852	18.150	.000	.274	18.150	.938
Error(METHOD)	TIME	Sphericity Assumed	7.297	48	.152					
		Greenhouse-Geisser	7.297	48,000	.152					
		Huynh-Feldt	7.297	48,000	.152					
		Lower-bound	7.297	48,000	.152					
	CORRECT	Sphericity Assumed	4.898	48	.102					
		Greenhouse-Geisser	4.898	48,000	.102					
		Huynh-Feldt	4.898	48,000	.102					
		Lower-bound	4.898	48,000	.102					
PATTERN	TIME	Sphericity Assumed	2.892	1	2.892	69.810	.000	.593	69.810	1.000
		Greenhouse-Geisser	2.892	1.000	2.892	69.810	.000	.593	69.810	1.000
		Huynh-Feldt	2.892	1.000	2.892	69.810	.000	.593	69.810	1.000
		Lower-bound	2.892	1.000	2.892	69.810	.000	.593	69.810	1.000
	CORRECT	Sphericity Assumed	1.701E-03	1	1.701E-03	.013	.911	.000	.013	.010
		Greenhouse-Geisser	1.701E-03	1.000	1.701E-03	.013	.911	.000	.013	.010
		Huynh-Feldt	1.701E-03	1.000	1.701E-03	.013	.911	.000	.013	.010
		Lower-bound	1.701E-03	1.000	1.701E-03	.013	.911	.000	.013	.010
Error(PATTERN)	TIME	Sphericity Assumed	1.988	48	4.142E-02					
		Greenhouse-Geisser	1.988	48,000	4.142E-02					
		Huynh-Feldt	1.988	48,000	4.142E-02					
		Lower-bound	1.988	48,000	4.142E-02					
	CORRECT	Sphericity Assumed	6.415	48	.134					
		Greenhouse-Geisser	6.415	48,000	.134					
		Huynh-Feldt	6.415	48,000	.134					
		Lower-bound	6.415	48,000	.134					
AREA	TIME	Sphericity Assumed	.837	2	.418	10.191	.000	.175	20.383	.934
		Greenhouse-Geisser	.837	1.601	.522	10.191	.000	.175	16.319	.874
		Huynh-Feldt	.837	1.648	.508	10.191	.000	.175	16.794	.883
		Lower-bound	.837	1.000	.837	10.191	.002	.175	10.191	.694
	CORRECT	Sphericity Assumed	1.320	2	.660	7.905	.001	.141	15.810	.840
		Greenhouse-Geisser	1.320	1.509	.875	7.905	.002	.141	11.925	.728
		Huynh-Feldt	1.320	1.547	.853	7.905	.002	.141	12.229	.739
		Lower-bound	1.320	1.000	1.320	7.905	.007	.141	7.905	.555
Error(AREA)	TIME	Sphericity Assumed	3.940	96	4.104E-02					
		Greenhouse-Geisser	3.940	76.860	5.127E-02					
		Huynh-Feldt	3.940	79.100	4.981E-02					
		Lower-bound	3.940	48,000	8.209E-02					
	CORRECT	Sphericity Assumed	8.014	96	8.348E-02					
		Greenhouse-Geisser	8.014	72.412	.111					
		Huynh-Feldt	8.014	74.255	.108					
		Lower-bound	8.014	48,000	.167					

## Univariate Tests

Source	Measure		Type III Sum of Squares	df	Mean Square	F	Sig.	Partial Eta Squared	Noncent. Parameter	Observed Power <sup>a</sup>	
METHOD * PATTERN	TIME	Sphericity Assumed	1.686E-02	1	1.686E-02	.405	.528	.008	.405	.026	
		Greenhouse-Geisser	1.686E-02	1.000	1.686E-02	.405	.528	.008	.405	.026	
		Huynh-Feldt	1.686E-02	1.000	1.686E-02	.405	.528	.008	.405	.026	
		Lower-bound	1.686E-02	1.000	1.686E-02	.405	.528	.008	.405	.026	
	CORRECT	Sphericity Assumed	4.252E-02	1	4.252E-02	.467	.498	.010	.467	.028	
		Greenhouse-Geisser	4.252E-02	1.000	4.252E-02	.467	.498	.010	.467	.028	
		Huynh-Feldt	4.252E-02	1.000	4.252E-02	.467	.498	.010	.467	.028	
		Lower-bound	4.252E-02	1.000	4.252E-02	.467	.498	.010	.467	.028	
	Error(METHOD*PATTERN)	TIME	Sphericity Assumed	2.000	48	4.167E-02					
			Greenhouse-Geisser	2.000	48.000	4.167E-02					
			Huynh-Feldt	2.000	48.000	4.167E-02					
			Lower-bound	2.000	48.000	4.167E-02					
CORRECT		Sphericity Assumed	4.374	48	9.113E-02						
		Greenhouse-Geisser	4.374	48.000	9.113E-02						
		Huynh-Feldt	4.374	48.000	9.113E-02						
		Lower-bound	4.374	48.000	9.113E-02						
METHOD * AREA		TIME	Sphericity Assumed	2.041	2	1.021	34.025	.000	.415	68.050	1.000
			Greenhouse-Geisser	2.041	1.976	1.033	34.025	.000	.415	67.227	1.000
			Huynh-Feldt	2.041	2.000	1.021	34.025	.000	.415	68.050	1.000
			Lower-bound	2.041	1.000	2.041	34.025	.000	.415	34.025	.999
	CORRECT	Sphericity Assumed	.286	2	.143	2.400	.096	.048	4.800	.243	
		Greenhouse-Geisser	.286	1.692	.169	2.400	.106	.048	4.061	.211	
		Huynh-Feldt	.286	1.747	.164	2.400	.104	.048	4.194	.217	
		Lower-bound	.286	1.000	.286	2.400	.128	.048	2.400	.140	
	Error(METHOD*AREA)	TIME	Sphericity Assumed	2.880	96	3.000E-02					
			Greenhouse-Geisser	2.880	94.839	3.036E-02					
			Huynh-Feldt	2.880	96.000	3.000E-02					
			Lower-bound	2.880	48.000	5.999E-02					
CORRECT		Sphericity Assumed	5.714	96	5.952E-02						
		Greenhouse-Geisser	5.714	81.227	7.035E-02						
		Huynh-Feldt	5.714	83.876	6.813E-02						
		Lower-bound	5.714	48.000	.119						
PATTERN * AREA		TIME	Sphericity Assumed	1.459	2	.729	25.712	.000	.349	51.423	1.000
			Greenhouse-Geisser	1.459	1.958	.745	25.712	.000	.349	50.331	1.000
			Huynh-Feldt	1.459	2.000	.729	25.712	.000	.349	51.423	1.000
			Lower-bound	1.459	1.000	1.459	25.712	.000	.349	25.712	.990
	CORRECT	Sphericity Assumed	.422	2	.211	2.929	.058	.058	5.858	.315	
		Greenhouse-Geisser	.422	1.747	.241	2.929	.066	.058	5.118	.281	
		Huynh-Feldt	.422	1.808	.233	2.929	.064	.058	5.296	.289	
		Lower-bound	.422	1.000	.422	2.929	.093	.058	2.929	.178	
	Error(PATTERN*AREA)	TIME	Sphericity Assumed	2.723	96	2.836E-02					
			Greenhouse-Geisser	2.723	93.961	2.898E-02					
			Huynh-Feldt	2.723	96.000	2.836E-02					
			Lower-bound	2.723	48.000	5.673E-02					

## Univariate Tests

Source	Measure		Type III Sum of Squares	df	Mean Square	F	Sig.	Partial Eta Squared	Noncent. Parameter	Observed Power <sup>a</sup>	
Error(PATTERN*AREA)	CORRECT	Sphericity Assumed	6.912	96	7.200E-02						
		Greenhouse-Geisser	6.912	83.875	8.240E-02						
		Huynh-Feldt	6.912	86.781	7.964E-02						
		Lower-bound	6.912	48.000	.144						
METHOD * PATTERN * AREA	TIME	Sphericity Assumed	.261	2	.131	4.544	.013	.086	9.089	.531	
		Greenhouse-Geisser	.261	1.903	.137	4.544	.014	.086	8.650	.511	
		Huynh-Feldt	.261	1.980	.132	4.544	.013	.086	8.997	.527	
		Lower-bound	.261	1.000	.261	4.544	.038	.086	4.544	.302	
	CORRECT	Sphericity Assumed	.259	2	.129	1.754	.179	.035	3.508	.161	
		Greenhouse-Geisser	.259	1.913	.135	1.754	.180	.035	3.356	.156	
		Huynh-Feldt	.259	1.991	.130	1.754	.179	.035	3.492	.161	
		Lower-bound	.259	1.000	.259	1.754	.192	.035	1.754	.097	
	Error(METHOD*PATTERN*AREA)	TIME	Sphericity Assumed	2.760	96	2.875E-02					
			Greenhouse-Geisser	2.760	91.365	3.021E-02					
			Huynh-Feldt	2.760	95.037	2.904E-02					
			Lower-bound	2.760	48.000	5.750E-02					
CORRECT		Sphericity Assumed	7.075	96	7.370E-02						
		Greenhouse-Geisser	7.075	91.845	7.703E-02						
		Huynh-Feldt	7.075	95.569	7.403E-02						
		Lower-bound	7.075	48.000	.147						

a. Computed using alpha = .01

## Tests of Within-Subjects Contrasts

Source	Measure	METHOD	PATTERN	AREA	Type III Sum of Squares	df	Mean Square	F	Sig.	Partial Eta Squared	Noncent. Parameter	Observed Power <sup>a</sup>	
METHOD	TIME	Linear			46.179	1	46.179	303.762	.000	.864	303.762	1.000	
	CORRECT	Linear			1.852	1	1.852	18.150	.000	.274	18.150	.938	
Error(METHOD)	TIME	Linear			7.297	48	.152						
	CORRECT	Linear			4.898	48	.102						
PATTERN	TIME	Linear			2.892	1	2.892	69.810	.000	.593	69.810	1.000	
	CORRECT	Linear			1.701E-03	1	1.701E-03	.013	.911	.000	.013	.010	
Error(PATTERN)	TIME	Linear			1.988	48	4.142E-02						
	CORRECT	Linear			6.415	48	.134						
AREA	TIME	Linear			.281	1	.281	4.626	.037	.088	4.626	.309	
		Quadratic			.555	1	.555	26.072	.000	.352	26.072	.991	
	CORRECT	Linear			.653	1	.653	5.141	.028	.097	5.141	.350	
		Quadratic			.667	1	.667	16.696	.000	.258	16.696	.914	
	Error(AREA)	TIME	Linear			2.918	48	6.079E-02					
		Quadratic			1.023	48	2.130E-02						
CORRECT	Linear			6.097	48	.127							
	Quadratic			1.917	48	3.993E-02							
METHOD * PATTERN	TIME	Linear	Linear		1.686E-02	1	1.686E-02	.405	.528	.008	.405	.026	
	CORRECT	Linear	Linear		4.252E-02	1	4.252E-02	.467	.498	.010	.467	.028	
Error(METHOD*PATTERN)	TIME	Linear	Linear		2.000	48	4.167E-02						
	CORRECT	Linear	Linear		4.374	48	9.113E-02						
METHOD * AREA	TIME	Linear		Linear	1.916	1	1.916	71.776	.000	.599	71.776	1.000	
		Linear		Quadratic	.126	1	.126	3.773	.058	.073	3.773	.242	
	CORRECT	Linear		Linear	.255	1	.255	4.089	.049	.078	4.089	.267	
		Linear		Quadratic	3.061E-02	1	3.061E-02	.540	.466	.011	.540	.032	
	Error(METHOD*AREA)	TIME	Linear		Linear	1.281	48	2.669E-02					
		Linear		Quadratic	1.599	48	3.330E-02						
CORRECT	Linear		Linear	2.995	48	6.239E-02							
	Linear		Quadratic	2.719	48	5.665E-02							
PATTERN * AREA	TIME	Linear		Linear	1.208	1	1.208	37.647	.000	.440	37.647	1.000	
		Linear		Quadratic	.251	1	.251	10.177	.003	.175	10.177	.693	
	CORRECT	Linear		Linear	.255	1	.255	2.724	.105	.054	2.724	.163	
		Linear		Quadratic	.167	1	.167	3.310	.075	.065	3.310	.206	
Error(PATTERN*AREA)	TIME	Linear		Linear	1.540	48	3.208E-02						
		Linear		Quadratic	1.183	48	2.465E-02						
	CORRECT	Linear		Linear	4.495	48	9.364E-02						
		Linear		Quadratic	2.417	48	5.035E-02						
METHOD * PATTERN * AREA	TIME	Linear		Linear	.242	1	.242	10.297	.002	.177	10.297	.699	
		Linear		Quadratic	1.959E-02	1	1.959E-02	.576	.452	.012	.576	.033	
	CORRECT	Linear		Linear	4.082E-02	1	4.082E-02	.465	.498	.010	.465	.028	
		Linear		Quadratic	.218	1	.218	3.646	.062	.071	3.646	.232	
Error(METHOD*PATTERN*AREA)	TIME	Linear		Linear	1.127	48	2.347E-02						
	Linear		Quadratic	1.633	48	3.403E-02							
CORRECT	Linear		Linear	4.209	48	8.769E-02							
	Linear		Quadratic	2.866	48	5.970E-02							

a. Computed using alpha = .01

## Tests of Between-Subjects Effects

Transformed Variable: Average

Source	Measure	Type III Sum of Squares	df	Mean Square	F	Sig.	Partial Eta Squared	Noncent. Parameter	Observed Power <sup>a</sup>
Intercept	TIME	366.726	1	366.726	800.085	.000	.943	800.085	1.000
	CORRECT	472.328	1	472.328	3198.415	.000	.985	3198.415	1.000
Error	TIME	22.001	48	.458					
	CORRECT	7.088	48	.148					

a. Computed using alpha = .01

## Estimated Marginal Means

### 1. Grand Mean

Measure	Mean	Std. Error	99% Confidence Interval	
			Lower Bound	Upper Bound
TIME	.790	.028	.715	.865
CORRECT	.896	.016	.854	.939

## 2. METHOD

### Estimates

Measure	METHOD	Mean	Std. Error	99% Confidence Interval	
				Lower Bound	Upper Bound
TIME	1	.509	.026	.440	.579
	2	1.070	.038	.969	1.171
CORRECT	1	.952	.012	.920	.984
	2	.840	.027	.769	.911

### Pairwise Comparisons

Measure	(I) METHOD	(J) METHOD	Mean Difference (I-J)	Std. Error	Sig. <sup>a</sup>	99% Confidence Interval for Difference <sup>a</sup>	
						Lower Bound	Upper Bound
TIME	1	2	-.560*	.032	.000	-.647	-.474
	2	1	.560*	.032	.000	.474	.647
CORRECT	1	2	.112*	.026	.000	4.158E-02	.183
	2	1	-.112*	.026	.000	-.183	-4.158E-02

Based on estimated marginal means

\*. The mean difference is significant at the .01 level.

a. Adjustment for multiple comparisons: Bonferroni.

### Multivariate Tests

	Value	F	Hypothesis df	Error df	Sig.	Partial Eta Squared	Noncent. Parameter	Observed Power <sup>b</sup>
Pillai's trace	.867	153.667 <sup>b</sup>	2.000	47.000	.000	.867	307.334	1.000
Wilks' lambda	.133	153.667 <sup>b</sup>	2.000	47.000	.000	.867	307.334	1.000
Hotelling's trace	6.539	153.667 <sup>b</sup>	2.000	47.000	.000	.867	307.334	1.000
Roy's largest root	6.539	153.667 <sup>b</sup>	2.000	47.000	.000	.867	307.334	1.000

Each F tests the multivariate effect of METHOD. These tests are based on the linearly independent pairwise comparisons among the estimated marginal means.

a. Computed using alpha = .01

b. Exact statistic



### 3. PATTERN

#### Estimates

Measure	PATTERN	Mean	Std. Error	99% Confidence Interval	
				Lower Bound	Upper Bound
TIME	1	.860	.030	.780	.940
	2	.720	.029	.643	.796
CORRECT	1	.895	.026	.824	.966
	2	.898	.016	.855	.941

#### Pairwise Comparisons

Measure	(I) PATTERN	(J) PATTERN	Mean Difference (I-J)	Std. Error	Sig. <sup>a</sup>	99% Confidence Interval for Difference <sup>a</sup>	
						Lower Bound	Upper Bound
TIME	1	2	.140*	.017	.000	9.523E-02	.185
	2	1	-.140*	.017	.000	-.185	-9.523E-02
CORRECT	1	2	-3.401E-03	.030	.911	-8.428E-02	7.747E-02
	2	1	3.401E-03	.030	.911	-7.747E-02	8.428E-02

Based on estimated marginal means

\*. The mean difference is significant at the .01 level.

a. Adjustment for multiple comparisons: Bonferroni.

#### Multivariate Tests

	Value	F	Hypothesis df	Error df	Sig.	Partial Eta Squared	Noncent. Parameter	Observed Power <sup>b</sup>
Pillai's trace	.598	34.962 <sup>b</sup>	2.000	47.000	.000	.598	69.923	1.000
Wilks' lambda	.402	34.962 <sup>b</sup>	2.000	47.000	.000	.598	69.923	1.000
Hotelling's trace	1.488	34.962 <sup>b</sup>	2.000	47.000	.000	.598	69.923	1.000
Roy's largest root	1.488	34.962 <sup>b</sup>	2.000	47.000	.000	.598	69.923	1.000

Each F tests the multivariate effect of PATTERN. These tests are based on the linearly independent pairwise comparisons among the estimated marginal means.

a. Computed using alpha = .01

b. Exact statistic

## 4. AREA

## Estimates

Measure	AREA	Mean	Std. Error	99% Confidence Interval	
				Lower Bound	Upper Bound
TIME	1	.785	.029	.706	.863
	2	.746	.030	.667	.826
	3	.838	.032	.752	.924
CORRECT	1	.832	.023	.769	.895
	2	.944	.017	.899	.989
	3	.913	.028	.839	.988

## Pairwise Comparisons

Measure	(I) AREA	(J) AREA	Mean Difference (I-J)	Std. Error	Sig. <sup>a</sup>	99% Confidence Interval for Difference <sup>b</sup>	
						Lower Bound	Upper Bound
TIME	1	2	3.842E-02	.019	.151	-2.071E-02	9.754E-02
		3	-5.356E-02	.025	.110	-.131	2.337E-02
	2	1	-3.842E-02	.019	.151	-9.754E-02	2.071E-02
		3	-9.198E-02 <sup>a</sup>	.016	.000	-.143	-4.123E-02
	3	1	5.356E-02	.025	.110	-2.337E-02	.131
		2	9.198E-02 <sup>a</sup>	.016	.000	4.123E-02	.143
CORRECT	1	2	-.112 <sup>a</sup>	.028	.001	-.200	-2.484E-02
		3	-8.163E-02	.036	.084	-.193	2.958E-02
	2	1	.112 <sup>a</sup>	.028	.001	2.484E-02	.200
		3	3.061E-02	.021	.478	-3.556E-02	9.678E-02
	3	1	8.163E-02	.036	.084	-2.958E-02	.193
		2	-3.061E-02	.021	.478	-9.678E-02	3.556E-02

Based on estimated marginal means

\*. The mean difference is significant at the .01 level.

a. Adjustment for multiple comparisons: Bonferroni.

## Multivariate Tests

	Value	F	Hypothesis df	Error df	Sig.	Partial Eta Squared	Noncent. Parameter	Observed Power <sup>f</sup>
Pillai's trace	.506	11.511 <sup>b</sup>	4.000	45.000	.000	.506	46.043	.998
Wilks' lambda	.494	11.511 <sup>b</sup>	4.000	45.000	.000	.506	46.043	.998
Hotelling's trace	1.023	11.511 <sup>b</sup>	4.000	45.000	.000	.506	46.043	.998
Roy's largest root	1.023	11.511 <sup>b</sup>	4.000	45.000	.000	.506	46.043	.998

Each F tests the multivariate effect of AREA. These tests are based on the linearly independent pairwise comparisons among the estimated marginal means.

a. Computed using alpha = .01

b. Exact statistic

## 5. METHOD \* PATTERN

Measure	METHOD	PATTERN	Mean	Std. Error	99% Confidence Interval	
					Lower Bound	Upper Bound
TIME	1	1	.585	.030	.504	.666
		2	.434	.026	.364	.504
	2	1	1.135	.038	1.032	1.237
		2	1.005	.041	.896	1.115
CORRECT	1	1	.959	.016	.917	1.001
		2	.946	.018	.898	.993
	2	1	.830	.045	.710	.950
		2	.850	.026	.781	.920

## 6. METHOD \* AREA

Measure	METHOD	AREA	Mean	Std. Error	99% Confidence Interval	
					Lower Bound	Upper Bound
TIME	1	1	.585	.031	.500	.669
		2	.445	.027	.372	.519
		3	.498	.028	.422	.575
	2	1	.985	.036	.887	1.082
		2	1.047	.042	.934	1.160
		3	1.178	.045	1.057	1.299
CORRECT	1	1	.918	.027	.847	.990
		2	.990	.010	.962	1.017
		3	.949	.022	.890	1.008
	2	1	.745	.042	.633	.856
		2	.898	.029	.820	.976
		3	.878	.040	.770	.985

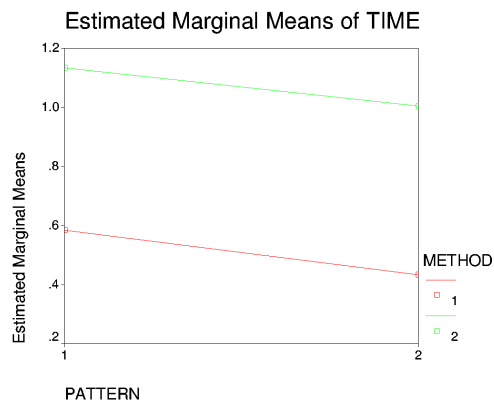
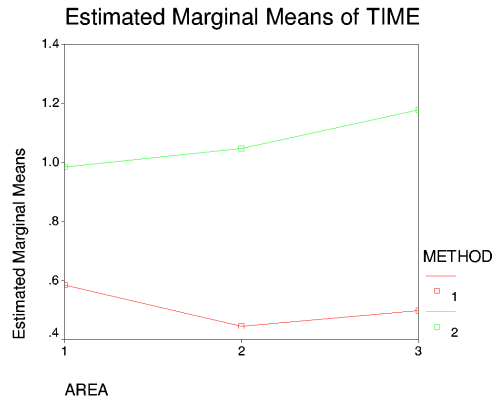
## 7. PATTERN \* AREA

Measure	PATTERN	AREA	Mean	Std. Error	99% Confidence Interval	
					Lower Bound	Upper Bound
TIME	1	1	.785	.031	.701	.868
		2	.846	.029	.768	.923
		3	.949	.037	.851	1.048
	2	1	.785	.034	.694	.876
		2	.647	.034	.556	.738
		3	.727	.033	.640	.815
CORRECT	1	1	.867	.035	.773	.961
		2	.918	.027	.847	.990
		3	.898	.036	.802	.994
	2	1	.796	.041	.686	.906
		2	.969	.017	.923	1.016
		3	.929	.029	.850	1.007

## 8. METHOD \* PATTERN \* AREA

Measure	METHOD	PATTERN	AREA	Mean	Std. Error	99% Confidence Interval		
						Lower Bound	Upper Bound	
TIME	1	1	1	.569	.033	.481	.658	
			2	.542	.034	.451	.632	
			3	.644	.042	.531	.756	
		2	1	.600	.040	.494	.706	
			2	.349	.030	.269	.429	
			3	.353	.024	.289	.418	
		2	1	1	1.000	.041	.890	1.110
				2	1.149	.040	1.043	1.256
				3	1.255	.045	1.134	1.375
	2		1	.969	.040	.862	1.077	
			2	.945	.051	.808	1.082	
			3	1.101	.054	.958	1.245	
	CORRECT	1	1	1	.959	.029	.883	1.036
				2	1.000	.000	1.000	1.000
				3	.918	.040	.812	1.024
2			1	.878	.047	.751	1.004	
			2	.980	.020	.925	1.034	
			3	.980	.020	.925	1.034	
2			1	1	.776	.060	.614	.937
				2	.837	.053	.694	.980
				3	.878	.047	.751	1.004
		2	1	.714	.065	.539	.889	
			2	.959	.029	.883	1.036	
			3	.878	.047	.751	1.004	

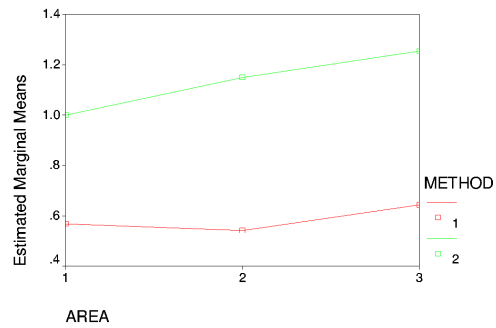
**Profile Plots**  
**TIME**



## AREA \* METHOD \* PATTERN

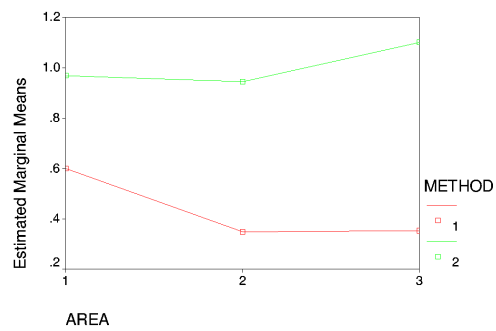
Estimated Marginal Means of TIME

At PATTERN = 1

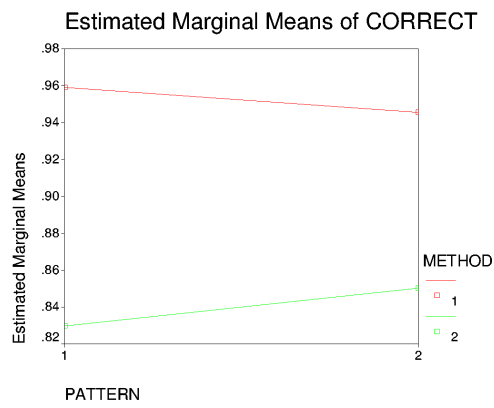
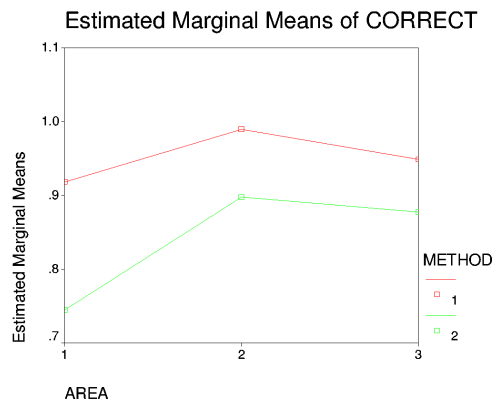


Estimated Marginal Means of TIME

At PATTERN = 2



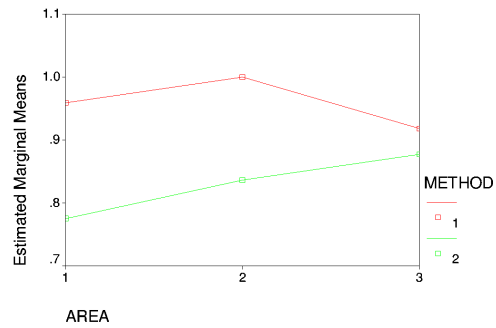
**CORRECT**



## AREA \* METHOD \* PATTERN

Estimated Marginal Means of CORRECT

At PATTERN = 1



Estimated Marginal Means of CORRECT

At PATTERN = 2

